

# **Contractor Report to RWM**

## **Bentonite in a High-temperature Environment**

### **Bentonite Erosion**

**December 2020**

Lennart Börgesson, Magnus Hedström, David Holton, Richard Metcalfe and Torbjörn Sandén



## Conditions of Publication

This report is made available under the Radioactive Waste Management Limited (RWM) Transparency Policy. In line with this policy, RWM is seeking to make information on its activities readily available, and to enable interested parties to have access to and influence on its future programmes. The report may be freely used for non-commercial purposes. RWM is a wholly owned subsidiary of the Nuclear Decommissioning Authority (NDA), accordingly all commercial uses, including copying and re publication, require permission from the NDA. All copyright, database rights and other intellectual property rights reside with the NDA.

Applications for permission to use the report commercially should be made to the NDA Information Manager.

Although great care has been taken to ensure the accuracy and completeness of the information contained in this publication, the NDA cannot assume any responsibility for consequences that may arise from its use by other parties.

© Nuclear Decommissioning Authority 2021 All rights reserved.

## Other Publications

If you would like to see other reports available from RWM, a complete listing can be viewed at our website <https://www.gov.uk/rwm>, or please write to us at the address below.

## Feedback

Readers are invited to provide feedback on this report and on the means of improving the range of reports published. Feedback should be addressed to:

RWM Feedback  
Radioactive Waste Management Limited  
Building 329  
Thomson Avenue  
Harwell Campus  
Didcot  
OX11 0GD  
UK

email: [rwmfeedback@nda.gov.uk](mailto:rwmfeedback@nda.gov.uk)



**Preface**

Radioactive Waste Management (RWM) carries out research activities into Geological Disposal Facility-relevant processes affecting the UK Radioactive Waste Inventory, in support of geological disposal of the UK's higher activity radioactive waste. The work presented in this report forms part of our engineered barrier systems research programme and was carried out by Clay Technology, Jacobs and Quintessa on our behalf. The work has been reviewed by RWM and by 2 independent peer reviewers. RWM accepts the data and conclusions in this report.



# **Bentonite in a High-temperature Environment**

## **Bentonite Erosion**

Lennart Börgesson<sup>1</sup>, Magnus Hedström<sup>1</sup>, David Holton<sup>2</sup>, Richard Metcalfe<sup>3</sup> & Torbjörn Sandén<sup>1</sup>

**Clay Technology AB, Lund, Sweden<sup>1</sup>; MCM Environmental, Bristol, UK<sup>2</sup>; Quintessa Ltd. Henley-on-Thames, UK<sup>3</sup>.**

**Report No. 208955-TA01**

December 2020

*Keywords:* Bentonite, Mechanical Erosion, Chemical Erosion

## Executive Summary

An international consensus has developed for the disposal of higher-activity radioactive wastes in domestic Geological Disposal Facilities (GDF). Radioactive Waste Management's (RWM's) generic illustrative disposal concepts for high level waste (HLW), spent fuel, highly enriched uranium (HEU) and plutonium in higher strength rock (HSR) and lower strength sedimentary rock (LSSR) are assumed to use bentonite clay as a buffer material to fulfil required safety functions.

In higher strength rock concepts, overseas waste management organisations have generally assumed a maximum waste container surface temperature of 100°C. For example, this temperature limit has been applied to the KBS3 concept, developed in Sweden by SKB, which has driven much research on the behaviour of bentonite. The Swiss waste management organisation, Nagra, assumes a mid-point buffer temperature of 125°C for disposal in a lower strength sedimentary rock. Accordingly, RWM's illustrative designs for high level waste assume a maximum container surface temperature of 100°C for higher strength rock and 125°C in the outer half of the buffer for lower strength sedimentary rock. However, these temperature thresholds are now potentially being challenged, in part due to disposal requirements for new nuclear build fuels. Consequently, there is limited research into the impacts of higher temperatures on bentonite barriers, particularly for higher strength rock disposal conditions. Bentonite possesses favourable properties due to its mineralogical make up; however, these minerals are known to undergo alteration in the presence of certain chemical species and under high temperatures. Such alteration can cause loss of the swelling capacity and associated plasticity, properties needed for the engineered barriers to fulfil their required safety functions. Further research is therefore required to improve our understanding of the alteration behaviour of bentonite at high temperatures in order to gain confidence in its safety function performance within a GDF environment.

Recognising these challenges, further research is required to address a number of outstanding tasks identified by RWM's Science and Technology Plan (RWM, 2016), which relate to bentonite piping and erosion, and the alteration of bentonite at temperatures >100°C. This review relates to Task 468 - Review of bentonite erosion work and identification of future research needs.

This report sets out a review of bentonite erosion by considering two important aspects:

1. **Mechanical erosion** - before the bentonite has produced a high swelling pressure, it may not prevent water inflow due to the pressure gradients that may prevail in the water bearing fractures at depth, whilst the GDF is operational. If the bentonite cannot resist these gradients, water will force its way through. This process, commonly referred to as *piping*, may result in transport of bentonite particles (mechanical erosion) with the flowing water.
2. **Chemical erosion** - chemical erosion refers to the loss of bentonite due to interaction with dilute groundwater.

These processes are relevant in HSR, where water-conducting fractures are in contact with the bentonite. The processes are not relevant in LSSR, where piping and erosion of bentonite

would not be possible owing to the very low hydraulic conductivity of the LSSR and lack of conductive fractures within it.

This report identifies gaps in knowledge relevant to mechanical and chemical erosion.

For mechanical erosion, the two main knowledge gaps are:

- Self-sealing of piping channels after water saturation: Although tests have shown that piping channels self-seal after water saturation, more tests under different conditions are required in order to assure that this will always be the case.
- Gel extrusion and formation of water/gel filled pockets: The knowledge of this process is still too immature to establish how and when it occurs.
- For the modelling of piping and erosion, it is concluded that general, the knowledge of these processes is too low to be able to form a model that can handle all the processes and identified variables.

Regarding the chemical erosion, the identified knowledge gaps concern:

- The effect of elevated temperatures and exposure to steam: there are indications that steam-exposed bentonite may have different gelling properties. This may affect erosion, but that process has not been investigated using steam-exposed bentonite
- The evolution of erosion rate with time: some studies suggest that the erosion rate decreases with time. However, it cannot be excluded that the erosion rate was influenced by artefacts. A few suggestions how to eliminate such artefacts are given.
- There are gaps in the theoretical and conceptual understanding, and the models that have been used so far are unreliable.

# Contents

1	Introduction .....	5
1.1	UK Context .....	5
1.2	International context – bentonite erosion .....	5
2	Potential Sub-Surface Conditions Near a UK GDF .....	9
2.1	Generic Geological Environments .....	9
2.2	Geological Settings .....	10
2.3	Temperature Gradients .....	11
2.4	Groundwater Flow Systems .....	12
2.5	Geochemical Conditions .....	13
2.6	Future Environmental Evolution .....	15
2.7	Key Issues for Bentonite Piping and Erosion.....	15
3	Mechanical erosion .....	17
3.1	Objectives.....	17
3.2	Method .....	17
3.3	Definition of piping and mechanical erosion .....	18
3.4	Summary of studied reports .....	19
3.5	Evaluation of different laboratory tests on erosion .....	36
3.6	Parameters and variables influencing piping and erosion.....	39
3.7	Governing processes influencing piping and erosion .....	43
3.8	The present capability to model piping and mechanical erosion .....	53
3.9	Influence of temperature on erosion.....	55
3.10	Identified gaps in the knowledge regarding piping and erosion .....	57
3.11	Conclusions .....	60
4	Chemical erosion.....	62
4.1	Definitions and concepts .....	62
4.2	Rheology of different clay phases .....	74
4.3	Erosion experiments involving bentonite or montmorillonite .....	82
4.4	Modelling work .....	94
4.5	Gap analysis .....	100
5	References .....	103

# 1 Introduction

## 1.1 UK Context

An international consensus has developed for the disposal of higher-activity radioactive wastes in domestic Geological Disposal Facilities (GDF). Radioactive Waste Management's (RWM's) generic illustrative disposal concepts for high level waste (HLW), spent fuel, highly enriched uranium (HEU) and plutonium in higher strength rock (HSR) and lower strength sedimentary rock (LSSR) are assumed to use bentonite clay as a buffer material to fulfil required safety functions. The bentonite buffer forms part of an engineered barrier, restricting flow of water and corrodants around the waste container and limits microbial activity that could otherwise accelerate container corrosion. The plasticity and swelling capacity of the bentonite allows self-sealing, in the event of physical disturbances in the host rock. Furthermore, released radionuclides would be attenuated, since transport of solutes through bentonite is by diffusion only.

In higher strength rock concepts, overseas waste management organisations have generally assumed a maximum waste container surface temperature of 100°C. For example, this temperature limit has been applied to the KBS3 concept, developed in Sweden by SKB, which has driven much research on the behaviour of bentonite. The Swiss waste management organisation, Nagra, assumes a mid-point buffer temperature of 125°C for disposal in a lower strength sedimentary rock. Accordingly, RWM's illustrative designs for high level waste assume a maximum container surface temperature of 100°C for higher strength rock and 125°C in the outer half of the buffer for lower strength sedimentary rock. However, these temperature thresholds are now potentially being challenged, in part due to disposal requirements for new nuclear build fuels. Consequently, there is limited research into the impacts of higher temperatures on bentonite barriers, particularly for higher strength rock disposal conditions. Bentonite possesses favourable properties due to its mineralogical make up; however, these minerals are known to undergo alteration in the presence of certain chemical species and under high temperatures. Such alteration can cause loss of the swelling capacity and associated plasticity, properties needed for the engineered barriers to fulfil their required safety functions. Further research is therefore required to improve our understanding of the alteration behaviour of bentonite at high temperatures in order to gain confidence in its safety function performance within a GDF environment.

Piping and erosion are relevant in HSR, where water-conducting fractures that cannot be durably sealed are in contact with the bentonite. The processes are not relevant in LSSR, where piping and erosion of bentonite would not be possible owing to the very low hydraulic conductivity of the LSSR and lack of conductive fractures within it.

Recognising these challenges, further research is required to address a number of outstanding tasks identified by RWM's Science and Technology Plan (RWM, 2016), which relate to bentonite piping and erosion, and the alteration of bentonite at temperatures >100°C. This review relates to Task 468 - Review of bentonite erosion work and identification of future research needs.

## 1.2 International context – bentonite erosion

Bentonite clay is planned to be used as an important component in many of the final repositories for spent nuclear fuel that are planned to be constructed in several countries

worldwide. The spent nuclear fuel is often encapsulated in canisters (copper or steel) which are deposited in the bedrock e.g. crystalline rock, sedimentary rock or clay formations, at a depth of 400-700 meters. Between the canisters and the rock, compacted bentonite is emplaced as buffer material, either in the form of blocks or as pellets/granules. The bentonite absorbs water and has after saturation a very low hydraulic conductivity that limits the flow of water. The bentonite also develops a swelling pressure that will keep the canister in place and the microbiological activity low.

An important function of the bentonite buffer, recognised internationally, is to minimise water flow through the deposition holes. The transport through the buffer is expected to be reduced and to be controlled principally by diffusion, both with regard to corrosive components in the groundwater and to corrosion products, and with regard to escaping radionuclides in case of a canister failure.

Figure 1-1 shows an example of the planned Swedish KBS-3 repository. The drawing illustrates the layout of part of a deposition tunnel and a scenario for water inflow into a deposition hole and a deposition tunnel during installation.

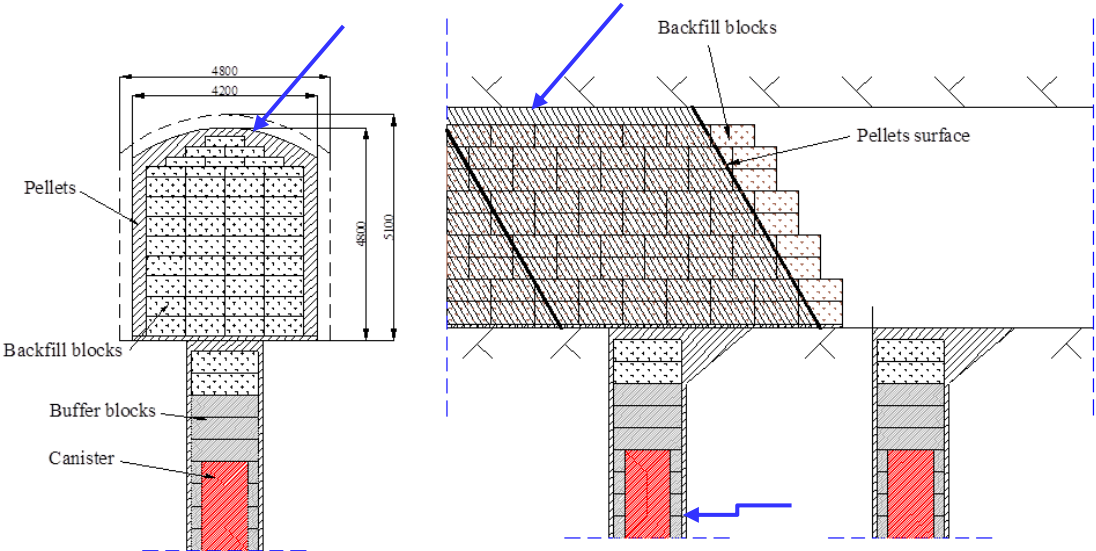


**Figure 1-1** Illustration of the layout of the deposition tunnel and holes (during ongoing installation) and a scenario of water inflow illustrated with blue arrows (Börjesson et al. 2015).

Bentonite is an excellent sealing material after full water saturation when the high swelling pressure and low hydraulic conductivity can prevent water from flowing through the deposition holes and deposition tunnels. However, before the bentonite has produced a high swelling pressure that acts on the rock surface, it cannot prevent water inflow due to the high pressures that prevails in the water bearing fractures at repository depth. If the water inflow is stopped the water pressure will rise in the fracture and since the bentonite e.g. a pellet filling between block and rock wall, cannot resist this pressure, water will break the seal and force its way through the pellet filling. This process, *pipng*, may result in a transport of bentonite particles with the flowing water, *erosion*, either out from the repository or internal from e.g. a deposition hole to the deposition tunnel.

The above described erosion process is in this report termed mechanical erosion, and is defined to take place when the drag force on the clay particle from the water movement is

higher than the sum of the friction and attraction forces between the particle and the clay structure.

The process that often has been termed chemical erosion refers to the loss of bentonite due to interaction with dilute groundwater. As will be described below, chemical erosion can be distinguished from mechanical erosion in that the particle release is not dependent on mechanical shear *per se*.

The sealing properties of bentonite are governed by the interaction between the mineral montmorillonite and water (Birgersson et al., 2017). Montmorillonite has high affinity for water which results in the build-up of an osmotic pressure or swelling pressure when bentonite is placed in a confined volume. This would be the situation in, e.g., a deposition hole during and after water saturation. However, at fractures intersecting the deposition hole, the bentonite is not restricted but can continue to swell until a steady state or equilibrium is reached. In sufficiently saline groundwater, the montmorillonite at the swelling front will form a gel that resists further water uptake and the swelling will halt a few centimetres into the fracture (Börgesson et al., 2018). The formation of a gel is sensitive to the chemical composition of the groundwater, hence the term chemical erosion, and in case the salinity falls below a critical concentration the montmorillonite at the swelling front turns into a colloidal sol, which is a liquid state from which colloidal montmorillonite particles can be released. This erosion process is therefore also referred to as colloid release (SKB, 2019). The sol, being a liquid, has no shear strength so the release of colloidal particles is not directly linked to the mechanical shear force from flowing water and it has been shown that gravity alone is sufficient to sustain erosion (Hedström et al., 2016; Schatz et al., 2013; Schatz and Akhanoba, 2017). Thus, the cause of chemical/colloid release erosion is different from mechanical erosion and requires an understanding of the different colloidal phases of bentonite/montmorillonite and, in particular, under what conditions the sol is stable (Shelton et al., 2018).

In the Nordic countries chemical erosion is an issue for the longevity of a repository for spent nuclear fuel, and adverse conditions may occur during and after a glaciation due to dilute groundwater intrusion at repository depth (Posiva OY, 2012; SKB, 2011). At the time SKB submitted its application for a permit to build a Spent Fuel Repository at Forsmark, the issue of chemical erosion was not yet resolved<sup>1</sup> and the need for a continued R & D program was acknowledged (SKB, 2011). This has led to continued international research, e.g., the BELBaR project (Shelton et al., 2018) and subsequent studies (Alonso et al., 2019). Present day groundwater conditions at repository depth are sufficiently saline not to present a problem of chemical erosion (Posiva OY, 2012; SKB, 2011). Similarly, in the UK, groundwaters with dissolved solid concentrations below the critical concentration are unlikely (Alexander et al., 2018). However, both in the Nordic countries and the UK, dilute groundwater may reach

---

<sup>1</sup> Comment by Claes Tegerström, CEO SKB, at the press conference when the application was submitted 2011, reported in “Ny Teknik”, a biweekly magazine distributed to all members of The Swedish Association of Graduate Engineers

repository depth during future periods of glaciation. The future environmental evolution with focus on UK conditions is discussed in section 2.6.

## 2 Potential Sub-Surface Conditions Near a UK GDF

Much of the existing knowledge about influences on the potential for bentonite piping and erosion comes from research focussed on the Swedish and Finnish radioactive waste disposal programmes. However, the geo-environmental conditions of a future UK GDF are likely to differ from those in the vicinity of the planned Swedish or Finnish radioactive waste repositories at Forsmark and Olkiluoto respectively. Therefore, existing knowledge based on studies of Swedish and Finnish sub-surface conditions may need to be extended to be applicable to a UK GDF.

The purpose of this section is to summarise briefly the environments in which a future UK GDF could plausibly be constructed. It is not the intent to give a detailed description of these environments, but rather to highlight important issues about them and their variability.

A GDF in the UK will in practice likely be sited in England or Wales. The Scottish Government has a different policy on radioactive waste disposal to that in the rest of the UK and is not participating in RWM's site selection programme for a GDF. There are also no plans to site a GDF in Northern Ireland, even though this province has been included in the national geological screening for a GDF<sup>2</sup>. Any future policy decision on geological disposal in Northern Ireland would be a matter for the Northern Ireland Executive.

### 2.1 Generic Geological Environments

RWM has defined 6 generic geological environments, each of which consists of one of three generic host rock types and either no cover rock sequence, or a sedimentary rock sequence (RWM, 2017):

1. Higher strength rocks (HSR) to surface;
2. HSR overlain by higher permeability sedimentary rocks;
3. HSR overlain by lower permeability sedimentary rocks;
4. Lower strength sedimentary rock (LSSR) overlain by higher permeability sedimentary rocks;
5. LSSR rock overlain by lower permeability sedimentary rock;
6. Evaporite overlain by a sedimentary sequence.

Plausible ranges of hydrogeological and geochemical parameter values for these generic environments are given in Metcalfe et al. (2015).

---

<sup>2</sup> A National Geological Screening exercise has been carried out by RWM to summarise the geology of England, Wales and Northern Ireland that is relevant to the safe disposal of higher-activity radioactive waste.

Real environments in the UK could have the specific characteristics of one of the six generic environments or they could have characteristics that are intermediate between two or more of the six generic environments

Radioactive waste disposal concepts including bentonite buffers could be adopted only in environments 1. to 5. Compacted bentonite buffers would not function properly in the highly saline groundwater that would occur within an evaporite sequence. In any case, bentonite buffers would be unnecessary if the host rock were to be halite, given the very low permeability and self-sealing properties of this material.

HSR may be igneous, metamorphic or older sedimentary rocks. They have a low matrix porosity and low permeability, and most groundwater flow occurs through connected fractures within the rock mass. Thus, only a small proportion of the rock mass is transmissive.

In contrast LSSR are fine-grained sedimentary rocks with a high clay mineral content that provides low permeability. Groundwater will not flow by advection through such rocks, but instead mass transport will be only by diffusion. LSSR are mechanically weak, meaning that open fractures cannot be sustained.

While there are some locations in England and Wales where HSR extends from the surface to depths of >200 m, in most locations where they occur, HSR is overlain by a sedimentary rock sequence, which may consist of higher-permeability rocks (e.g. sandstone aquifers), lower permeability rocks (e.g. shales), or, more commonly, an interstratified sequence of both kinds of sedimentary rock.

LSSR are, depending upon their location, similarly overlain by sedimentary rocks that are lower permeability, higher permeability, or a mixture of the two.

## **2.2 Geological Settings**

Although England and Wales are relatively small countries (130,279 km<sup>2</sup> and 20,779 km<sup>2</sup> respectively), they are geologically diverse, with solid rocks ranging in age from late Precambrian (c. 700 Ma) to Tertiary.

Igneous rocks crop out over only small areas of England and Wales, mostly in southwest England, northern England, northwest Wales and southwest Wales. However, igneous rocks occur beneath sedimentary cover rocks in much larger areas of both countries.

An important feature of the geological setting of England and Wales are a number of Mesozoic sedimentary basins. These basins typically contain large evaporite sequences of Permian and Triassic age, and consequently very saline groundwater, which may be near halite saturation (around 6 molal at 25°C). Rock sequences that lie adjacent to these basins may also contain very saline groundwater, the salinity originating in halite dissolution within the basins.

RWM's recent national geological screening exercise has considered the geology up to 20 km offshore, in recognition of the possibility that a GDF may be constructed under the present seabed but accessed by tunnels from a location onshore. Therefore, offshore geological conditions also need to be considered. The offshore areas of England and Wales are dominated by sedimentary basins, most of which contain evaporite sequences of Permian and Triassic age.

## 2.3 Temperature Gradients

Temperatures in a GDF may influence the performance of bentonite buffers. After waste emplacement in a GDF the temperature of the buffer will initially increase due to radioactive decay of the waste, reaching a peak after a few tens of years (depending upon the disposal concept and geological environment), before substantially decreasing over a period of perhaps a few thousand years. For most, if not all, of the period of enhanced temperatures due to radiogenic heating, any bentonite buffer may not be fully water-saturated. Therefore, the elevated temperatures may not affect erosion significantly. Nevertheless, the characteristics of the host rocks at a GDF location could also influence the temperature evolution of the bentonite. For example, HSR may have thermal conductivities in the range  $2.2 \text{ Wm}^{-1}\text{K}^{-1}$  to  $3.8 \text{ Wm}^{-1}\text{K}^{-1}$ , while LSSR may have thermal conductivities in the range  $0.62 \text{ Wm}^{-1}\text{K}^{-1}$  to  $3.2 \text{ Wm}^{-1}\text{K}^{-1}$ .

However, in the longer-term the temperature will be governed by the natural heat flow. The significance of this for bentonite erosion needs to be considered.

The average geothermal gradient in the UK is  $26^\circ\text{C}/\text{km}$  (Busby, 2014, 2010). However, there is considerable variation in heat flow across the UK (Figure 2-1). The highest heat flows correspond to granite batholiths in southwest England and northern England. Temperatures at a depth of 1000 m in these areas reach up to about  $50^\circ\text{C}$ ; Manning et al. (2007) report a geothermal gradient of  $60^\circ\text{C}/\text{km}$  above the Weardale Granite of northern England. Within the Mesozoic sedimentary basins, the gradient can reach around  $35^\circ\text{C}/\text{km}$  (Busby, 2014). At the maximum depth at which a GDF could be sited, 1000 m, maximum temperatures in the range 40 to  $50^\circ\text{C}$  are plausible.

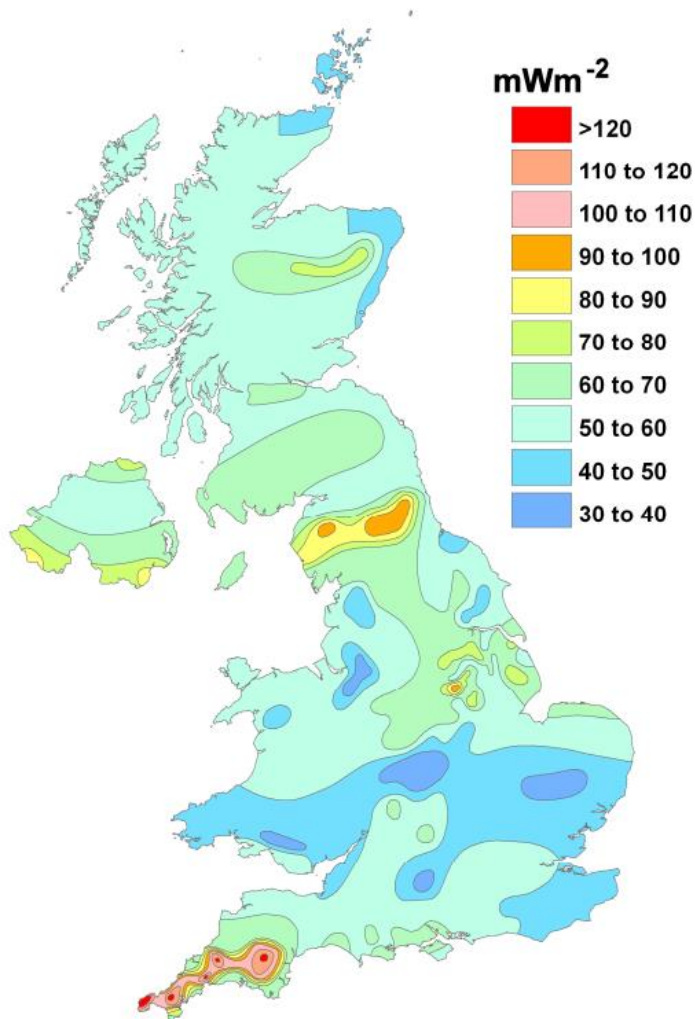


*Figure 2-1 Heat flow across the UK. After Busby (2010).*

## 2.4 Groundwater Flow Systems

In England and Wales groundwater flow in the depth range relevant to a GDF is driven mainly by topographic head gradients, which may be modified by density gradients related to the dissolution of evaporite minerals. Examples are given Metcalfe et al. (2000) and Bath et al. (2006). Thermal gradients may also influence groundwater flow patterns/rates in some cases (Busby, 2014).

Within sedimentary basins that contain evaporite sequences, there is a general tendency for groundwater to dissolve halite in more central regions, gain in density and consequently flow towards the basin margins (although the details of groundwater flow are much more complex). Onshore, the basin margins tend to coincide with areas of meteoric recharge which drives groundwater to flow towards the basin centre. There is, therefore, likely to be a transition between fresher water at shallower depths and closer to the basin margins, and more saline water at depth and towards the basin centre (e.g. in northwest England; Bath et al. (2006); Metcalfe et al. (2007); Milodowski et al. (2018)).

When assessing the potential for bentonite piping and erosion in a UK GDF, it is necessary to consider the potential for steep salinity and chemical gradients to occur, across or near the

GDF site. It is also necessary to consider the possibility that these gradients may change locations in response to changing groundwater flow patterns and/or fluxes. These changes may be caused by variations in environmental conditions, principally rainfall, glaciation and sea level change (which may be related to isostasy caused by local glaciation and/or global (eustatic) sea level change due to glaciation).

## **2.5 Geochemical Conditions**

Geochemical conditions at likely GDF depths<sup>3</sup> in England and Wales will depend on the nature of the site. However, representative compositions are specified in Table 2-1, taken from Metcalfe et al. (2015). It is impossible to guarantee that all actual water compositions can be matched by mixtures of these compositions. Nevertheless, it is expected that the general chemical compositions of the majority of real groundwaters in England, Wales and Northern Ireland can be approximated at an appropriate level for the current generic stage of RWM's programme by mixtures of these water compositions.

These compositions in Table 2-1 are based on real water compositions taken from published literature, as specified in the references. However, only a sub-set of the constituents present in these real waters (major cations and anions) is presented. The compositions have been modified to ensure that they are internally consistent (i.e. charge-balanced). Internal consistency was achieved by calculating values for some parameters using Geochemist's Workbench v 6.0.3 in conjunction with the thermodynamic databases thermo.dat or thermo\_hmw.dat, which are distributed with Geochemist's Workbench (Bethke, 2008, 1996).

---

<sup>3</sup> Depending on the site, waste would be emplaced at a depth between 200 m and 1000 m)

**Table 2-1 Model water compositions specified to describe water chemistry in the 6 generic geological environments considered by RWM (from Metcalfe et al., 2015).**

	Meteoric Water	Seawater	Basinal Brine	Crystalline Basement	Fresh Sandstone Groundwater	Fresh Chalk Groundwater	Mudrock Porewater
Basic Source	Shand et al. (2007)	Summerhayes and Thorpe (1996)	Bath et al. (2006), Nirex (1998)	Manning et al. (2007), Salas et al. (2010)	Smedley and Edmunds (2002)	Bath and Edmunds (1981)	De Craen et al. (2004)
Rationale	Lowest Cl reported. Approximates recharge	Mean Seawater composition	Most saline groundwater sampled in the Sellafield area	Most saline water reported from crystalline basement	Most alkaline sample reported in the above source from the East Midlands Triassic aquifer	Flowing water in limestone aquifer, near mean Ca and HCO <sub>3</sub> reported for Chalk (e.g. Smedley et al., 2004)	Reference porewater for Boom Clay at Mol. This formation originally contained seawater that has been flushed by meteoric water
Model	GWB v 6.0, Thermo.dat database, Atmospheric equilibration, charge balance on Cl	GWB v 6.0, Thermo.dat database, Atmospheric equilibration, charge balance on Cl	GWB v 6.0, thermo_hmw.dat database, pH constrained by calcite equilibrium, remove water to halite and anhydrite saturation, HS set at detection limit. charge balance on Cl	GWB v 6.0, Thermo.dat database, pH set to highest value calculated by Salas et al. (2010) for Forsmark, equilibration, HS set at detection limit. charge balance on Cl	GWB v 6.0, Thermo.dat database, HS set at detection limit. charge balance on Cl	GWB v 6.0, Thermo.dat database, HS set at detection limit. charge balance on Cl	GWB v 6.0, Thermo.dat database, HS from difference between reported total S and SO <sub>4</sub> , charge balance on HCO <sub>3</sub> .
Parameter	Concentration mg l <sup>-1</sup>						
O <sub>2</sub> (aq)	12.0	8.6	0.0	0.0	0.0	0.0	0.0
Na	0.47	10770	100000	9732	49.7	41	372
K	0.04	399	458	652	6.2	2.9	7.45
Ca	0.07	405.4	2237	5214	112.1	120	1.41
Mg	0.06	1286	449	72.6	36.86	12.5	1.66
TIC	0.21	23.68	13.77	9.26	26.98	67.35	187.4
SO <sub>4</sub>	0.85	2708	1760	47.7	369	66	2.28
Cl	1.28	19380	159100	24970	44.85	104.2	27
HS <sup>-</sup>	0.00	0.00	0.1	0.1	0.1	0.1	0.01
Total Dissolved Solids (TDS)	2.98	34,972	264,018	40,703	646	414	600

## 2.6 Future Environmental Evolution

Future climate change is the main factor that will affect the evolution of the groundwater system at a GDF site over the next 1 Ma, a timescale relevant to safety assessment e.g. RWM (2017). The potential for dilute recharge water to flow to GDF-relevant depths owing to future glaciation needs to be considered. Were this to happen, bentonite erosion could be affected significantly. Potentially glaciation and deglaciation cycles could repeatedly change the groundwater conditions around the bentonite.

In contrast, plate tectonics and related processes (earthquakes, volcanism) are unlikely to affect the long-term evolution of a GDF significantly over this timescale because the UK lies in a stable continental setting on the passive continental margin of the Atlantic Ocean.

It follows that the likelihood of fault rupture at between 200 and 1000m depth in a GDF site is very low. However, were sufficiently large fault movements to occur they could affect groundwater flows in a GDF, even if the fault does not intersect the GDF. Such effects could be transient when the fault moves, but if the porosity and permeability of the fault and related fractures changed due to the rupture, there could be a permanent influence on groundwater flow. In more seismically active countries such effects have mostly been reported following earthquakes that are much larger than those typically recorded in the UK. Nevertheless, the largest recorded earthquake in the UK, which occurred in 1931, about 120 km offshore from eastern England had a magnitude of 6.1  $M_L$ . An earthquake of such a magnitude could potentially affect groundwater flow, depending upon where it occurred. Furthermore, seismicity caused by glacial loading and unloading in the future may be significantly greater than at the present. For these reasons, the possibility needs to be considered that transient changes in groundwater in a GDF could be related to fault rupture.

During the next 1 Ma, in the absence of anthropogenic forcing, there would be alternating glacial and interglacial periods in cycles of between 100 ka and 150 ka (depending on the climate model), like those that are predicted to occur in the Nordic countries. Without this forcing, the next interglacial maximum is expected to occur at around 100 ka, after which continental ice will rapidly melt, leading to an interglacial minimum (RWM, 2017) However, taking anthropogenic forcing into account, the onset of the next glacial period will be delayed by approximately ~50-70 ka. In this case, the first major northern hemisphere glaciation is estimated under these models to occur between about 170 and 180 ka (RWM, 2017). However, there is considerable uncertainty, not least caused by the rate at which anthropogenic CO<sub>2</sub> emissions change in the next few decades.

As in the Nordic countries, in the UK glaciation and deglaciation will cause isostatic subsidence and uplift respectively. Present uplift in the north of the UK and subsidence in the south, together with seismicity in the UK, are driven largely by glacio-isostasy.

## 2.7 Key Issues for Bentonite Piping and Erosion

The key differences between the geosphere conditions of relevance to bentonite piping and erosion in a UK GDF and repositories in Sweden and Finland are:

- The Swedish and Finnish repositories are both in a “HSR to surface” environment (using current RWM generic GDF environment terminology). There are no sedimentary cover rocks at either the Swedish or Finnish site that could influence groundwater flows or groundwater chemistry.

- In the UK, LSSR is being considered as a generic host rock. In such a host rock, piping and erosion of bentonite would not be possible owing to the very low hydraulic conductivity of the LSSR and lack of conductive fractures within it.
- The maximum groundwater salinities that might occur in a UK GDF site are much higher than the maximum groundwater salinities that occur in the Swedish and Finnish sites. It is plausible that at a UK GDF site, maximum salinities approaching halite saturation could be encountered (ionic strength around 6M at 25°C). If such highly saline waters were to occur at a UK GDF site, appropriate research and development would need to be undertaken to ensure that engineered barriers are adequately matched to the environment.
- Relatively steep salinity and groundwater chemical gradients are possible in or near a GDF in the UK. These gradients could be steeper than those encountered at the Swedish and Finnish repository sites. At a UK GDF site consideration needs to be given to the possibility that the salinity gradients could change and / or move in response to climatic changes and related processes (e.g. isostasy). Thus, in future bentonite might be exposed to temporally changing groundwater chemistry and salinity, the latter possibly being much higher or much lower than at the time of bentonite emplacement.
- Depending upon a UK GDF's location, the geothermal gradient could be higher than that at either Forsmark or Olkiluoto. Maximum temperatures at the depth of bentonite emplacement in a UK GDF could be substantially higher than at either Forsmark or Olkiluoto. At Forsmark the geothermal gradient is about 10°C/km at 300 m depth and about 13°C/km at 700 m depth, with the temperature at repository depth of c. 500 m being about 11°C (Sundberg et al., 2008). Similarly, at Olkiluoto, the geothermal gradient is around 14°C/km and at the repository depth of 400 m temperatures are around 10°C (Sedighi et al., 2014). In contrast the mean geothermal gradient in the UK is 26°C/km, but may reach 60°C/km. Furthermore, at the present generic stage, the UK GDF programme is open to the possibility that waste could be emplaced at depths up to around twice the depths planned for waste emplacement at Forsmark or Olkiluoto. Therefore, natural temperatures at which bentonite may be emplaced in a UK GDF could plausibly be up to 40°C to 50°C.
- The characteristics of the host rocks at a GDF location could also influence the temperature evolution of the bentonite due to radiogenic heating by the wastes in the first few thousand years after GDF closure. For example, HSR may have thermal conductivities in the range 2.2 Wm<sup>-1</sup>K<sup>-1</sup> to 3.8 Wm<sup>-1</sup>K<sup>-1</sup>, while LSSR may have thermal conductivities in the range 0.62 Wm<sup>-1</sup>K<sup>-1</sup> to 3.2 Wm<sup>-1</sup>K<sup>-1</sup> (Metcalf et al., 2015).

## 3 Mechanical erosion

### 3.1 Objectives

The properties of buffer and backfill in a future repository are to great extent depending on the installed dry density. Water flowing into the repository will affect the different bentonite components both in conjunction with the installation but also after closure and the following water saturation. Flowing groundwater can result in a redistribution of the installed bentonite material within the repository area but can also transport material out from the repository e.g. to adjacent tunnels. This may result in local regions with lower density than intended.

This review of mechanical erosion has focused on three topics (see Wood Proposal Ref: CRM149197):

1. **Performed erosion tests.** A review of several tests performed with the objective to determine erosion of bentonite at different conditions has been made. The methodologies, the results and the interpretation of results are all important aspects of such tests.
2. **Utilisation of erosion data.** Erosion data have been used for the definition of tightness requirement of tunnel plugs. For this type of calculations, it is important to have an erosion model to translate the acceptable mass loss to an acceptable water volume passing through a deposition hole to define a leakage requirement on the plug.
3. **Development of conceptual understanding.** For example, the stability of erosion channels and the hydrochemical mechanisms behind such channels, the erosion potential which corresponds to the formation of stable channels and the time scale of water saturation for system hydrated through erosion channels.

Another important objective has been to identify gaps in the existing knowledge e.g. how high temperatures, > 100°C, influence the erosion of bentonite.

### 3.2 Method

A review of the present knowledge regarding mechanical erosion of bentonite has been made by performing a literature study. Reports and articles have been found by searching in different data bases. A compilation of the reports and articles included in the study is provided in Table 3-1.

The review has been used to reveal the processes that are governing piping and erosion and to identify parameters and variables that affect these processes. An attempt has also been made to grade the influence of the variables and parameters on the different processes and to grade the knowledge and understanding of the governing processes. The results of these investigations have been used to identify gaps in the knowledge of piping and erosion.

### 3.3 Definition of piping and mechanical erosion

#### 3.3.1 Mechanical erosion and chemical erosion

A review of the present knowledge regarding mechanical erosion of bentonite material has been undertaken. During the work, it has been noted that there is some conceptual confusion between “mechanical erosion” and “chemical erosion”. In this report we define chemical erosion to occur at the release of bentonite colloidal suspension, which is produced when the material is exposed to very low salinity water. Mechanical erosion is defined to take place when the drag force on the clay particle from the water movement is higher than the sum of the friction and attraction forces between the particle and the clay structure.

#### 3.3.2 Piping

Piping is defined by Börgesson et al. (2015). The following text is taken from that report.

If water inflow into a repository, deposition hole or deposition tunnel, is localised to fractures that carry more water than the swelling bentonite can absorb, there will be a water pressure in the fracture acting on the buffer. Since the swelling bentonite initially has a very low density (a gel), which increases with time as the water goes deeper into the bentonite, the gel may be too soft to stop the water inflow. The results from such a scenario, may be piping in the bentonite, formation of a channel and a continuing water flow and erosion of soft bentonite gel. There will be competition between the swelling rate of the bentonite and the flow and erosion rate of the buffer.

*Piping* will take place and the pipes remain open if the following three conditions are fulfilled:

1. The water pressure  $p_{wf}$  in the fracture, when water flow is prevented, must be higher than the sum of the counteracting confining pressure from the clay and the shear resistance of the clay.
2. The hydraulic conductivity of the clay must be so low that water flow into the clay is sufficiently retarded to keep the water pressure at  $p_{wf}$ .
3. There is a downstream location available for the flowing water and the removal of eroded materials for the pipe to stay open.

Piping probably only occurs before complete water saturation and homogenisation since the swelling pressure of the buffer material after homogenisation is high and the hydraulic gradient in the rock after re-establishment of original water pressure will be low. The consequence of piping will be a channel and outflow of water to dry or unfilled parts of the repository. Since the clay swells the channel will reduce in size with time but, on the other hand, erosion will counteract and abrade bentonite particles and thus increase the size of the channel. There is thus a competition between swelling clay and eroding clay. If the inflow is low and the increase in water pressure slow the pipe may seal before water pressure equilibrium has been reached.

Results from different investigations indicate influence of several factors on the piping process such as geometry, water inflow rate and rate of water pressure increase. The type of bentonite and the degree of water saturation will also have an impact on the occurrence of piping.

After water saturation of the repository and re-establishment of the hydraulic gradients, piping is not judged to be an issue.

### **3.3.3 Mechanical erosion**

Water flowing in a channel through bentonite after piping had occurred, may result in *erosion* of bentonite. Erosion will take place if the drag force on the clay particle from the water movement is higher than the sum of the friction and attraction forces between the particle and the clay structure. The detached bentonite particles will follow the water flow either out from the repository area or to another place within the repository (internal erosion). It is very difficult for the bentonite to stop the water inflow before water pressure equilibrium has been reached and the swelling bentonite has sealed the pipe.

The erosion process is largely dependent on the water inflow rate, the number of inflow points, and the inflow rate to other parts of the repository. For example, a tight tunnel end plug will efficiently decrease internal erosion since the hydraulic gradients within the repository will decrease very fast. Other important factors influencing the erosion process are: the bentonite properties and the water chemistry.

## **3.4 Summary of studied reports**

This report has reviewed several reports where investigations of piping and erosion processes have been made. A compilation of the reports is provided in Table 3-1 together with information regarding the content i.e. if laboratory tests are included, description of processes, modelling or scenario descriptions. A compilation of the most important results and conclusions made in the reports is provided in section 3.4.1 to 3.4.17.

**Table 3-1 Compilation of reports**

Report	Laboratory tests	Process descriptions	Modelling	Scenario descriptions
<b>Asensio et al. 2018.</b> Salinity effects on the erosion behaviour of MX-80 bentonite: A modelling approach.			Modelling pinhole tests described in (Laurila et al. 2013).	
<b>Börgesson and Sandén, 2006.</b> Piping and erosion in buffer and backfill materials. Current knowledge.	Review of earlier performed tests.	Piping and erosion		Piping and erosion in buffer and backfill.
<b>Börgesson et al. 2005.</b> Studies of buffer behaviour in KBS-3H concept.	Small scale piping/erosion/sealing tests			Scenarios concerning the KBS-3H design
<b>Börgesson et al. 2015.</b> Consequences of water inflow and early water uptake in deposition holes. EVA-project.	Piping, erosion, water flow in pellet filling, self-sealing, formation of gel-pockets, ability to stop piping	Review of several processes and parameters influencing piping and erosion	Water absorption rate, piping, erosion, sealing. Inflow scenarios.	Water inflow and water uptake, erosion consequences
<b>Halonnen and Adesola, 2020.</b> Downscaled Tests on Buffer Pellet Behaviour in Steel Cells.	Erosion tests on pellet fillings			
<b>Johannesson et al. 2010.</b> Characterization of backfill candidate material, IBECO-RWC-BF. Baclo Project-Phase 3.	Piping and erosion on block and pellets.	Healing ability.		
<b>Karnland et al., 2009 a.</b> Long term test of buffer material at the Äspö Hard Rock Laboratory, LOT project. Final report on the A2 test parcels.	Laboratory investigations on bentonite exposed for high temperature in field tests.			
<b>Karnland et al. 2009 b.</b> Long term test of buffer material at the Äspö HRL, LOT project. Final report on the A0 test parcel.	Laboratory investigations on bentonite exposed for high temperature in field tests.			
<b>Laurila et al. 2013.</b> Current Status of Mechanical Erosion Studies of Bentonite Buffer.	Free swelling, erosion: pinhole tests and simulated deposition hole	Review of several processes and parameters influencing piping and erosion	Empirical modelling of swelling, erosion in pinhole tests	

<b>Report</b>	<b>Laboratory tests</b>	<b>Process descriptions</b>	<b>Modelling</b>	<b>Scenario descriptions</b>
<b>Leupin et al., 2014.</b> Montmorillonite stability under near-field conditions. Technical Report 14-12. Nagra.	Laboratory investigation on bentonite exposed for high temperature.	Theoretical review of alteration and transformation processes that may affect the bentonite.		
<b>Navarro et al. 2016.</b> Swelling and mechanical erosion of an MX-80 bentonite: Pinhole test simulation.			Swelling and erosion. Simulating pinhole tests described in (Laurila et al. 2013).	
<b>Pintado et al. 2013.</b> Downscaled tests on buffer behaviour.	Mock-up tests simulating buffer behaviour during early saturation.			
<b>Sandén and Börgesson, 2008.</b> Deep repository Engineered barrier system. Piping and erosion in tunnel backfill. Laboratory tests to understand processes during early water uptake.	Piping and erosion on block and pellets. Healing ability.			
<b>Sandén et al. 2008.</b> Deep repository Engineered barrier system. Erosion and sealing processes in tunnel backfill materials investigated in laboratory.	Piping and erosion on block and pellets. Healing ability.	Piping and erosion.	Modeling erosion.	
<b>Sandén and Börgesson, 2010.</b> Early effects of water inflow into a deposition hole.	Piping and erosion tests, water flow in pellet filling	Piping and erosion		Effects of water inflow into a deposition hole.
<b>Suzuki et al. 2013.</b> Experimental investigation of piping phenomena in bentonite-based buffer materials for an HLW repository.	Piping and erosion on block and pellets. Pinhole tests.			
<b>Wilson J, Bond A, 2016.</b> Impact of elevated temperatures on bentonite buffers.		Theoretical review and modelling of alteration and transformation processes.		
<b>Åkesson M, 2012.</b> Temperature Buffer test. Final report. SKB TR-12-04.	Laboratory investigations on bentonite exposed for high temperature in field tests.			
<b>Åkesson et al. 2012.</b> Temperature Buffer test. Hydro-mechanical and chemical/mineralogical characterizations.	Laboratory investigations on bentonite exposed for high temperature in field tests.			

### 3.4.1 Salinity effects on the erosion behaviour of MX-80 bentonite: A modelling approach (Asensio et al., 2018)

#### **Overall description**

Pinhole tests (Laurila et al., 2013) with different salinity of the eroding water have been modelled in order to study if the influence of the salt concentration in the water can be modelled. Two different models were used: a hydro-mechanical formulation with a constant erodibility coefficient and a hydro-chemo-mechanical formulation with an erodibility coefficient dependent on salinity. In the latter approach the expansive behaviour of bentonite is a function of salinity, which will affect how it is eroded. The aim was to assess the feasibility of these two modelling approaches.

The models were implemented in COMSOL and solved in a coupled manner. Both models used an erosion model derived by Navarro et al. (2016). It is a mechanical erosion model that links the bentonite mass loss to the shear stress exerted by a water flow. The rate of mass loss per unit area  $\dot{m}_B$  (kg/m<sup>2</sup>/s) is calculated with the following expression:

$$\dot{m}_B = k_e \max(\tau_Q - \tau_C, 0) \quad (1)$$

where  $\tau_Q$  is the hydraulic shear stress produced by the water flow,  $\tau_C$  is the critical shear stress at which the mass removal starts, and  $k_e$  is the erodibility coefficient, which is a property of the material being eroded.

The erodibility coefficient in the hydro-mechanical model was calibrated to yield good results for the different salinities regarding the normalised cumulated mass loss. One coefficient was used for low salinity (0 and 10 g/l) and one for high salinity (35 and 70 g/l). The agreement with measurements were good for low salinity, but the very high erosion rate in the beginning of the test and the strongly reduced erosion rate at the late phase of the high salinity tests were not captured.

In the hydro-chemo-mechanical model the same erodibility coefficient was used as in the low saline water, but in this model the influence of the salinity was captured by the swelling model, with a faster swelling for higher salinity. The results of this model were similar to the results of the hydro-mechanical model, but the change in erosion rate with time was slightly better captured, although not adequately.

The conclusion of the results was that the erosion phenomenon is strongly coupled with hydro-chemo-mechanical effects, which highlights the importance of having an accurate coupled deformability model and using a multi-physics approach to analyse such processes.

#### **Comments**

As noted in the conclusions of the study it shows that the influence of the chemistry on the swelling rate is important in order to model the erosion with water flowing through a circular hole in bentonite adequately. Unfortunately, the results do not include an analysis of the change in hole radius as described in the article by Navarro et al. (2016).

### **3.4.2 Piping and erosion in buffer and backfill materials (Börgesson and Sandén, 2006)**

#### ***Overall description***

This is a brief report summarising the present knowledge of piping and erosion processes, describing the results from relevant tests.

#### ***Comments***

Three types of laboratory tests are described:

1. Small scale piping erosion tests. The main purpose of the tests was to find the levels of water pressure and water flow at which the bentonite is sealed, and the water flow is prevented.
2. Sealing tests in scale 1:10 simulating a KBS-3H repository.
3. Large scale sealing tests simulating a KBS-3H repository.

Some example of important conclusions and observations based on the results from the laboratory tests are listed below:

- Pellet filling or bentonite gel does not have high enough resistance to piping unless the water pressure is very low or the geometry favourable.
- It takes a long time (several years) until a swelling pressure is high enough to withstand the expected high-water pressures in fractures. This means that for the installation phase that process will probably not be able to stop piping and erosion.
- Once an open pipe that leads water (water-conducting pipe) has been formed it is very difficult for the bentonite to stop the water flow. It requires either that the flow temporarily is stopped so that the bentonite has time to swell and seal or that both the flow rate and the rate of increase in water pressure are slow enough.

### **3.4.3 Studies of buffer behaviour in KBS-3H concept (Börgesson et al., 2005)**

#### ***Overall description***

The report describes mainly laboratory tests that are specific for the KBS-3H design. However, one chapter describes piping and erosion tests at the small scale. These tests were performed on highly compacted MX-80 bentonite blocks with the diameter 50 mm and the height 120 mm.

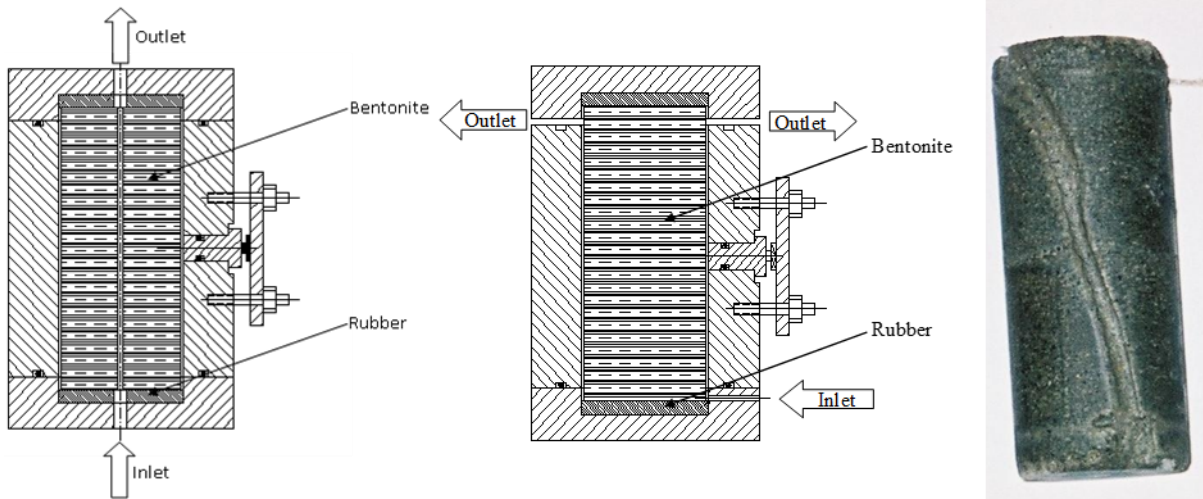
Two types of “pin-hole” like tests were performed. In one test type water was allowed to flow in a 0.5 mm slot between the block and the steel tube confining the block. In the other test type the water was led through a hole (2 or 4 mm in diameter) in the centre of the block. Altogether 42 tests were made. The variables were

- Different constant flow rate with measurement of water pressure
- Different constant water pressure with measurement of flow rate
- Different water composition

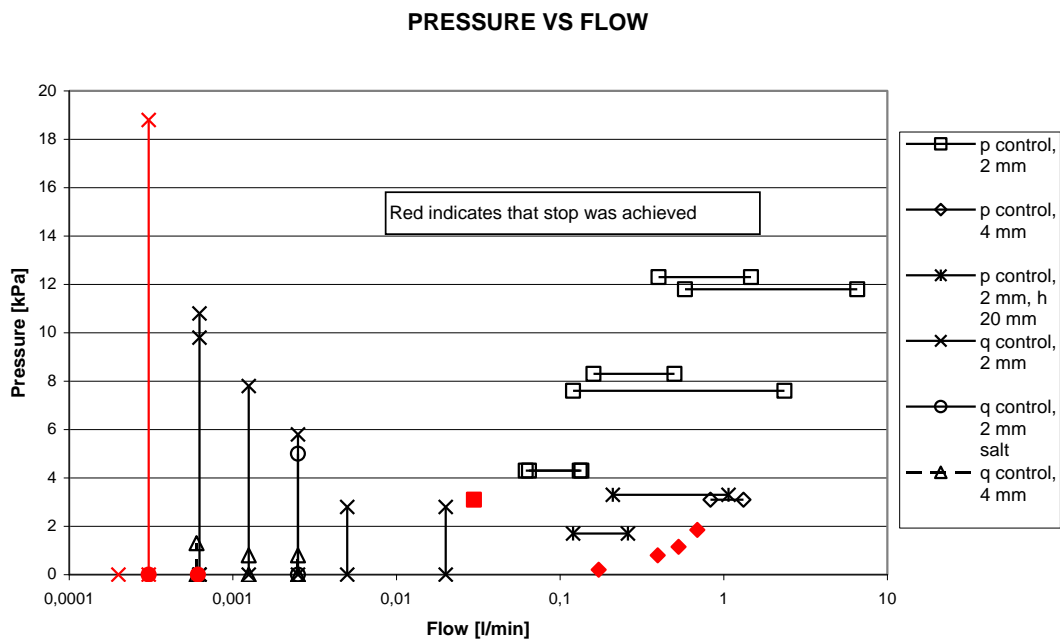
In some tests, measurement of the eroded mass in the outflowing water was made.

Figure 3-1 shows the set-up of the tests and an example of an erosion channel.

Figure 3-2 shows a compilation of results plotted as the applied or measured water pressure as a function of the applied or measured water flow rate. The results with flow rate  $<0.02$  l/min are derived from tests with applied constant water pressure and measured flow rate, while the results with higher flow rates are derived from tests with constant flow rate and measured water pressure. The results marked in red are from tests where the flow stopped due to sealing of the channel.



**Figure 3-1** Devices for the two types of tests and an example of erosion channel formed in the device with flow along the periphery.



**Figure 3-2** Example of results with the applied or measured water pressure as a function of the applied or measured water flow rate. Red symbols indicate when the flow was stopped.

## **Comments**

Several conclusions and comments were derived from the results of the laboratory tests. The two most important conclusions are:

1. Very low water pressure is sufficient to cause piping and erosion at constant water pressure (2-4 kPa).
2. Very low water flow rate is sufficient to cause piping and erosion at constant water flow rate (less than 0.001 l/min).

### **3.4.4 Consequences of water inflow and early water uptake in deposition holes. EVA project (Börgesson et al., 2015)**

#### **Overall description**

This report describes the results of a comprehensive project that has included both laboratory experiments, considering a review of the different processes influencing piping and erosion, and a description of the status regarding modelling of mechanical erosion. The report also includes a scenario description, describing the evolution of the hydraulic and mechanical processes in the bentonite in a deposition tunnel in the time period from the installation until the end plug takes all the water pressure.

#### **Laboratory tests**

Many tests have been performed with the purpose to investigate piping, erosion, sealing ability, self-sealing of piping channels and sealing of fractures in the rock. Additional processes that have been observed and which may be detrimental for the buffer is the formation of water or gel filled pockets in a pellet filling and following outflow of bentonite gel. These are processes that could be very damaging since the amount of bentonite that is transported away is much larger than by ordinary erosion.

#### **Modelling of mechanical erosion**

A conceptual model describing piping, erosion and sealing in a repository is described. This model is based on many erosion tests but entirely empirical and was at first presented in Sandén and Börgesson, (2010).

The model says that the eroded mass depends on the total volume of eroding water that has passed the erosion channel. This has been investigated for other bentonite materials and follows the following relation:

$$m_s = \beta m_w^\alpha \quad (2)$$

where

$m_s$  = accumulated mass of eroded bentonite (g)

$m_w$  = accumulated mass of eroding water (g)

$\beta = 0.02-2.0$  = parameter defined by the level of erosion at a certain accumulated water flow

$\alpha = 0.65$  = parameter defined by the inclination of the straight-line relation plotted in a log-log diagram

The results reported, indicate that for upwards water flow, the range of  $\beta$  is between 0.02 and 2.0. The total amount of eroded material can thus be estimated if the total volume of eroding water is known.

It should be noted that this expression does not take the pipe length into consideration but considers only the erosion in the deposition hole and not in the backfill.

The work estimates erosion from the deposition holes in the planned repository at Forsmark using the modelling of water inflow distribution in all deposition holes and deposition tunnels.

### Process model

An attempt to model the erosion is also presented in this report. The model is (as the other models described) based on flow in a cylindrical pipe. It includes that there is a “competition” between some processes that tend to increase the diameter of the pipe and some processes that tend to decrease the diameter. Mechanical erosion of bentonite particles from the walls by the shear forces caused by the flowing water in the channel leads to an increase in pipe diameter. The swelling of the bentonite by the water uptake leads to a decrease of the pipe diameter. The model also includes possible sedimentation of the eroded bentonite. Figure 3-3 illustrates the processes.

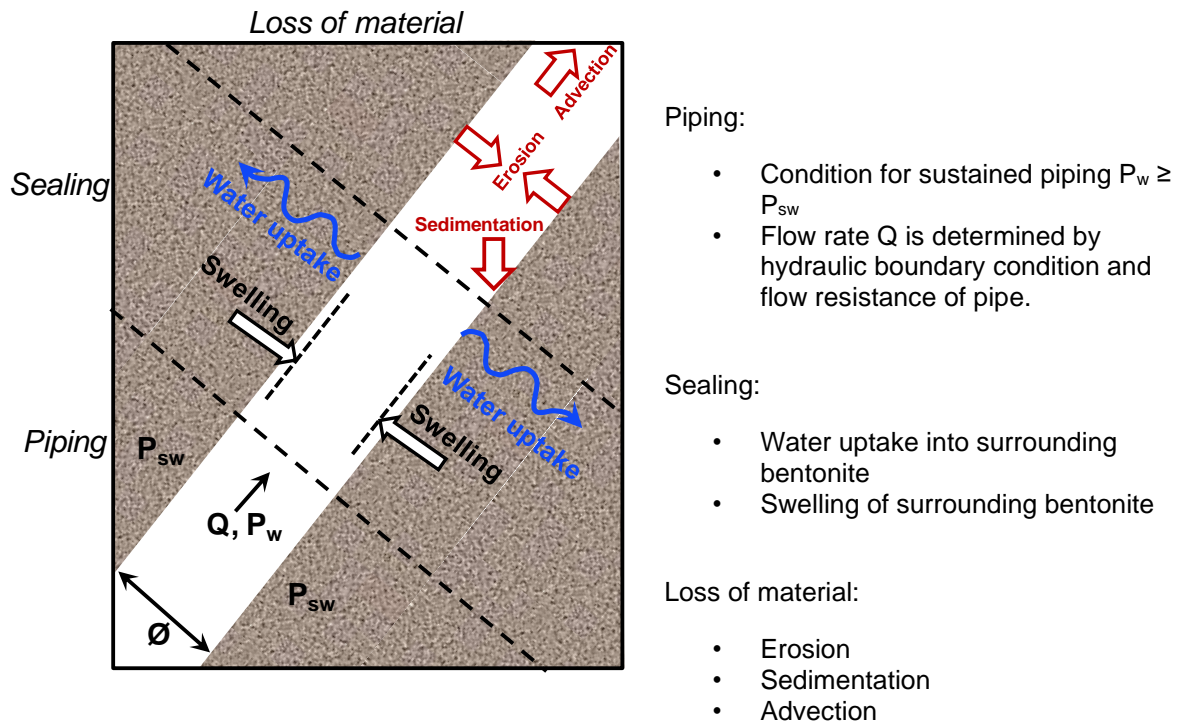


**Figure 3-3 Schematic illustration of piping, sealing and loss of material.**

However, the theoretical basis for the model includes additional considerations. The model includes an influence of the water pressure in the pipe that counteracts swelling. It includes an influence of the clay concentration in the flowing water on the erosion rate. Also, the swelling was not based on traditional water uptake/swelling processes but on a radial density profile relation between the pipe radius (initial and current), the dry density (initial and at the pipe wall), the amount of lost material, and a (time-dependent) radius representing a saturation front.

The modelling was performed with the MathCad software.

## Comments

Important conclusions from the presented work were:

- The erosion follows the suggested empirical model describing the erosion rate as a function of the accumulated amount of eroding water.
- Piping and subsequent erosion will occur and be maintained until the water pressure gradient is located at the plug and the flow rate out from the backfill is lower than  $10^{-4}$  l/min. This flow rate is chosen since the process studies show that at lower flow rates the flow channels will be self-sealed, and piping and erosion will stop. This means that piping and erosion may continue at least during the lifetime of the plug i.e. 100 years, since the plug is not expected to have a lower leakage rate.
- Self-sealing of fractures in the plug or the rock will not occur. This is a pessimistic assumption based on that no real proof of sealing of fractures has been derived.
- Erosion channels with limited radial extension (1-2 cm) will be sufficiently healed, in order not to have a major influence on the hydraulic properties of the bentonite, when stagnant water pressure has been established.
- Formation of water or gel pockets may occur at low inflow rates.
- The process model maps out a promising way to model the erosion processes. However, there is no comparison with measured data, but only references to measured trends. In addition, the model described is incomplete and needs to be further developed. Such a development has been performed for Posiva, but the results are not reported in referable publications.

The results from the modelled inflow distribution at Forsmark were used in scenario analyses. The following basic presumptions were used in the scenario analyses:

- The analyses have considered the time span up to 100 years after closure of a deposition tunnel, except for the analyses of the effect of a malfunctioning plug where longer times also have been considered.
- The erosion damages have pessimistically been assumed to be located at the inflow point where all eroded material has been lost
- The following allowable loss of dry bentonite mass has been assumed:
  - Buffer in a deposition hole: 100 kg
  - Backfill in a deposition tunnel: 1 000 kg

Since a leakage through the plug and the rock is inevitable such scenarios have also been studied. The scenario analyses yielded the following conclusions regarding the influence of leakage through the plug and the rock:

- At a leakage less than 0.1 l/min all combinations of inflow rates into deposition holes and tunnel are acceptable for the buffer if the inflow rate into separate deposition holes are less than 10% of the inflow into the deposition tunnel.

- At a theoretical leakage less than 1.0 l/min all combinations of inflow rates into the deposition holes and tunnel are acceptable if the inflow rate into separate deposition holes are less than 10% of the inflow into the deposition tunnel except for if the inflow rate into the hole higher than 0.01 l/min.
- At a plug leakage higher than 0.1 l/min there may also be significant erosion damage in the backfill.

Some scenarios with a non-functioning plug were also studied. The conclusions of these studies were that there are cases when no requirements on the plug tightness are needed but also that this largely depends on the time to resaturate the repository.

### **3.4.5 Downscaled tests on buffer pellet behavior in steel cells (Halonen and Adesola, 2020)**

#### ***Overall description***

The report describes four erosion tests performed on pellets. The tests were performed in large test cells, diameter 350 mm and height 800 to 900 mm. The pellets were made of MX-80 and the water had a salinity of 10 g/l (6.47g NaCl: 3.53 g CaCl<sub>2</sub>). The flow rate was varied between 0.002 and 0.1 l/min.

#### ***Comments***

In the two tests with lowest flow rate, 0.002 and 0.01 l/min, no erosion was detected during the test time. Depending on the low flow rates, the bentonite had time to swell and seal which resulted in that a counter pressure was built up (0.01 l/min).

An average erosion rate of 0.4 g/litre was measured in the two tests over the test period when using a flow rate of 0.1 l/min.

### **3.4.6 Characterization of backfill candidate material, IBECO-RWC-BF. (Johannesson et al., 2010)**

#### ***Overall description***

The report describes the results from a comprehensive characterization of a bentonite material, IBECO-RWC-BF. The work includes several different investigations: block manufacturing, determination of geotechnical parameters (compressibility, evaluation of elastic parameters, block strength, compression properties of unsaturated pellet filling, swelling pressure, hydraulic conductivity). Of significant interest for this report are the erosion tests and self-healing tests performed on both blocks and pellets.

#### ***Comments***

- The erosion rate is higher for the blocks compared to pellets.
- Interesting results were observed when performing tests with low water flow rates (0.01 l/min):
  - Block tests. All water was adsorbed by the blocks that started to swell. After 24 hours, no water had left the test setup and depending on the swelling it was not possible to continue the tests.
  - Pellet tests. In some tests, a resistance to water flow was built up and sealed the bentonite which resulted in separation and that the water pressure started to act

on a “wall” of bentonite. This is a phenomenon that have been observed also in other investigations, see e.g. Börgesson et al. (2015).

**3.4.7 1: Long term test of buffer material at the Äspö Hard Rock Laboratory, LOT project. Final report on the A2 test parcels. (Karnland et al., 2009a)  
2: Long term test of buffer material at the Äspö HRL, LOT project. Final report on the A0 test parcel. (Karnland et al., 2009b)**

***Overall description***

The LOT test series can be described as a multi-task experiment in which relatively small test parcels are exposed to field conditions. The test series include in total seven test parcels of which three have been exposed to conditions similar to those in a KBS-3 repository and four parcels have been exposed to conditions with accelerated alteration processes (increased temperature).

These reports describe the dismantling of the field test A0 and A2. After dismantling, several laboratory investigations were performed on the material.

No erosion tests have been performed in the LOT project. The reason for including the reports here is that some bentonite parcels have been exposed to high temperatures over a significant time.

***Comments***

The bentonite in Test A0 and A2 was exposed to maximum temperatures between 130-150° closest to the heater. The test duration was two and six years respectively. The main objective with the test series was validation of buffer performance after water saturation e.g. regarding swelling pressure, hydraulic conductivity and rheological properties. Another objective was to check existing models regarding buffer degrading processes, e.g. mineral redistribution and montmorillonite alteration.

Important results from the performed analyses can be summarised as follows:

- Redistribution of easily dissolved accessory minerals in the bentonite, in particular CaSO<sub>4</sub>
- No formation of illite or any other typical montmorillonite alteration minerals
- Diffusive transports of trace elements were in accordance with previous studies

An overarching conclusion was that the observed mineralogical alteration, as a consequence of the water saturation process and the exposure to high temperature, are small, and that this alteration did not change the physical properties to such an extent that the buffer function is jeopardised.

**3.4.8 Current status of mechanical erosion studies of bentonite buffer (Laurila et al., 2013)**

***Overall description***

This is a comprehensive report describing the knowledge regarding mechanical erosion of bentonite. The report includes a description of different parameters and processes affecting erosion but also results from laboratory experiments. A description of the status regarding modelling of mechanical erosion is also provided.

## Laboratory tests

The laboratory tests were in general focused on the Finnish concept for a final repository i.e. regarding bentonite materials, densities and salinity concentrations.

The laboratory tests can be divided into three parts:

1. Free swelling tests. Compacted bentonite blocks had access to water with different salinity. The bentonite could only swell in one direction.
2. Erosion tests (pinhole). Tests were performed using compacted blocks with a central hole. A constant water flow, 0.1 l/min in all tests, was applied through the hole. The tests were performed using blocks manufactured of both MX-80 and Friedland clay. In total fifty tests were performed. The parameters varied were e.g. the length of the test cell, the diameter of the hole and the salinity of the water.
3. Erosion tests (block/pellets). These tests are reported in Pintado et al. (2013) and are only briefly described in this report. The test design simulates a deposition hole with a central block stack and pellets filling up the gap between block and the test cell wall. A constant water flow was applied in the bottom and the piping and following erosion was studied/measured.

## Modelling of mechanical erosion

Efforts were made to model the pinhole test results with a combination of a simple swelling model and a simple erosion model. The swelling model was based on a density dependent diffusivity model with two constants, the swelling diffusivity  $D_s$  and a friction factor  $F_c$  that opposes swelling. These constants were calibrated with results from one-dimensional swelling tests for different salinities of the water. The erosion model was similar to the model by Asensio et al. (2018) and Navarro et al. (2016) with a constant erodibility constant  $E_s$ . This constant was calibrated by the pinhole tests using the calibrated swelling constants. The model was solved using the COMSOL Multiphysics FEM solver software. The results were also compared to the power law model with a double logarithmic relation between the total mass of eroded mater and the total volume of water flow through the channel described by Börgesson et al. (2015).

They concluded that the data are not sufficient to determine the usefulness of the model and that more research is needed both experimentally and from a theoretical basis to provide better confidence in the approach.

## Comments

The report is written several years before the two modelling articles by Asensio et al. (2018) and Navarro et al. (2016), and the model presented in the report thus less developed.

### 3.4.9 Montmorillonite stability under near-field conditions. (Leupin et al., 2014)

#### Overall description

This report describes the knowledge regarding potential alteration of bentonite by focusing on experimental and modelling results under thermal conditions. To complement the findings in the literature review of published studies, three sets of experiments were also performed to study potential changes to the safety relevant properties of bentonite during the high temperature of a repository.

The conclusion was “*Based on the review and additional studies performed, it can be concluded that the swelling pressure and the hydraulic conductivity, which are important safety function indicators for clay barriers, are not expected to be significantly affected by the thermal transient that will occur in the discussed repositories.*”

### **Comments**

This is a comprehensive report where a thorough review has been made regarding the thermal stability of montmorillonite. The first part of the report is a literature review focusing on the transformation of montmorillonite to a non-swelling clay mineral illite. The laboratory studies focus on potential changes to the safety relevant properties of bentonite during the high temperature of a repository.

#### **3.4.10 Swelling and mechanical erosion of an MX-80 bentonite: Pinhole test simulation (Navarro et al., 2016)**

##### **Overall description**

Several pinhole tests (Laurila et al., 2013) have been used to test a model developed for modelling erosion and swelling of highly compacted MX-80 bentonite with an initial water content of 17%. These are the same tests used in the modelling article described in section 3.4.1 (Asensio et al., 2018). The loss of mass at the water-soil interface is described by means of a simplified erosion model, assuming the “instantaneous” activation of erosion, which is the same erosion model as was used as in the article by Asensio et al. (2018). A double-porosity formulation was adopted based on the Barcelona Expansive Model to describe the deformability of the bentonite. The model was implemented in the multi-physics partial differential equation solver Comsol Multiphysics (CM). Only tests with non-saline water were modelled.

##### **Conclusions from the tests**

According to the article: Satisfactory data fits were obtained by simulating a variety of pinhole tests on MX-80 samples of various configurations. Thus, although more experimental validation is needed, and the approach could be further improved (introducing, e.g., the effect of water salinity), the obtained results indicate that this method is a useful starting point for describing and quantifying the coupled erosion and swelling of MX-80 bentonites.

### **Comments**

Although the model, according to the article, simulates the measured erosion it is difficult to understand how a decreased value of the coefficient of bentonite erosion  $k_e$  can yield a decreased inner radius with time (sealing of the hole) and at the same time an increased erosion rate (Figures 11 and 12 in the article), or is there an error in Figure 12?

#### **3.4.11 Downscaled tests on buffer behaviour (Pintado et al., 2013)**

##### **Overall description**

The report describes two mock-up test series simulating deposition holes:

1. X-Boy. The test equipment was manufactured of steel. The simulated deposition hole had a diameter of 350 mm and a height of 800 mm. Two tests were performed, one with pellets in the gap between buffer blocks and the simulated rock and one without pellets. Both tests were performed using tap water and with a water flow rate of 0.1 l/min

2. Transu. The test equipment is manufactured of transparent PVC. The simulated deposition hole had a diameter of 269 mm and a height of 800 mm. Four tests were performed, two with pellets in the gap between buffer blocks and rock and two without pellets. All tests were performed with a water flow rate of 0.1 l/min. The water used in the tests were either tap water (one test) or water with a salinity of 1% (one test) or 3.5% (two tests).

### **Comments**

The test duration varied between one and four months. Erosion was measured continuously in all tests.

Some comments to the test results:

- The determined erosion rate varied between 0.14 g/l and 2.11 g/l.
- The lowest erosion rates were measured in tests performed with tap water and with no pellets in the gaps.
- The highest erosion rates were measured in tests performed with saline water and with a pellet filled gap.
- Higher erosion rates were observed when the water salinity was increased.

### **3.4.12 Piping and erosion in tunnel backfill. Laboratory tests to understand processes during early water uptake (Sandén and Börgesson, 2008)**

#### **Overall description**

The report describes the results from an investigation of erosion properties of both compacted blocks of Friedland clay and pellets manufactured of MX-80. The tests with pellets were made both using Plexiglas tubes but also a large slot ( $2 \times 1 \times 0.1$  m). In addition, tests have been made to study the sealing ability of a backfill material consisting of 30% bentonite and 70% crushed rock.

### **Comments**

- The erosion tests on blocks made of Friedland clay showed that the erosion rate was strongly depending on the water flow rate. The erosion rate decreased with time. The influence of water salinity on erosion was very clear. An increase of the salinity from 0 to 1%, increased the erosion rate by about five times.
- The pellets tests showed that at low flow rates, 0.001 l/min, the pellets have time to take up water and seal which results in a high flow resistance. At higher flow rates, the water is mainly flowing in one channel.
- The erosion tests on pellets showed that the erosion rate was high in the beginning but clearly decreasing with time. The effect of water flow rate and salinity in the water was obvious.

### **3.4.13 Erosion and sealing processes in tunnel backfill materials investigated in laboratory (Sandén et al., 2008)**

#### **Overall description**

This is a comprehensive report describing the results from investigations performed on backfill materials. The tests have focused on erosion of block and pellets, self-healing ability

of piping channels in different materials, and relative humidity induced swelling and cracking of compacted blocks. The report also includes a suggestion for an empirical model describing erosion of bentonite as function of the accumulated mass of eroding water.

### **Comments**

- The influence of fine material in a pellet filling was investigated. The results from these tests showed that the influence of fine material was strong in the beginning of the tests (if fine material was present, the erosion rate increased) but after 24 hours the erosion rate was the same in all tests.
- Erosion tests of pellets were performed in Plexiglas tubes with an inner diameter of 100 mm. The influence of salt in the water on the erosion rate was investigated. A high salt content (3.5%) resulted in fast swelling and sealing of pellets and in combination with low flow rates (0.01 l/min), a high flow resistance was built up and it was not possible to measure erosion in these tests. At higher flow rates (0.1 l/min) and a high salt content (3.5%), the erosion rate was very high during the first hours but after 24 hours the erosion rate was the same as in tests performed with water with a salt content of 1%.
- An erosion model based on erosion tests has been suggested. It assumes a linear relation between accumulated eroded material and accumulated water flow in a double logarithmic diagram. It includes two parameters:  $\alpha$  that corresponds to the inclination of the linear relation and  $\beta$  that determines the level of the accumulated erosion. See also sections 3.4.4 and 3.4.14.

### **3.4.14 Early effects of water inflow into a deposition hole (Sandén and Börgesson, 2010)**

#### **Overall description**

The report describes the results from laboratory tests simulating water inflow to a deposition hole after installation. Besides studying the heaving of the buffer, the wetting of pellets and buffer blocks, erosion measurements have also been performed. The report also includes results from erosion tests made in Plexiglas tubes on pellets and a long-term test where erosion of a pellet filling placed in a large vessel (inner diameter= 650 mm and height 1300 mm) was measured for four months. In addition, scenario descriptions regarding erosion of bentonite from a deposition hole are provided.

### **Comments**

Some important conclusions from the tests were:

- All results from the erosion measurements are well between the limits of the erosion model (see section 3.4.8).
- Erosion rate in vertical direction seems to be lower than in horizontal direction. The influence of gravity can be one explanation for this behaviour.
- The influence of test length on the erosion rate is still not known. There does not seem to be a proportional relation between test length and erosion rate.
- The decrease in erosion rate by time characterised by the empirical erosion model continued also in the long-term test (four months).

- The phenomena when a flow channel is sealed, and the water pressure starts to act on an “arch” of wetted pellets occurred in two of the tests. This is a phenomenon that needs to be further studied.

### **3.4.15 Experimental investigations of piping phenomena in bentonite-based buffer materials for an HLW repository (Suzuki et al., 2013)**

#### ***Overall description***

Laboratory investigation of piping and erosion properties. The tests were performed using equipment in two different scales. Small scale tests were performed in test cells where the diameter of the specimens was 110 mm and the height 50 mm. Corresponding figures for large scale tests were 50 mm diameter and a height of 1000 mm. Both test apparatuses were manufactured out of acrylic i.e. they were transparent which facilitated the evaluation of the tests.

The tests were performed using both pre-compacted blocks and pellets. The blocks were manufactured of a mixture of 70% Kunigel V1 bentonite and 30% silica sand, and the pellets with 100% Kunigel V1. The water used in the tests were either distilled or saline (0.5 M NaCl).

In total fourteen tests were made, ten in the small scale and four in the large scale.

#### ***Conclusions from the tests***

- Piping will occur in the gap between the test cell and the buffer material, block or pellets, if there is a water inflow of 0.1 l/min. The maximum water pressure during piping and erosion was below 100 kPa i.e. the swelling pressure after saturation could not be expected in the early stage of saturation, which could have prevented piping.
- The silica sand in the blocks settles in the piping channels and prevents the self-sealing of the bentonite i.e. the water pathways with high hydraulic conductivity might exist for a considerable time. This must be considered in the design and engineering as well as in the long-term assessment.
- Piping will not occur if the inflow rate is less than 0.001 l/min or if the gap is filled with bentonite by compaction or spraying methods.
- To protect against piping and erosion it will be necessary to either reduce the water inflow to less than 0.001 l/min or to stop the water movement within a deposition hole by using a temporary plug.

#### ***Comments***

Although these tests were made on a rather different material with lower swelling pressure than MX-80 the observations and conclusions were similar as those for MX-80.

### **3.4.16 Impact of elevated temperatures on bentonite buffers (Wilson and Bond, 2016)**

#### ***Overall description***

This report provides a review of the effect of heat on bentonite, specially, process of smectite illitisation and bentonite cementation phenomena including the effect of steam on bentonite properties. Models are then used to explore the potential for such processes to occur in a GDF

(Geological Disposal Facility) that includes bentonite and wastes with heat outputs that are representative of UK legacy wastes.

There are basically two main conclusions in the report:

1. According to the smectite illitisation models, it is difficult to see how illitisation (transformation of strongly swelling smectite into illite) could result in sufficient deleterious effects to a bentonite buffer to prevent it from performing its safety functions for disposal concepts and waste packages in the DSSC (Disposal System Safety Case).
2. While alteration itself does not appear to pose a threat to buffer performance, some alteration, most probably associated with silica cementation, seems likely. Silica cementation may be associated with illitisation, which releases silica, or it may result from other processes such as movement of water vapour (steam). The review has shown that even relatively short duration exposure to water vapour at elevated temperatures can result in dramatic loss of swelling pressure, and associated increase in stiffness. This is not entirely consistent with the conclusions made in (Leupin et al. 2014).

### **Comments**

The second conclusion is not in agreement with the conclusion drawn in the report by Leupin et al. (2014) as described in section 3.4.9.

### **3.4.17 1: Temperature buffer test. Final report (Åkesson, 2012). 2: Hydro-mechanical and chemical/mineralogical characterizations (Åkesson et al., 2012)**

#### **Overall description**

The Temperature Buffer Test (TBT) was a joint project between SKB and ANDRA, supported by ENRESA and DBE. The project aimed to improve the understanding and to model the thermo-hydro-mechanical behaviour of buffers made of swelling clay submitted to high temperatures during the water saturation process. No erosion studies were undertaken in this project but the effect of high temperature on the general properties and behaviour of bentonite was analysed.

One report gives a detailed description of the hydro-mechanical and chemical/mineralogical laboratory tests and the other gives a summary of all work performed within the TBT project.

### **Comments**

Example of conclusions from the performed laboratory tests are provided below:

#### *Hydro-mechanical analyses*

- A reduction in swelling pressure was observed on re-saturated specimens, especially on those from the innermost part
- A scatter but a tendency towards an increase in hydraulic conductivity of re-saturated specimens drilled from the innermost part was observed as well as a similar tendency of ground and re-compacted specimens and specimens prepared from dried material

- Triaxial tests: Brittle behaviour involving high stiffness, high shear strength, and low strain at failure, was seen on specimen from the inner part

#### *Chemical and mineralogical analyses*

- Sulfate was redistributed under the thermal and hydration gradients that were prevalent during the test. Anhydrite accumulated at some distance from the heater, whereas gypsum was dissolved in the peripheral parts of the buffer where water was supplied
- Cristobalite was dissolved at the bentonite/heater contact
- Calcite was dissolved in the warmest parts of the block
- Exchangeable sodium was replaced by calcium in the warmest parts, probably as an effect of calcite dissolution, which must have affected the porewater composition
- At the steel heater, the iron content of the bentonite was significantly increased due to corrosion of the steel.
- The distribution of non-exchangeable magnesium displayed a clear gradient with a distinct maximum at the heater, suggesting a transfer of magnesium along the thermal gradient.

Most of the observed chemical changes are limited to the accessory minerals in the bentonite (gypsum / anhydrite, cristobalite, calcite). However, the redistribution of magnesium may involve changes to the montmorillonite, but data are inconclusive and both the source and the sink of magnesium remain to be identified (Åkesson et al., 2012).

### **3.5 Evaluation of different laboratory tests on erosion**

#### **3.5.1 Test types**

Different types of laboratory tests have been performed in order to measure the erosion rate of bentonite pellet fillings, compacted bentonite blocks or a combination of block and pellets. In the tests, the bentonite has been exposed to different conditions regarding water flow rates, water salinity and geometry.

#### ***Pellet fillings***

Pellet fillings have mainly been tested with two different techniques:

##### **1. Plexiglas tubes.**

- a. Single tubes with different lengths (typically one meter) and diameter (typically 0.1 m inner diameter) have been filled with bentonite pellets. The tubes were equipped with endplates, one used to apply a constant water flow rate (point inflow) and the other with a leaking grid where the outflowing water could be collected. Examples of this test type are described in Sandén and Börgesson (2008), Sandén and Börgesson (2010), Sandén et al. (2008) and (Suzuki et al. (2013).
- b. Double tubes i.e. one with large diameter (0.29 m) and one with smaller diameter (0.2 m) with bentonite pellets between the tubes. With this design, a circular slot with a width of 0.045 m was formed. The slot simulated a pellet filled slot between bentonite blocks and rock walls in a deposition hole. The slot was filled with pellets and a water flow applied from one end of the tubes.

At the other end there was a leaking grid where the outflowing water was collected. Examples of this test type are described in (Börgesson et al. 2015).

2. **Large slot tests.** Equipment consisting of two Plexiglas walls mounted on a steel frame. The slot,  $2 \times 1 \times 0.1$  m, was open in one end. A constant water flow rate was applied at the middle of one wall and the wetting behaviour could then be studied. The water flowing out at the front was collected. Examples of this test type are described in Sandén and Börgesson (2008) and Sandén et al. (2008).

### **Compacted blocks**

Erosion of compacted blocks have been studied with three different techniques:

1. **Blocks placed in a groove.** Compacted blocks (brick size) were placed in a steel groove and a constant water flow rate was applied from one end by use of a tube. The water was flowing along the block surface (the steel groove was placed with an inclination of 1 %) and the outflowing water at the other end was collected. Examples of this test type are described in Sandén and Börgesson (2008) and Sandén et al. (2008).
2. **Blocks placed in a transparent PVC tube.**
  - a. The tube had an inner diameter of 269 mm. The blocks had a diameter of 210 mm i.e. there was an annular gap with a width of 29.5 mm. Examples of this test type are described in Pintado et al. (2013).
  - b. Small scale tests are described in Suzuki et al. (2013). The test cell had a diameter of 110 mm and height 50 mm. Tests were also performed in another test cell with a height of 1000 mm and an inner diameter of 50 mm.
3. **Pinhole tests.** In these tests, water is flowing through a small borehole (typically between 2 and 12 mm diameter) drilled through a compacted bentonite block. The outflowing water at the other end was collected. Examples of this test type are described in Börgesson et al. (2005), Laurila et al. (2013) and Suzuki et al. (2013).

### **Pellets and blocks (simulated deposition holes)**

Tests simulating downscaled deposition holes, including both buffer blocks and a pellet filled slot have been performed. In these tests, a point inflow was applied at the bottom of the simulated deposition hole, into the pellet filling. The water flowing out at the top was collected and the amount of eroded material determined. This test type has been performed both as a closed system with a tight lid at the top of the test device, see Pintado et al. (2013) but also with an open top simulating the situation immediately after installation, see Sandén and Börgesson (2010).

#### **3.5.2 Water flow rates**

The main parts of all erosion tests have been performed using water flow rates between 0.01 to 0.1 l/min. Few tests have been made at flow rates up to 1 l/min but due to practical problems to handle this large amount of water the test duration have only been a few hours, see e.g. Sandén and Börgesson (2008).

Tests have also been performed at lower flow rates, e.g. 0.002 l/min by Halonen and Adesola (2020), 0.001 l/min by Sandén and Börgesson (2010, 2008), and Suzuki et al. (2013). A few tests have been performed with flow rates as low as 0.0001 l/min but in these tests, it has not

been possible to measure any erosion, instead the water has been taken up by the bentonite that has swelled and sealed.

### 3.5.3 Water salinity

As mentioned in section 3.5.2, the groundwater salinity and composition i.e. the concentration and distribution of monovalent and divalent cations, is expected to be an important factor regarding erosion, and this has also been seen in many experiments.

Most test series have included tap water and water with different salinities. The salinity of the waters has been described in different ways in the reports:

1. Total Dissolved Solids, TDS i.e. g/l.
2. Concentration in mol.
3. Concentration in percent.

The salinities used in the tests have mainly been between 10 g/l and 35 g/l and in some case 70 g/l.

The solutions used have been composed of NaCl and CaCl<sub>2</sub>, either using only one of the salts or with different Ca<sup>2+</sup>:Na<sup>+</sup> mass ratios e.g. 1:1, 1:2. Several tests have been performed using a composition of 50:50, Na:Ca by weight.

### 3.5.4 Evaluation methods

The amount of eroded clay in the water flowing out from the test setups have been determined in different ways:

1. **Collecting effluent samples at decided intervals.** This method has been used when the flow rates have been rather high (an inflow rate of 0.1 l/min corresponds to 144 l/24 hours which means that it is difficult to collect all outflowing water). Samples have been taken at decided intervals depending on e.g. total test duration, daytime/night etc. The samples, approximately 1 litre in a glass jar, have been dried in 105°C for 24 hours (or more if needed) and the residue determined. The remaining mass has been corrected for salt present in the water. The method involves quite significant effort. An automatic sampling carousel has been used to collect samples outside office hours, see description in Laurila et al. (2013).
2. **Collecting all effluent.** When performing tests with low water inflow rates, < 0.1 l/min, it is possible to save all outflowing water (0.01 l/min corresponds to 14.4 l/24 hours) and then evaporate the fluid. However, it will be necessary to have access to several ovens.
3. **Collecting all effluent in sedimentation vessels.** The outflowing water is collected in sedimentation vessels, tentatively in three steps. The accumulated sediment is collected and dried at decided intervals. With this method, all eroded material is collected, which is favourable.
4. **Weighing and drying the residual sample mass.** The overall mass loss is determined by comparing the dry mass at installation with the mass after dismantling and drying. This is a method to ensure the reliability of the erosion measurements.

### 3.5.5 Comments

When performing erosion tests on bentonite, pellets or block, there are several important issues that must be addressed:

- **Evaluation method.**
  - When collecting effluent samples at decided intervals, the determined concentrations in the single samples are interpolated over the corresponding time period to calculate the accumulated amount of eroded material and present it as a function of the accumulated outflow. This interpretation must, however, be performed carefully to ensure any temporary changes in erosion rate can be properly captured.
  - The method to collect all effluent in sedimentation vessels has significant advantages to ensure all eroded material is collected. When using saline water, the sedimentation of bentonite is rapid, and it is possible to remove a significant proportion as a clear fluid. This means that only a minor volume of water must be evaporated. The method can advantageously be used in long term tests where the erosion rate is low.
  - Independent of the sampling method, it should be noted, that the calculated mass of eroded material must be compensated for the salt present in the evaporated water i.e. the sample must be weighed before and after drying, see also bullets below.
- **Water salinity.** It is important to compensate for the salt present in the water when determining the amount of eroded material. If a high salt content is used in the test, e.g. 35 g/litre, the mass of salt present in the vessel after evaporation of the water, can be much greater than the mass of the eroded bentonite. It is recommended to take samples of the water used in the test continuously, e.g. after mixing of a new batch, to check the salt content.
- **Determining the salt content.** In the performed tests, the salt content in the water has been determined by evaporating the water in an oven. When using NaCl in the water it is enough to have a temperature of 105°C. However, when using CaCl<sub>2</sub>, the water molecules are more significantly attached to the crystals and it is necessary to increase the evaporation temperature to 130°C. When drying samples with higher salinities, a surface layer of crystallised salt can be formed in the jar containing the water sample. This layer slows down the drying and longer drying durations will be necessary. In some cases, it will be necessary to mechanically break down the layer to make it possible to dry the sample completely. If the determined salt content is incorrect, the calculated amount of eroded material will be incorrect. The drying time can vary strongly depending on the amount of water, salinity and the capacity of the oven.

### 3.6 Parameters and variables influencing piping and erosion

In the reviewed reports, several parameters and variables influencing piping and erosion have been identified:

1. Bentonite material

- Density and water content
  - Montmorillonite content
  - Accessory minerals
2. Water composition
  3. Water inflow rate and water pressure increase rate at sealing
  4. Geometry
  5. Time
  6. Temperature

This section gives an overview of the different parameters and variables and their influence on piping and erosion.

### **3.6.1 Bentonite**

#### ***Material***

Bentonites with different origin and quality are available on the market. MX-80 bentonite is a reference material in the area of constructing final disposals for spent nuclear fuel and have therefore been used in many laboratory investigations. MX-80 is dominated by natural mainly sodium dominated montmorillonite clay, ~ 80% by weight. The main accessory minerals are e.g. quartz, tridymite, cristobalite, feldspars and muscovite/illite. Dispersed in distilled water the clay fraction (grain size < 2 µm) makes up around 80% (Karnland et al., 2006; Wilson et al., 2011).

#### ***Properties***

##### **Density and water content (degree of saturation)**

The properties of the bentonite depend both on the material i.e. mainly the montmorillonite content, but also on the density of the exposed bentonite and in what shape it is emplaced e.g. block or pellets.

The density and the water content of the bentonite has a large influence on the erosion properties. In bentonite blocks that have been compacted to high density, the cohesive and frictional forces in the bentonite material have increased, which results in higher shear forces being needed for detachment. Blocks that have been compacted with the optimal water content (the water content where the highest density is reached for a certain compaction pressure) have higher resistance against erosion. This depends probably on the low content of air-filled voids in the block i.e. the degree of saturation is high. Blocks that have been loosely compacted from dryer material (e.g. water content of 10%) will have a high content of air-filled voids. Low water content in compacted blocks will result in high suction which means that the wetting and following swelling will be faster which will increase the initial erosion.

Bentonite pellets are more vulnerable for erosion. In a pellet filling there are a lot of voids which are connected to each other, and where the water can flow initially. Another explanation for the higher erosion of pellets is that the exposed bentonite surface is large.

### **Montmorillonite content and accessory minerals**

The montmorillonite content is an important measure for characterising bentonite (Karnland, 2010). Both swelling pressure and hydraulic conductivity are strongly depending on the content of swelling minerals. Characterizations of bentonite material from piping channels has shown that preferentially montmorillonite particles are eroded while larger bentonite grains are enriched in the channel, see e.g. Börgesson et al. (2015). Montmorillonite is also expected to be relatively susceptible to detachment as it swells into the water in the channel.

The montmorillonite content is also important as it acts as a binding material when compacting bentonite to blocks. Tests have shown that blocks compacted with a material with a low montmorillonite content seems to be more sensitive to erosion.

According to Laurila et al. (2013), the component that detaches more easily is removed at first, leaving a surface that is more resistant to erosion. This effect can be referred to as armouring or shielding. In bentonite the resulting armouring layer is expected to be enriched in accessory minerals. This has also been observed in some experiments, but not in Börgesson et al. (2015). In addition, the swelling of bentonite is expected to decrease the effect of armouring.

The influence of the montmorillonite content on the erosion rate is not quite clear. In general, a high bentonite content seems to be less erodible than a low, at least at high flow rates. However, it seems to depend both on the flow rate and the montmorillonite type as well as the duration of the erosion. It seems logical that at very low flow rates, the montmorillonite particles will erode more than the accessory mineral particles as they are less dense. It is also obvious that Ca dominated bentonite is more prone to erosion than Na dominated.

#### **3.6.2 Water salinity and composition**

Groundwater salinity and composition i.e. the concentration and distribution of monovalent and divalent cations, has a large influence on forces between montmorillonite layers and thus on the microstructure of bentonite. It is thus expected to be an important factor regarding erosion, and this has also been seen in many experiments.

Expected groundwater composition at repository level (Sweden and Finland) will tend to change MX-80 bentonite from sodium to a calcium dominated bentonite. Calcium bentonite tends to form aggregates and therefore the sides of a piping channel get brittle and a grainy structure appears. According to Börgesson et al. (2015), water with calcium chloride initially seems to give higher outflow concentrations than water with sodium chloride but with time, the outflow concentrations in calcium chloride water will decrease to values less than in a sodium water. The slow decrease in erosion when exposed to sodium chloride water can be an effect of sol forming tendencies in a sodium bentonite, a sol that is slowly swelling out inwards the channel and is continuously carried away by the flowing water. In contrast, the calcium bentonite aggregates are too large and heavy to be transported in the flow once the channel has widened. Therefore, erosion is quickly reduced with calcium chloride water.

Salinity affects the rate of wetting and swelling of the bentonite. Higher salinity allows for faster wetting. The total swelling after saturation is, however, more in less saline water.

#### **3.6.3 Water inflow rate and rate of increase in water pressure at sealing**

Piping is assumed to occur when the water pressure in the water inflow point exceeds the sum of the swelling pressure and the shear strength of the bentonite, see definition of piping in section 3.3.2.

Piping and subsequent erosion will occur and will be maintained as long as there is a water pressure gradient and the flow rate is higher than  $10^{-4}$  l/min (Börgesson et al., 2015) (process studies show that at lower flow rates, the flow channels will be self-sealed and piping and erosion will stop).

An empirical model describing the amount of accumulated eroded material as function of the accumulated water flow is described in Börgesson et al. (2015). According to this model there is no influence of flow rate on the total amount of eroded material at a specified accumulated flow volume.

The rate of increase in water pressure affects the bentonites possibility to self-heal. If the bentonite can swell and seal a piping channel for a certain time it can withstand high water pressures. In the sealing tests performed within the KBS-3H project (Börgesson et al., 2005) a water pressure increase rate of 100 kPa/h was used.

### **3.6.4 Geometry**

In several reports, mainly Sandén and Börgesson, (2010) and Börgesson et al. (2015), two parameters concerning the geometry have been identified that have an influence on the erosion rate:

1. Direction of the piping channel. Erosion in vertical direction e.g. in a deposition hole seems to be lower than in horizontal direction. The influence of gravity is probably an explanation for this behaviour.
2. The length of the piping channel. The effect of the piping channel length on erosion rate is not fully known. However, there does not seem to be a proportional relation between the length of the piping channel and the erosion rate. In Laurila et al. (2013) it has been observed that an increase of the length of the piping channel with a factor of 4 will result in a mass loss increase of a factor 2. If not taking this into account, there will be a risk that the total erosion at full scale will be overestimated especially in the backfill.

Tests have also shown that the geometry of a pellet filled volume does not seem to influence the erosion rate, anyway not at the flow rate 0.1 l/min.

### **3.6.5 Time**

The erosion rate obviously decreases with the time passed since start of erosion. Laboratory tests have shown high erosion rates in the beginning, approximately 10-100 g/litre, but after a certain accumulated flow volume, about 100 litres, the erosion rates have decreased to between 0.01 to 1 g/litre. This is in fair agreement with the suggested erosion model described by Eq. 2. It should be noted that this expression does not take the pipe length into consideration. The erosion model does not include time but only the accumulated water flow, which seems to work to some extent. Since the total time used for the experiments is mostly less than two weeks any significant extrapolation of the experiment to longer time-scales is likely to be problematical.

Initially, eroded material from bentonite contains more grains than fine, but with time fine grained material will dominate in the eroding water. The fines are finally washed out and the material left in the channel is coarser grained than the reference material (Börgesson et al., 2015).

### 3.6.6 Temperature

No tests on the influence of temperature on the piping and erosion properties of bentonite have been performed. However, the referred reports analyse the influence on temperature on the general properties and behaviour of bentonite. See section 3.9.

## 3.7 Governing processes influencing piping and erosion

In addition to the parameters and variables several processes influencing piping and erosion have been identified:

1. Water absorption and free swelling
2. Properties of piping channels
3. Mass detachment
4. Mass entrainment into flow and re-deposition
5. Self-sealing of pipe channels during erosion
6. Self-sealing of fractures
7. Self-sealing of piping channels after water saturation
8. Gel extrusion and formation of water/gel filled pockets

These processes are linked to each other and are also strongly dependent on the different parameters listed in section 3.6. This section gives an overview of the different processes and their influence on piping and erosion.

Many of the results are taken from the Eva-project (Börgesson et al., 2015). In this project two types of MX-80 bentonite pellets were used, pillow shaped, and rod shaped as shown in Figure 3-4.



***Figure 3-4 Pictures of the two pellets types used in the erosion tests in the Eva-project. Extruded rod-shaped pellets to the left and roller compacted pillow shaped to the right.***

### 3.7.1 Water absorption and free swelling

Unsaturated bentonite, powder or compacted blocks and pellets, has high affinity for taking up water. The water can be taken up either as liquid or as vapor (bentonite is a hygroscopic material i.e. it can both absorb and emit moisture from the surrounding environment).

The theory behind the water uptake process of bentonite is described by Karnland et al. (2006):

*“Due to the electrically negatively charged montmorillonite layers and the charge compensating cations in the interlayer space, an analogue with salt is relevant to some extent.*

*Ions in a water solution reduce the chemical potential, and a concentration difference between solutions normally leads to water transport from the high potential (low concentration) to the low potential volume. In parallel, ions will diffuse from the high concentration to low concentration volume, and the equilibrium condition i.e. equal chemical potentials, leads to uniform ion concentration.*

*In bentonite, water molecules can be intercalated between the individual montmorillonite layers to create an interlayer ionic solution. However, the cations cannot freely diffuse away from the mineral surface because of the demand for electrical neutrality. Water will consequently be transported into the interlayer space, if water with a higher chemical potential is available, and the interlayer distance will increase which is synonymous with bentonite swelling. This water uptake will continue until the chemical potentials equal, which in the case of pure water source theoretically leads to infinite swelling. The extent of water uptake in bentonite may thereby be orders of magnitude larger and have a different character compared to other materials.*

*In a fixed total volume, the water uptake into the interlayer space will reduce the volume of initially larger pores. The uptake is forced to stop when the total available pore volume is completely filled with introduced water. At this full water saturation condition, water will continue to move in order to level the ion concentration in the system. The interlayer distances will thus increase in interlayer space with high ion concentration on the expense of interlayer space with low concentration, and the final distances will be a function of the local montmorillonite layer charge. The remaining difference in ion concentration, between the high concentration interlayer solution and the water supplying solution, leads to an osmotic pressure build-up in the clay (swelling pressure), which equals the chemical potential of water in the system.”*

The swelling capacity of the bentonite is an important property regarding erosion, piping and the self-healing of piping channels. The free swelling of bentonite into a piping channel where water is flowing will contribute to increase the erosion rate. Depending on the interlamellar cations in the bentonite (early swelling) and in the water (the counter ions in the bentonite will with time be exchanged to the available cations in the flowing water), the bentonite will have different swelling properties. If the dominating exchangeable cations are calcium (or other divalent cations), the expansion is limited but if it instead is sodium (monovalent cation) the bentonite can expand much more.

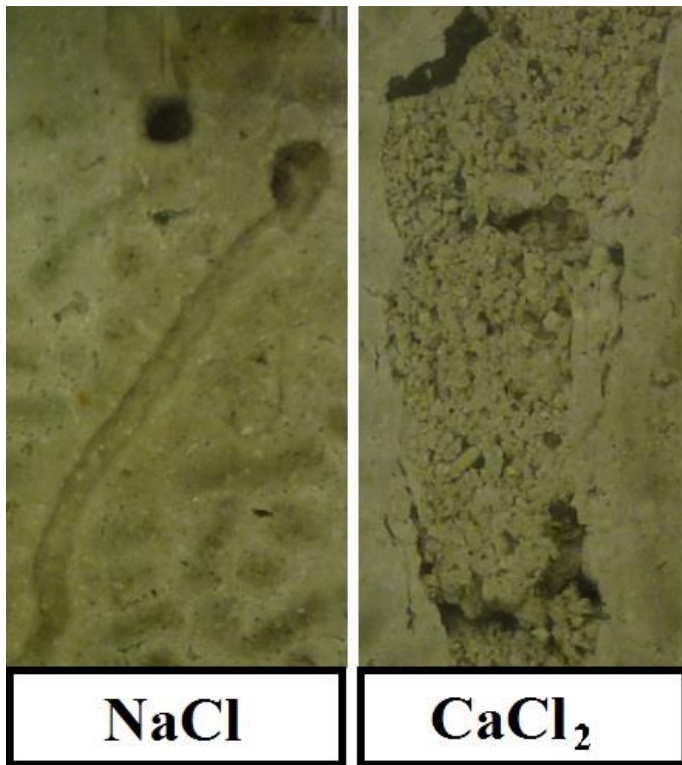
As described above, the magnitude of the swelling pressure depends on the groundwater salinity and composition i.e. the concentration and distribution of monovalent and divalent cations. It is thus expected to be important factors regarding erosion, and this has also been seen in many experiments.

### 3.7.2 Properties of piping channels

The design of many repositories includes that the gaps between compacted buffer blocks or backfill blocks and the surrounding rock surfaces are filled with pellets. This means that inflowing water from the rock will initially create piping channels in pellet fillings. The proportion of voids in a pellet filling is between 45 to 50%. This means that the inflowing water will initially flow in several channels but after a certain time, when the bentonite has started to swell and seal flow paths where the flow rate is low and the pipe diameter small, all water will flow in some single channels.

Bentonite surrounding a piping channel with a certain water flow, will take up water and swell but since the swelling flakes/aggregates are transported away continuously, no swelling pressure will initially be built up.

As previously mentioned, higher water salinity seems to induce both sealing and gel extrusion. The effects of water salinity were evaluated within the EVA erosion test studies (section 3.4.4). One of the main conclusions in that study was that the presence of calcium chloride in the eroding water causes an ion-exchange in the bentonite which changes the material properties. All tests in this study were performed with water with a 50/50 mix (by weight) of sodium chloride and calcium chloride and it was also seen in the EVA erosion tests that this 50/50 mix at 1% salinity was sufficient for ion exchange to take place. When the sodium dominated MX-80 bentonite is transformed into a calcium bentonite aggregates will form. These aggregates are occasionally ripped off from the sides of the flow channel and the channel may often quickly widen and be filled with loose material. Figure 3-5 shows a comparison of flow channels formed by pure sodium chloride water and pure calcium chloride water (both 1% salinity). The aggregates formed by the calcium chloride water are clearly seen in the figure.



←→ ~10 mm

**Figure 3-5 Comparison of flow channels formed by different types of salt water. The left channel is formed by sodium chloride water and the right channel is formed by calcium chloride water.**

This explains why the flow channel tends to widen and the loose bentonite aggregates accumulate in the channel. Increased water salinity seems to induce sealing and clogging of the channel and the occurrence of gel extrusion, which would be expected with increased amounts of loose material in the channel.

### 3.7.3 Mass detachment

Water flowing in the piping channel imply a frictional force on the pipe wall, which tends to detach bentonite particles from the wall and drag them with the flowing water. This process can be simplified and described by Eq. 1 (reproduced below) as reported in section 3.4.1

$$\dot{m}_B = k_e \max (\tau_Q - \tau_C, 0)$$

where  $\dot{m}_B$  is the rate of mass loss per unit area ( $\text{kg}/\text{m}^2/\text{s}$ ),  $\tau_Q$  is the hydraulic shear stress produced by the water flow,  $\tau_C$  is the critical shear stress at which the mass removal starts, and  $k_e$  is the erodibility coefficient, which is a property of the material being eroded.  $k_e$  is a critical parameter that has been calibrated for some very special situations measured in the laboratory. The usefulness of this relation is very limited since  $k_e$  and  $\tau_C$  are probably dependent on not only the bentonite type and the water salinity but also on the flow rate and the conditions of the pipe wall.

### 3.7.4 Mass entrainment into flow and re-deposition

When bentonite has been detached from the pipe wall it will be transported with the water and either be re-deposited further away or transported out of the tunnel either through a potential

plug or through a fracture in the rock. These processes (erosion, advection and sedimentation) are indicated in red in Figure 3-3. If the flow rate is low the gravity will tend to make the detached bentonite settle on the bottom of the pipe or if the pipe is vertical as in a deposition hole even settle against the flow direction. The large difference in behaviour of the erosion, when 1% CaCl<sub>2</sub> was added to the flowing water compared to when 1% NaCl is added to the water, as shown in Figure 3-5, yields large difference in settlement of the eroded bentonite in the channel. In the case with CaCl<sub>2</sub>, the settling of large flocks of bentonite was clearly visible.

The influence of the channel length is as noted earlier unclear. There may be several reasons for not having an erosion rate that is proportional to the length. The model attempt made by Åkesson (Börgesson et al., 2015) and then further developed (not referable reports) includes an influence of the clay concentration in the eroding water on the erosion rate, which thus means that the erosion rate will be strongly reduced for long flow distances. However, tests have showed that this model was not correct. Another reason for reduced erosion rate with channel length is of course the settlement and re-deposition of eroded clay particles. The more clay particles in the flowing water the larger re-deposition, so in a long channel the re-deposition may be in the same order as the erosion.

It is of course very important to know where the eroded material ends up, in order to evaluate the effect of the erosion. In the erosion calculations made in Börgesson et al. (2015), it is assumed that all eroded material from the buffer leaves the deposition hole. This may be pessimistic, but we do not have evidence enough to exclude this assumption.

### **3.7.5 Self-sealing of pipe channels during erosion**

The ability of the bentonite to stop the piping is an important critical process since it will also stop the erosion and the subsequent loss of bentonite. This process is of course tightly linked to piping and the process when piping occurs. The present view is that piping cannot be stopped until all the pellet-filled voids are filled with water and the water pressure gradient from the rock to the buffer and backfill inside the plug is moved to the plug. This process is treated in section 3.7.7. However, this is not self-evident and there are processes that may stop the water inflow and subsequent piping earlier.

The swelling pressure in a pellet filling is too low to prevent piping because the water pressure that builds up when the inflow is prevented can be several MPa. However, there are two other sub-processes that may stop piping:

1. The bentonite blocks in contact with the pellet filling swell and compress the pellet filling and will progressively build up swelling pressure in the pellet filling, which can close the channel and stop piping. This takes a long time and requires rather low water inflow rate.
2. Vault formation in the pellet filled slot, which is caused by interaction between the pellet pillows and formation of a vault that can take high pressures. In order to prevent piping, corresponding vault formation in the gel between the pellet pillows, is required. The vault is created by gel getting stuck between the swelling pellet granules. This phenomenon has been observed in the laboratory and is related with the process described in section 3.7.8 (gel extrusion and formation of water or gel-filled pockets).

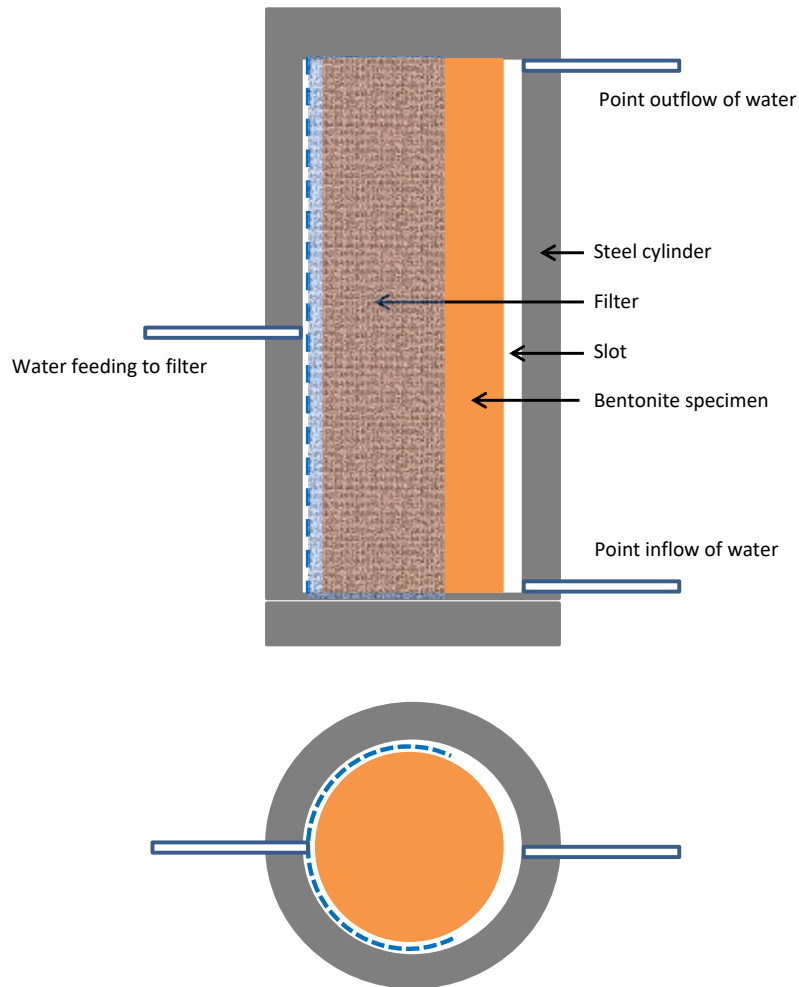


**Figure 3-6 Equipment used to study the ability of the bentonite to stop piping by swelling of neighbouring highly compacted bentonite. The inner height of the equipment is 12 cm and the diameter 6 cm. The slot between the bentonite specimen and the cylinder was 5 mm.**

A large number of tests were performed in the Eva project in order to investigate the ability of sub-process 1 to stop ongoing piping and erosion (Börgesson et al., 2015). Figure 3-6 shows the set-up of the test. Water was led from a lower inlet to a higher-placed outlet in a slot between a bentonite block and a cylinder at the same time as the bentonite block had access to water from a filter placed at the other side of the block. With time the water saturation and swelling of the bentonite block caused a compression of the slot and eventual sealing of the pipe.

The test durations varied between a couple of hours and 38 days, the flow rate between 0.01 and 0.001 l/min. The salt concentration in the water was 1% with 50/50 NaCl and CaCl<sub>2</sub>.

The results were not encouraging regarding the ability to stop piping this way. A few tests reached a stop after a few hours at an increased water pressure to 1 MPa but only one held that for a longer time and the process that stopped piping could not be the swelling from the bentonite block but probably vault formation. All long-time tests failed to heal.

There are uncertainties in the test methods and there were not many tests that finally could be used to evaluate the ability of the bentonite to stop piping. Despite that, the conclusion was that the tests do not show that piping can be stopped by swelling bentonite blocks. Additional

larger-scale tests, with higher densities and longer test times must be done if this process is considered decisive for the function of the buffer.

### 3.7.6 Self-sealing of fractures

In the context of the UK's broad classification of host rocks, the self-sealing of fractures is probably only relevant to HSR (i.e. hard fractured rocks). Studies have generally focused on understanding these processes in deposition tunnels filled with bentonite. After plugging of a deposition drift with an end plug there will probably be leakage between the in-situ cast plug and the rock but also in fractures in the rock, which has been observed in the Vault Plug Test and in the Backfill and Plug Test. The tightness of the plug is an important factor for the bentonite erosion if the plug is not able to keep a water pressure inside the plug that is high enough to prevent continuous water flow in the erosion channels and thereby start the self-healing process of the channel as described in section 3.7.7. If the bentonite transported in the water flowing through a fracture can seal the fracture it would strongly improve the tightness of the rock or the plug and reduce the total mass of eroded bentonite.

In order to check the ability of bentonite to seal off these leakage paths a number of tests with an artificial fracture in contact with bentonite pellets were performed (Börgesson et al., 2015). The parameters varied were the aperture of the slots (leakage ways), the water flow rates, the salt content in the water and the stiffness of the fracture. Figure 3-7 shows the equipment.

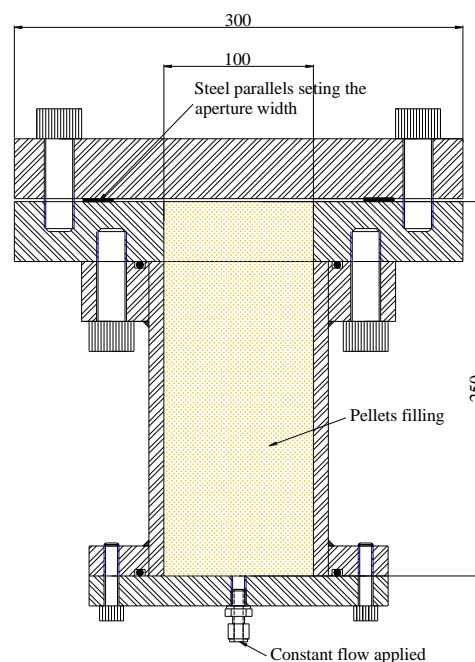


**Figure 3-7** Left: Picture from the laboratory showing the assembled equipment just before test start. Right: Schematic drawing of the test equipment.

There was a large scatter in results, which were not conclusive regarding the sealing ability of the bentonite. The tests though showed that the sealing ability depends on several factors:

- Fracture aperture
- Water flow rate
- Water pressure increase rate

- Fracture stiffness
- Maximum water pressure

Common to most tests was that sealing was reached when the fracture aperture was small (<0.1 mm), the water flow rate was low (<0.1 l/min) and the pressure increase rate at sealing was low (<2 MPa/h). Figure 3-8 shows an example of the bentonite left in the fracture after test termination and removal of the upper part of the artificial fracture when sealing was reached.



*Figure 3-8 Distribution of bentonite in the fracture after removal of the upper part in test 12 (aperture 0.05 mm, flow rate 0.1 l/min and pressure increase rate 2 MPa/h). The pellet-filled cylinder is seen in the centre. The strips are placed for fixing the slot width.*

The overall conclusion was that a lot of information and knowledge was gained by the performed tests but also that the uncertainties are still very large and additional knowledge is desired.

### **3.7.7 Self-sealing of piping channels after water saturation**

When the bentonite in the deposition holes and the deposition tunnel is completely water saturated and the water flow and subsequent erosion (hopefully) stopped by the plug, the piping channels will be filled with swelling bentonite and sealed. An interesting question for the tightness of the bentonite is the properties of the sealed channel. Will it have the same properties as the rest of the bentonite or does the density and composition of the sealed channel deviate from the surrounding bentonite to an extent that may discriminate the sealing function of the bentonite.

Erosion tests have shown that the composition of the bentonite in and around the channels will change due to the erosion. The following changes were noted:

- Concentration of coarser material inside the channels due to that the finer clay particles are more vulnerable to erosion, especially at upwards water flow.
- Ion exchange of the bentonite in the case of high Ca-concentrations in the flowing water

Both effects may adversely affect the buffer's ability to seal erosion channels. Therefore, a study of the properties of the former channels after piping, erosion and self-sealing after some time of erosion was performed (Börgesson et al., 2015).

Although there was a limited amount of useful test results and although some increase in hydraulic conductivity was noted in the former channel, the conclusion was that the change in properties was not so large that it affected the overall behaviour and properties of the bentonite. However, the self-healing of pipe channels is important for the function of the buffer and backfill and more investigations are needed.

### 3.7.8 Gel extrusion and formation of water or gel-filled pockets

An undesirable process that has been observed in several erosion tests is that erosion can be stopped and increasing water pressure at that location causes compression of the pellet in front of the stop and this forms water or gel pockets. This is a general problem and not site- or geometry-specific. These pockets with high pressure may lead to the bentonite gel formed before the erosion stop is extruded through the outflow opening. Figure 3-9 shows examples of water-pocket formation and gel extrusion.



**Figure 3-9** Examples of pocket formation (left) and gel extrusion (Börgesson et al., 2015).

Tests were made with both types of pellets used (rod-shaped and pillow-shaped as shown in Figure 3-4). The tests were made in a double cylinder in order to simulate the pellet filled slot in a deposition hole with varying flow rate (0.00125-0.01 l/min) and water salinity (1% and 3.5%). Altogether, 14 tests were performed and only 4 of them continued without clogging, formation of gel-pockets or gel extrusion. All these 4 tests were performed on rod-shaped pellets.

No clear influence on flow rate or salt content was observed although earlier experiences had shown that the flow rate needs to be rather low. Pillow shaped pellets seems to be more vulnerable to these processes than the rod shaped. Any conclusion on why these processes occurred in some cases and not in other could not be drawn. It is however obvious that this will occur in pellet filled geometries. Additional investigations should be performed in order to better be able to avoid these processes.

- Comments

Table 3-2 shows a compilation of the different processes and how they are affected by the different parameters and variables. How strong the processes are affected by the different

parameters and variables is rated from 0 to 3 with the strongest affect rated 3. The parameters and variables are included in the table with the following symbols

- Bentonite material  $B$
- Density  $\rho$
- Water content  $w$
- Montmorillonite content  $M_c$
- Accessory minerals  $m_a$
- Water composition  $w_{comp}$
- Water inflow rate  $v_i$
- Water pressure increase rate at sealing  $v_p$
- Geometry  $G$
- Time  $t$
- Temperature (0-100°C)  $T$

**Table 3-2 Compilation of the governing processes influencing piping and erosion and how strongly they are influenced by the different parameters and variables. 3 = very strong influence, 2 = medium strong influence, 1 = small influence, 0 = no influence. The knowledge of the different processes is graded A-D with A having the highest level of knowledge and D the lowest level.**

	$B$	$\rho$	$w$	$M_c$	$m_a$	$w_{comp}$	$v_i$	$v_p$	$G$	$t$	$T$	Knowledge
<b>Water absorption and free swelling</b>	3	3	2	3	0	3	1	1	2	3	1	A
<b>Properties of piping channels</b>	3	2	1	3	0	3	2	1	0	2	0	B
<b>Mass detachment</b>	3	2	2	3	2	3	3	1	0	3	0	B
<b>Mass entrainment into flow and re-deposition</b>	3	2	2	2	1	3	3	1	2	3	1	C
<b>Self-sealing of pipe channels during erosion</b>	3	3	2	3	1	3	3	3	2	2	1	C
<b>Self-sealing of fractures</b>	2	2	1	2	0	2	3	3	3	1	0	C
<b>Self-sealing of piping channels after water saturation</b>	3	3	0	3	0	2	1	0	1	0	0	B
<b>Gel extrusion and water/gel filled pockets</b>	2	2	2	2	0	3	3	3	2	1	0	D
<b>Sum</b>	22	19	12	21	4	22	19	13	12	15	3	

The rating is of course somewhat uncertain and subjective; however, it is based on the expert judgement of the authors. However, it is obvious that the most important factors influencing piping and erosion are: the bentonite material  $B$ , the density  $\rho$ , the montmorillonite content

$M_c$ , the water composition  $w_{comp}$  and the flow rate  $v_i$ . The least important factors are the accessory minerals  $m_a$  and the temperature below 100°C  $T$ .

An estimate of the understanding or knowledge of the different processes is also included in the table. The best-known process is judged to be “Water absorption and free swelling” and the most uncertain is “Gel extrusion....”.

Temperature above 100 °C has not been included in the table since there is too little information available. See also section 3.9.

### **3.8 The present capability to model piping and mechanical erosion**

Some attempts to model the processes in piping and mechanical erosion have been made and are reported in section 3.4. They all consider water flow in an idealised channel. Most of the presented models include the two main processes eroding bentonite particles by the shear stress from the flowing water and swelling of the bentonite surrounding the pipe. There is also the simple empirical model described by Eq. 2.

The process models are rather embryonic in nature. They refer to a few tests that have mainly been used to calibrate parameters. None of these models are good enough in order to yield accurate predictions of the effect of erosion.

Due to the lower density of the bentonite in contact with the rock surface and the high water pressure at repository depths there will almost always be piping when the water inflow in a fracture intersecting a bentonite filled cavity in the rock unless the inflow rate is very low. In Börjesson et al. (2015) it was concluded that piping will take place and the pipe will be kept open unless:

- There is a stop in the flow for at least 10-15 minutes
- The water flow rate is lower than 0.1 ml/min
- The water pressure is lower than 10 kPa

This conclusion is based on results from many different tests in the laboratory. A good erosion model should be able to predict when the swelling of a pipe is larger than the eroding transport of clay and thus the piping and erosion will stop when the pipe radius has been reduced to zero. However, that would lead to an increase in water pressure on the bentonite in the pipe, which in turn would open up the pipe when the water pressure is approximately higher than the sum of the swelling pressure and the shear resistance in the clay.

However, there may be another phenomenon that can stop piping temporarily: if there is vault formation in the pipe, the increasing water pressure that will be generated may compact the bentonite in front of the pipe and thus hinder further flow and stop piping. This may on the other hand lead to another problematic process described in section 3.7.8, namely gel extrusion and water or gel-filled pockets.

Currently, there is no model that can model these kinds of behaviours. There is probably no need to be able to model when piping occurs since it will, as concluded, either always occur unless the inflow rate is very low or cause other problems as gel extrusion and pocket formation. A pessimistic way to proceed is to do as was done in Börjesson et al. (2015) to

assume that all inflowing water will yield piping and try to estimate the consequences of the erosion in the pipes.

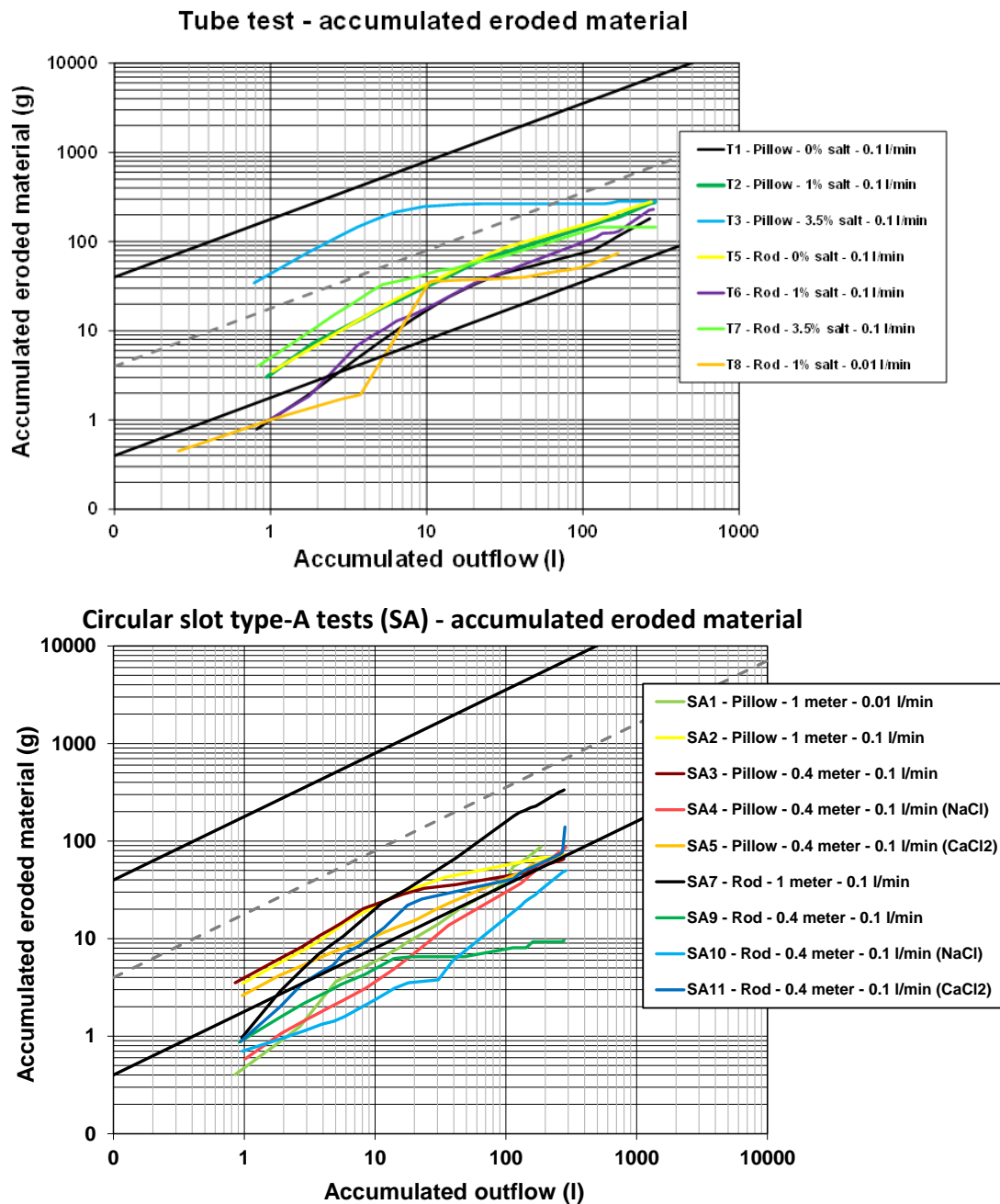


*Figure 3-10 Two examples of results from erosion tests on different pellets types, with different flow lengths, flow rates and salt content in the flowing water. The accumulated weight of the eroded dry mass is plotted as a function of the accumulated volume of flowing water. The straight black lines describe a model of expected maximum and minimum accumulated eroded material (Sandén and Börgesson, 2010). The dashed grey line shows the later suggestion of upper limit of the model for upwards water flow using  $b < 0.2$  (Börgesson et al., 2015).*

It is very important to be able to predict the amount of material that may erode from certain parts of a repository in order to assure that the remaining bentonite density is high enough.

The model used by Börjesson et al. (2015), Eq. 2, is perhaps a crude technique but all laboratory results show that the erosion lies below the upper limit set in this model  $\beta < 0.2$ .

Figure 3-10 show two examples of measurements and comparisons with the model (Börjesson et al., 2015).

Some exceptions of this limit have been observed but these exceptions are caused by other phenomena that cannot be modelled such as gel extrusion and pocket formation. Figure 3-11 shows examples of results where gel extrusion occurred in two tests.

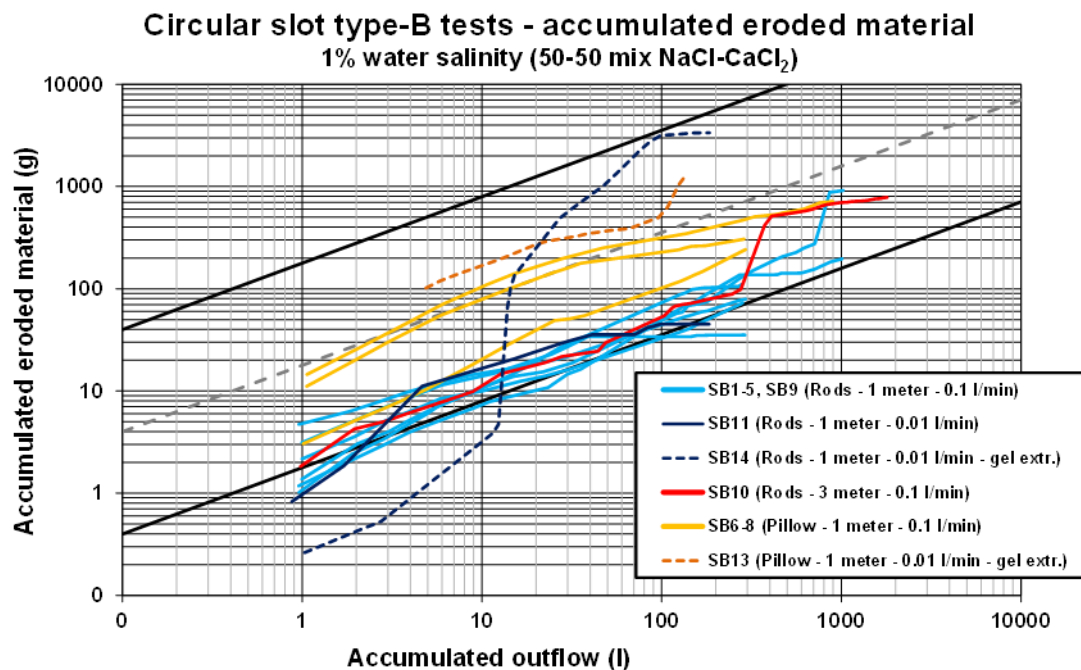


*Figure 3-11 Examples of erosion test results on different pellet types and different flow lengths. At two of the tests (marked with dashed lines) gel extrusion occurred, which explains the high “erosion” figures (Börjesson et al., 2015).*

To our knowledge there are two more studies, which also include attempts to model erosion. These were done by Clay Technology and financed by Posiva. These studies are not published in referable documents and can thus not be reported here. However, these studies did not lead to any useful model although they cast additional light on the complicated processes of erosion.

### 3.9 Influence of temperature on erosion

#### 3.9.1 Bentonite properties

The decaying fuel in a repository for spent nuclear fuel, will increase the temperature of the canister and the bentonite buffer. Bentonite is known to degrade at high temperatures and therefore there are often upper temperature limits for the buffer in the different nuclear waste concepts. The upper limit is often specified to be 100°C. This limit is set to prevent deleterious processes such as illitisation and cementation of the bentonite.

The increased temperature will initially give rise to a thermal gradient over the bentonite buffer by which original water in the bentonite will be redistributed. In parallel, there is an uptake of water from the surrounding rock going on. The inflowing water from the rock may lead to

erosion of bentonite if the inflow rate is high enough and if the bentonite cannot swell fast enough to seal the flow.

The temperature may influence the erosion in two ways. In the beginning, a high temperature will likely only influence the properties of the water, mainly viscosity, since the temperature needs some time to affect the bentonite chemically. This is also the time when the bentonite is exposed to water inflow that may cause erosion. After some time, the temperature will decrease and the bentonite be closer to water saturation and thus less exposed to erosion, but also be more affected by the high temperature.

Several investigations have been made to investigate how exposure of bentonite buffer to high temperature influences the bentonite properties, see e.g. Leupin et al. (2014) and Wilson and Bond (2016). In these reports, a review of the possible processes such as smectite illitisation and bentonite cementation phenomena including the effect of steam on bentonite properties, have been made. The reports also include modelling and laboratory investigations. One main conclusion is that it is not believed that illitisation (transformation of strongly swelling smectite into illite) could result in sufficient deleterious effects to a bentonite buffer. There seems, however, be somewhat divided opinions whether silica cementation, as a result of exposure to water vapour at elevated temperature is a problem for the bentonite. In (Wilson and Bond, 2016) it is concluded that the silica cementation can result in dramatic loss of swelling pressure, and associated increase in stiffness.

Additional information regarding the influence of temperature on bentonite can be found from different laboratory investigations e.g. Karnland et al. (2009a) and Åkesson et al. (2012) made on bentonite specimens taken from large scale field tests where the bentonite have been exposed to high temperature, 130-150°C. These investigations have shown that some changes of the bentonite properties have occurred:

1. **Reduction of swelling pressure.** A reduction in swelling pressure has been observed on specimens taken from the hottest parts. This suggests that the amount of swelling mineral has decreased or changed properties. The swelling and following sealing of gaps and/or channels may take longer time, and this reduction of swelling pressure is thus something that is believed to increase the exposure for erosion.
2. **Changes in strength.** Tests have shown that the stress-strain behaviour of the bentonite changes. The bentonite become brittle involving high stiffness, high shear strength and low strain at failure. How this change in strength influences the erosion properties of the bentonite is not known.
3. **Redistribution of minerals.** The increased temperature has also resulted in a redistribution of easily dissolved accessory minerals e.g. CaSO<sub>4</sub>. The accessory minerals are in general larger particles than the montmorillonite. They are therefore not transported as readily by the water flow and are expected to resist detachment more. How the redistribution of minerals by exposure to high temperature influence the erosion properties of the bentonite is not known.
4. **Exchangeable cations.** Exchangeable sodium was replaced by calcium in the warmest parts, probably as an effect of calcite dissolution which have affected the porewater composition. In different erosion experiments it has been noted that a change of cations in the bentonite results in that aggregates are formed. The aggregates accumulate in the flow channels that are clogging. This is a phenomenon that is believed to result in so called “gel extrusion”.

It should be observed that the noted changes have occurred on specimens taken close to the heaters i.e. in the warmest parts. In a repository, inflowing water from the rock will mainly flow close to the rock where the temperature is lower and not in the parts close to the canister.

The influence of these possible changes of the bentonite buffer on the erosion properties of the bentonite is, however, not known. If the amount of montmorillonite decreases depending on e.g. alteration processes, it is believed that the bentonite will be more prone to erode. See also section 3.5.1.

It is questionable if erosion can occur in temperatures above 100°C, since the water will be transformed to water vapour unless the vapour pressure is high, which it is unlikely to be the case before water saturation has been reached and water pressure has recovered. It may however take place after the temperature peak when the temperature has decreased below 100°C and the bentonite thus has been affected by the high temperature.

### **3.9.2 Water properties**

The viscosity of water changes with temperature. The viscosity at 100°C is about a quarter of the viscosity at 20°C. This may probably influence the erosion properties, but it has not been investigated and is thus not known.

### **3.10 Identified gaps in the knowledge regarding piping and erosion**

- A large number of tests on piping and mechanical erosion in bentonite and several attempts to model these processes have been made. The laboratory tests have yielded a strong increased knowledge but have also revealed that the processes are very complicated and influenced by many factors. As shown in

Table 3-2 there are many subprocesses and the influence of different parameters and variables are very different. This means of course that modelling piping and erosion has not been very successful.

- In order to analyse and identify gaps in the knowledge,

Table 3-2 is also included here.

- 

Table 3-2 shows the influence of different parameters and variables on the important processes of the piping and erosion behaviour of bentonite, how much they affect the behaviour (the sum of the influence grade) and the level of knowledge of the different processes. However, the table does not show the level of importance of the different process for the piping and erosion behaviour. At first a column that graded the level of importance of each process was included but removed since all processes seem to be very important. However, the process “Self-sealing of pipe channels after erosion” is perhaps more important than the other ones, since if the channels would not heal the sealing properties of the bentonite may be compromised.

**Table 3-2 Compilation of the governing processes influencing piping and erosion and how strongly they are influenced by the different parameters and variables. 3 = very strong influence, 2 = medium strong influence, 1 = small influence, 0 = no influence. The knowledge of the different processes is graded A-D with A having the highest level of knowledge and D the lowest level.**

	$B$	$\rho$	$w$	$M_c$	$m_a$	$w_{comp}$	$v_i$	$v_p$	$G$	$t$	$T$	Knowledge
<b>Water absorption and free swelling</b>	3	3	2	3	0	3	1	1	2	3	1	A
<b>Properties of piping channels</b>	3	2	1	3	0	3	2	1	0	2	0	B
<b>Mass detachment</b>	3	2	2	3	2	3	3	1	0	3	0	B
<b>Mass entrainment into flow and re-deposition</b>	3	2	2	2	1	3	3	1	2	3	1	C
<b>Self-sealing of pipe channels during erosion</b>	3	3	2	3	1	3	3	3	2	2	1	C
<b>Self-sealing of fractures</b>	2	2	1	2	0	2	3	3	3	1	0	C
<b>Self-sealing of piping channels after water saturation</b>	3	3	0	3	0	2	1	0	1	0	0	B
<b>Gel extrusion and water/gel filled pockets</b>	2	2	2	2	0	3	3	3	2	1	0	D
<b>Sum</b>	22	19	12	21	4	22	19	13	12	15	3	

Note that all parameters and variables in the table are rather easy to determine except for the water pressure increase rate at sealing  $v_p$ . However, the influence on the different processes are not so easy to determine.

In order to evaluate the different processes and identify important gaps in knowledge, we will consider them process by process.

### **Water absorption and free swelling**

This process is probably the best-known process. Numerous tests have been made on water uptake and swelling of bentonite both of water saturated and unsaturated bentonite and at different confinements. Many models and modelling attempts have also been made in different projects. In spite of this there are still problems to model some scenarios that include swelling. However, no additional investigations for the special purpose of piping and erosion are probably needed.

## **Properties of piping channels**

This includes both the properties and behaviour of possible material in the channels and in the walls of the channels. As shown in Figure 3-5 the channels can be very different depending of the salt type and the salt content in the flowing water. Several tests have been made and the knowledge and understanding are rather good but far from enough in order to model the behaviour.

### **Mass detachment**

This is of course an important process since it determines the amount of eroded material. The models used are rather simple (Eq. 1). More knowledge is required if modelling is judged to be important.

### **Mass entrainment into flow and redeposition**

The entrainment of the detached material and how and where it may be redeposited are of course important for the understanding and the possibility to model erosion. The knowledge is, however, very limited and very difficult to investigate. In most erosion tests the eroded material leaving the channel is collected and it is unknown if or how much material that has been redeposited in the erosion channel. However, some tests reported by Börgesson et al, showed that the material left in the channels were slightly coarser grained than the material left in the walls of the pipes, which is logical. In addition, the results with different flow length indicate that the total amount of erosion is not proportional to the flow length. This means that either material has been redeposited or that the mass detachment is decreased with flow length or both.

Also, for this process more knowledge is required if modelling is judged to be important.

### **Self-sealing of piping channels during erosion**

As described in section 3.7.5, piping can be stopped in mainly two ways:

- Swelling of adjacent saturated bentonite and by that closing the pipe
- Vault formation in the pipe front

Experiments indicated that vault formation was the only way to stop piping. However, the base for this conclusion is small and more testing is needed. Otherwise, piping and erosion must be assumed not to stop until full water saturation and reestablishment of natural ground water pressure in the rock and the bentonite, which was done in the scenario analyses in Börgesson et al (2015).

### **Self-sealing of fractures**

- In addition to the variables and parameters included in

Table 3-2 there are a few others that influence the ability seal a fracture in the rock or in a plug, namely the aperture width and the fracture stiffness. Tests showed that the fracture aperture needs to be small and the water flow rate and the water pressure increase rate need to be low, for the fracture to self-seal stop the erosion. Also for this process, more investigations must be done otherwise self-sealing of fractures must be considered not to take place and

pipng and erosion must be assumed to continue until full water saturation and natural ground water pressure in the rock and the bentonite have been re-established.

### **Self-sealing of piping channels after water saturation**

As mentioned, this is probably the most important process, since if the flow channels would stay open after full water saturation and homogenisation the sealing properties of the bentonite may be destroyed. A limited number of tests have showed that the sealing properties were sufficient after erosion and self-sealing. However, additional testing is desirable due to the high importance of this process.

### **Gel extrusion and formation of water/gel filled pockets**

This is probably the least known process, and potentially also a very harmful one in the sense that it may create low density pockets in the pellet filling. It has occurred so many times in different experiments that it must be considered inevitable. It may cause large damage due to the occurrence of voids. More testing is needed in order to better understand the consequences.

## **3.11 Conclusions**

### **3.11.1 General**

A literature review has been undertaken in order to find and study reports and articles dealing with piping and mechanical erosion in bentonite fillings as well as the effect of high temperatures on the properties of bentonite. Altogether 19 reports were found interesting and have been reviewed. 13 of them dealt with piping and mechanical erosion while 6 dealt with high temperature effects. The most important information was found in the report of the EVA project (Börgesson et al., 2015).

Altogether 8 different subprocesses that affect the piping and erosion behaviour were identified. 11 different variables that have an influence of these subprocesses were also identified.

An attempt to grade the influence of the different variables on the subprocesses by ascribing each variable the values 0-3 was made as well as an attempt to grade the present knowledge of the subprocesses from A (largest) to D. The most important factors influencing piping and erosion were the bentonite material  $B$ , the density  $\rho$ , the montmorillonite content  $M_c$ , the water composition  $w_{comp}$  and the flow rate  $v_i$ . The least important factors were the accessory minerals  $m_a$  and the temperature below 100°C  $T$ . The most well-known subprocess was “Water absorption and free swelling” and the least known process was “Gel extrusion and water/gel filled pockets”.

### **3.11.2 Knowledge gaps**

In general, the knowledge of piping and erosion in bentonite is too low to be able to form a model that can handle all the processes and variables found. If such a model is desired more investigations on the following subprocesses are required:

- Properties of piping channels
- Mass detachment
- Mass entrainment into flow and re-deposition

- Self-sealing of pipe channels during erosion

If reliable models cannot be formed or considered not required, the conclusion must be that piping and erosion must be handled as suggested by Börgesson et al (2015), where the scenarios of piping and erosion were assumed to be inevitable and will continue until the bentonite fill is water saturated and natural ground water pressure re-established. Under those circumstances, increased knowledge about the following two subprocesses are needed:

- Self-sealing of piping channels after water saturation
- Gel extrusion and formation of water/gel filled pockets

Although tests have shown that piping channels self-seal after water saturation more tests under different conditions are required in order to assure that this will always be the case.

The final process of gel extrusion and formation of water or gel filled pockets may damage the pellet filling in a way that risks the intended function and the knowledge is still too immature to establish how and when it occurs. More investigations are needed.

The conclusion is thus that these two last subprocesses are the most important to investigate.

In addition, it is important to estimate how large the erosion will be if the assumption that it cannot be stopped is made. Since almost no erosion test has resulted in a larger erosion than modelled by Eq. 2, with  $\beta = 0.2$ , it is recommended to use that equation, which was done in the scenario analyses in Börgesson et al. (2015). However, it would be very valuable to make additional such tests, with the test setup similar to the special conditions that are considered, since they can differ from the conditions in previous tests.

If very high temperatures are considered, addition tests on bentonite at such temperatures should be made since the present viewpoint on the effect of temperatures above 100°C are inconclusive and ambiguous.

## 4 Chemical erosion

The process that often has been termed chemical erosion refers to the loss of bentonite due to interaction with dilute groundwater. This scenario is most likely to occur in a GDF during and after future periods of glaciation, which could cause dilute glacial meltwaters to reach repository depth. The periods of potential erosive conditions can also be expected to last for up to tens of thousands of years (Posiva OY, 2012). The long period of time is a challenge for making prediction. Therefore, it is especially important that the process understanding is based on as well-known and well-established physics and chemistry as possible.

The understanding of the conditions that prevent chemical erosion is relatively good. For example, the importance of divalent counterions or at which ionic strength montmorillonite forms a gel (Birgersson et al., 2009; Hedström et al., 2016; Jönsson et al., 2009).

On the other hand, it has been difficult to determine the severity of the chemical erosion problem and to estimate the amount of montmorillonite that may be lost during periods of dilute melt water. This chapter will address the most relevant colloidal phases of montmorillonite and provide an overview of the relevant forces acting between montmorillonite particles. As far as possible, rheology and erosion will be described, at least qualitatively, based on these forces. The most illustrative erosion test have been performed using artificial fractures. Several such tests are examined.

Models describing swelling and erosion will also be analysed based on the colloidal forces. The chapter concludes by identifying the most important knowledge gaps for assessing chemical erosion.

### 4.1 Definitions and concepts

#### 4.1.1 Montmorillonite phases

A schematic phase or state diagram for Na-montmorillonite in contact with aqueous NaCl solution is shown in Figure 4-1. It contains the phases: sol, gel and paste. In principle the same diagram could be used for a mixed Ca/Na system if the amount of Na<sup>+</sup> in the interlayer is larger than ~20%. For the mixed system, the ionic strength must be set an appropriate mix of Na and Ca salts, e.g. NaCl and CaCl<sub>2</sub>, to avoid ion exchange (Birgersson et al., 2011, 2009; Kahn, 1958).

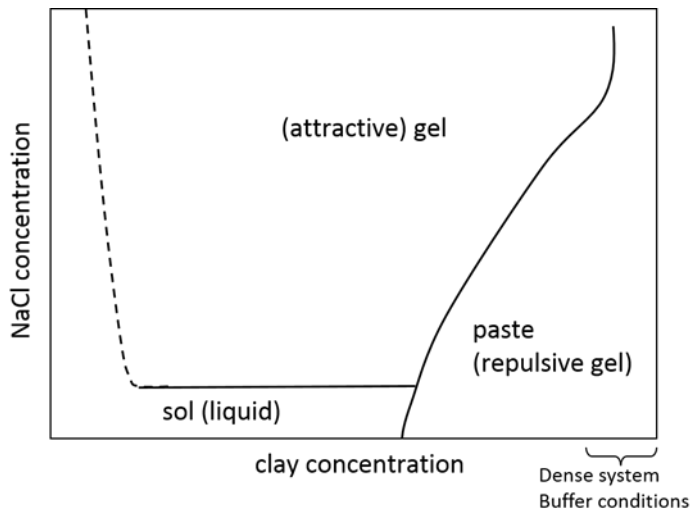


**Figure 4-1 Schematic phase (state) diagram for Na-montmorillonite modified from Hedström et al. (2016).**

Regarding different montmorillonite phases, a consistent terminology facilitates communication. The terminology below strives to adhere to the definitions recommended by either the National Institute of Standards and Technology, NIST (Hackley and Ferraris, 2001) or by the International Union of Pure and Applied Chemistry, IUPAC (Alemán et al., 2007). The terms attractive and repulsive gels are often seen in the literature but are somewhat inconsistent as exemplified below.

**Sol:** A liquid dispersion containing particles of colloidal dimensions (NIST). The IUPAC recommended definition of a sol is “a fluid colloidal system of two or more components”. A montmorillonite sol is thus a liquid state that may be susceptible to erosion by flowing groundwater or by gravity as the sol has larger density than water.

**Gel:** Bicontinuous structure with a solid and a liquid component. The solid network may consist of particles or polymers, held together by covalent, ionic or dispersion (physical) forces. The network may be elastic, viscoelastic, or plastic. The scale of the mesh of the network (distance between cross links) is of colloidal dimensions (NIST). The recommended definition of a gel by IUPAC is a “non-fluid colloidal network or polymer network that is expanded throughout its whole volume by a fluid”.

In view of the NIST definition, the word “attractive” is superfluous since the particles in a gel are “held together” which implies attraction. However, in the literature the terms attractive and repulsive clay gels often occur (Abend and Lagaly, 2000). The montmorillonite gel is only formed when the salinity is above a critical value, the critical coagulation concentration CCC. The most likely mechanism for forming a gel is attraction between positive edges and negative faces of individual montmorillonite layers (Delhorme et al., 2012a; Goh et al., 2011; Hedström et al., 2016; Jönsson et al., 2008; Martin et al., 2006). Identifying the conditions for the formation of montmorillonite gel is important because it is the only bentonite-specific mechanism that can prevent clay erosion at a transmissive fracture.

**Paste:** The term paste was, in the context of montmorillonite/bentonite, proposed in Hedström et al. (2016) to avoid confusing use of the term gel and it has subsequently been adopted by other authors (Neretnieks and Moreno, 2018a; Smith et al., 2017). Montmorillonite paste denotes a phase that is governed by repulsive forces (Hedström et al., 2016). Unconfined clay paste expands in contact with water, while confined paste develops a swelling pressure if

contacted to water via a filter or membrane that is impervious to the clay particles. On a short timescale, this phase does not flow, and it has yield strength (Börgesson et al., 2018; Eriksson and Schatz, 2015). The origin of the solid-like behaviour is the repulsive forces that lead to a lack of free volume; every displacement of a particle would take it to a volume of increasing repulsion (Martin et al., 2002). In the literature, the paste is sometimes called “repulsive gel” although the presence of a network, which defines a gel, has never been demonstrated for this phase.

#### 4.1.2 Forces in colloidal systems

In this section the forces that govern bentonite/montmorillonite phase behaviour will be reviewed. The problem of chemical erosion concerns the longevity of the repository for spent nuclear fuel which makes a fundamental understanding of the forces involved especially important.

Montmorillonite and other smectite clays consist of ~1 nm thick aluminosilicate layers with lateral dimensions typically in the range 50-500 nm (Michot et al., 2004; Ploehn and Liu, 2006). These so called 2:1 clay layers consists of two tetrahedral silicon oxide sheets sandwiching an octahedral aluminium oxide sheet. The smectite clay layers have a permanent negative charge due to isomorphous substitutions of, e.g., Mg for Al in the octahedral sheet or Al for Si in the tetrahedral sheets. This permanent charge is compensated by exchangeable cations and thus the origin of the cation exchange capacity (CEC). The permanent layer charge together with the cations is the main cause of clay swelling or the build-up of swelling pressure when the clay is confined (Hensen and Smit, 2002; Hsiao and Hedström, 2017; Karnland et al., 2005; Quirk and Marčelja, 1997; Tambach et al., 2004). At the edge of the clay layer, the 2D crystal structure is disrupted and the covalent bonds are broken. It is also only at these edges that the octahedral sheet is exposed to the solvent. The edge groups are titratable and may, depending on pH and ionic strength, become positively charged due to protonation as illustrated in Figure 4-2 (Avena et al., 2003). The opposite charges of edges and faces (basal surfaces) are considered to promote the association of clay particles which can give rise to flocculation or gelation (van Olphen, 1964).

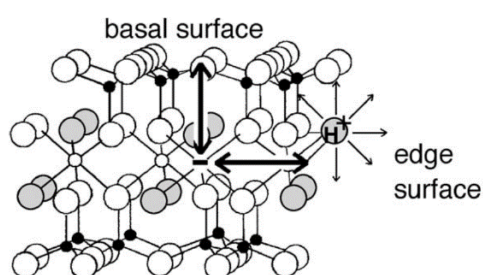


**Figure 4-2** Scheme of a 2:1 dioctahedral phyllosilicate layer indicating protonation at the edge surface. The double-headed arrows have the same size and indicate the distances between a negative structural charge in an average octahedral position and both the basal and edge surfaces (Avena et al., 2003).

For many charged colloidal particles, the DLVO theory, named after Derjaguin, Landau, Verwey, and Overbeek, has been central for explaining colloidal stability (Derjaguin and Landau, 1941; Verwey and Overbeek, 1948). In that theory, two types of forces are considered. The repulsion between colloidal particles is represented by electrostatic double-layer forces, calculated from the Poisson-Boltzmann equation, and the attraction is calculated from the van der Waals forces. The colloidal stability or instability is explained by the competition between the double-layer force and the van der Waals force. The double-layer

force is influenced by the electrolyte concentration while the van der Waals force is not. This explains the sensitivity to salt concentration on the colloid stability or instability, which is a major achievement of the DLVO theory and allows for calculation of the critical coagulation concentration (CCC) for many systems (Evans and Wennerström, 1999; Goodwin, 2009; Hamley, 2007; Verwey and Overbeek, 1948). However, it has long been apparent that one must include additional forces beyond the DLVO theory to understand the complex coagulation behaviour of smectite clays (Guldbrand et al., 1984; Kahn, 1958; Kjellander et al., 1988; Swartzen-Allen and Matijevic, 1976; van Olphen, 1956).

### **Repulsive forces**

It is mainly montmorillonite/bentonite dominated by  $\text{Na}^+$  as a counterion that may swell extensively in dilute groundwater and thereby lead to the release of colloidal montmorillonite particles. Therefore, much effort has been put into the description of the most adverse scenario which is the swelling and erosion of homoionic Na-montmorillonite (Birgersson et al., 2009; Hedström et al., 2016; Neretnieks et al., 2009; Schatz et al., 2013). It is now established that the DLVO theory for parallel clay layers provides a quantitatively good account of the swelling pressure in Na- and Li-smectites over a large range of dry densities and sub-molar salinities (Karnland et al., 2005; Quirk and Marčelja, 1997; Zhang et al., 1995). As mentioned above, the repulsive force in the DLVO theory is calculated from the Poisson-Boltzmann (PB) equation which is used to determine the distribution of ions between two negatively charged clay layers. An example of the solution to the PB equation for two parallel charged layers in equilibrium with aqueous NaCl solution is given in Figure 4-3. Treating montmorillonite or any other laminar system in this fashion assumes that all porewater is evenly distributed in the interlayers between clay layers. This assumption is also supported by numerous experiments (Holmboe et al., 2012; Martin et al., 2006; Norrish, 1954; Norrish and Rausell-Colom, 1962). Because of thermodynamic equilibrium, all interlayers are equal, so it is enough to study one of them and its equilibrium with the external bulk electrolyte (Birgersson et al., 2017; Engström and Wennerström, 1978; Martin et al., 2006).

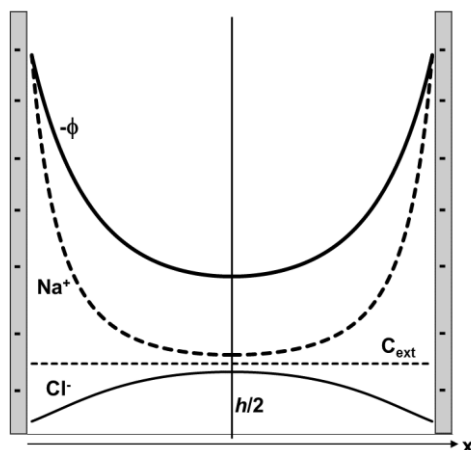


**Figure 4-3 Schematic illustration of sodium and chloride concentration profiles in the interlayer between two clay layers with equal surface charge density. The negative of the mean electrostatic potential  $\phi$  is also included. The horizontal dashed line indicates the external or bulk NaCl concentration. The separation between the clay layers is  $h$ . Due to symmetry the electric field,  $d\phi/dx$ , vanishes at the midplane,  $x=h/2$ . Reproduced from (Hedström and Karnland, 2011).**

Water is treated as a continuum and enters the PB equation in the form of a dielectric constant, normally taken to be the bulk value also for the interlayer solution. To solve the

model of parallel surfaces in Figure 4-3 one also assumes that the lateral dimensions of the layers approach infinity, which makes the problem one-dimensional and depend only on the  $x$ -coordinate which is perpendicular to the surfaces. The one-dimensional PB equation for parallel layers is

$$\epsilon_0 \epsilon_r \frac{d^2 \phi}{dx^2} = -e \sum_i Z_i c_{i,0}^* \exp(-Z_i e \phi(x) / k_B T) \quad (3)$$

where  $\epsilon_0 \epsilon_r$  is the dielectric constant for water and  $\phi$  the mean-field electrostatic potential (Evans and Wennerström, 1999). The right-hand side of Eq. 3 represents the charge density expressed as a Boltzmann distribution, where  $e$  stands for the elementary charge,  $Z_i$  is the ion valency of ion  $i$ ,  $k_B$  the Boltzmann constant, and  $T$  the absolute temperature.  $c_{i,0}^*$  is the concentration of ion  $i$  at a reference point where  $\phi = 0$ . For a system in osmotic equilibrium with a bulk saline solution, it is convenient to choose the bulk solution as the reference (Dubois et al., 1992). With the bulk solution as reference, the concentrations  $c_{i,0}^*$  represents the bulk concentrations. Further, in Eq. 3, the concentrations  $c_{i,0}^*$  are “number concentrations”, i.e., number of ions per cubic metre and not molar concentrations. The internal concentration at  $x$  in the interlayer is given by  $c_{i,0}^* \exp(-Z_i e \phi(x) / k_B T)$ .

Figure 4-3 illustrates the solution of the PB equation for montmorillonite in equilibrium with an external 1:1 salt solution, labelled as NaCl, but note that there is no ion-specific information contained in Eq. 3, only the valence. The electrostatic potential depends on the clay layer surface charge density ( $\sigma$ ) as well as the positions of the ions in the interlayer solution outside. Further, Eq. 3 is not solved for any specific configuration of ions in the interlayer but instead for the average distribution, and the resulting mean potential. Thus, the PB equation represents a mean-field theory (Evans and Wennerström, 1999). Even for the seemingly simple system in Figure 4-3, Eq. 3 has to be solved numerically for the most general situation (Dubois et al., 1992; Evans and Wennerström, 1999). Based on Figure 4-3 we will here discuss some features of the solution. The clay layers are assumed to be identical, so the system has a symmetry plane at  $x = h/2$ . This symmetry implies that the electric field at the midplane is zero ( $\left. \frac{d\phi}{dx} \right|_{x=h/2} = 0$ ), thus there is no direct electrostatic interaction between the two negatively charged layers. At the midplane the layer charge is fully balanced by the ions, and by integrating Eq. 3 once from  $x = 0$  to  $h/2$  one arrives at the boundary condition  $\left. \frac{d\phi}{dx} \right|_{x=0} = -\frac{\sigma}{\epsilon_0 \epsilon_r}$ . The layer charge in montmorillonite originates from permanent substitutions in the crystal structure, in contrast to titratable groups, therefore  $\sigma$  can be viewed as constant. This implies that the slope of  $\phi$  at the surface will not depend on the bulk electrolyte concentration. On the other hand, the potential at the surfaces ( $\phi_0 = \phi(0) = \phi(h)$ ) is influenced by the electrolyte concentration and its magnitude decreases with increasing concentration. In montmorillonite and other smectites  $\sigma < 0$  and thus  $\phi < 0$  in the interlayer region, as indicated in Figure 4-3. Consequently, the concentration of cations is enhanced in the interlayer compared to the bulk concentration whereas the concentration of anions is suppressed as shown in Figure 4-3. The difference between the average interlayer concentrations of cations and anions equals the cation concentration needed to compensate the montmorillonite layer charge. The two clay layers in Figure 4-3 repel each other, but as shown above, it is misleading to view this force as a direct electrostatic force. The repulsion is entropic and proportional to the difference in ion concentration at the midplane and in the bulk (Evans and Wennerström, 1999).

The PB equation is not valid for divalent counterions so we only explicitly state the pressure (force/area) for montmorillonite in equilibrium with a 1:1 salt (NaCl) with external concentration  $c_0^*$

$$\frac{F_{PB}(h)}{\text{area}} = k_B T c_0^* (e^{-e\phi(h/2)/k_B T} + e^{e\phi(h/2)/k_B T} - 2) \quad (4)$$

The first two terms in Eq. 4 represents the interlayer contributions from  $\text{Na}^+$  and  $\text{Cl}^-$ , respectively and the last term is the ideal osmotic pressure of the bulk solution. The expression for the DLVO osmotic pressure is obtained by adding the attractive term originating from van der Waals interaction (Eq. 9 below) to Eq. 4. While it is clear that there is no direct electrostatic interaction between the two charged layers in Figure 4-3, it is equally obvious that Eq. 4 only makes sense for charged colloids, since neutral colloids do not require any charge compensating counterions. The origin of the repulsion in the DLVO theory is thus electrostatic but is manifested as an entropic term.

Both cations and anions contribute to the PB pressure in Eq. 4. An increase in  $c_0^*$  leads to lower pressure because  $|\phi|$  and in particular  $|\phi(h/2)|$  will decrease.  $F_{PB} > 0$  but approaches zero as  $\phi(h/2)$  eventually vanish at high  $c_0^*$ . If the charged layers in Figure 4-3 are not held in place with an opposing force the system will expand,  $h_1 \rightarrow h_2 > h_1$ , and  $F_{PB}(h_2) < F_{PB}(h_1)$ , thus  $|\phi(h_2/2)| < |\phi(h_1/2)|$ . The system responds to increasing layer separation similarly to increasing salt concentration. For the case of high salinity or large layer separation, Eq. 4 can be approximated by

$$\frac{F_{PB}}{\text{area}} = 64k_B T c_0^* \tanh^2\left(\frac{Ze\Phi_0}{4k_B T}\right) \exp(-\kappa h) \quad (5)$$

where  $\kappa$  is the inverse Debye screening length

$$\frac{1}{\kappa} = \left(\frac{k_B T \epsilon_0 \epsilon_r}{\sum_i (Z_i e)^2 c_{i,0}^*}\right)^{1/2} \quad (6)$$

and  $\phi_0$  can be found from

$$\sinh\left(\frac{Ze\Phi_0}{2k_B T}\right) = \frac{\sigma}{(8k_B T c_0^* \epsilon_0 \epsilon_r)^{1/2}} \quad (7)$$

The approximation to the PB pressure in Eq. 5 is valid for symmetric  $Z:Z$  salts but should, due to the limitation of the mean-field approach that underlies the PB theory, only be applied to 1:1 salts, i.e.  $Z = 1$ . Eq. 5 is derived by linearising the PB equation and is valid for  $\kappa h \gg 1$  (Dubois et al., 1992). Eq. 3 is in fact virtually indistinguishable to the exact numerical solution to the PB equation for  $\kappa h \geq 2$  (Liu and Neretnieks, 2008). Note that  $\kappa^{-1}$  is the Debye screening length in the external bulk electrolyte and  $h$  refers to the interlayer thickness. For a 1:1 electrolyte at 25°C, one finds that  $\kappa^{-1}(\text{nm}) = 0.304/\sqrt{c_0}$  where the concentration  $c_0$  is given in molar. For Na-montmorillonite in contact with 1 mM NaCl, Eq. 5 is applicable when  $h > 20$  nm, which corresponds to dry densities  $\rho_d < 130 \text{ kg/m}^3$ . With 100 mM NaCl, Eq. 5 will replicate the exact numerical solution for  $h > 2$  nm or  $\rho_d < 920 \text{ kg/m}^3$ . Na-montmorillonite with  $\rho_d = 110 \text{ kg/m}^3$  in 1 mM NaCl is a paste with considerable yield stress  $\sim 1$  kPa which is much above expected shear forces from flowing groundwater after resaturation of the buffer has occurred. (Eriksson and Schatz, 2015). Insofar as the PB theory describes the repulsion between charged colloids, Eq. 5 is an accurate representation covering the relevant dry densities, from paste to sol, that are important for colloid release erosion.

Eq. 5 can be used to judge the effect of temperature on the swelling pressure. The repulsive force in Na-montmorillonite increases with increasing temperature but the relationship is more complicated than the direct proportionality in Eq. 5, because the relative permittivity of water ( $\epsilon_r$ ) is temperature dependent and decreases with increasing  $T$ . This temperature dependence influences  $\kappa$  in addition to its explicit  $T$  dependence (Eq. 6), and  $\phi_0$  as shown in Eq. 7. Both  $\kappa$  and the magnitude of  $\phi_0$  increases with  $T$ . Their effect on Eq. 5 is dominated by the exponential dependence on  $\kappa$  so the temperature influence on the pressure is less than direct proportionality.

For high dry densities, above  $1400 \text{ kg/m}^3$  which is equivalent to an average separation between the clay layers of 1 nm or less, the molecular nature of water and ions becomes important which gives rise to additional repulsive forces (often termed hydration forces) not included in the DLVO theory (Hsiao and Hedström, 2017; Ruths and Israelachvili, 2008). Having a repository of spent nuclear fuel in mind, the DLVO theory is relevant starting point to describe the most adverse scenario, i.e., sodium-dominated bentonite swelling into a fracture filled with dilute water.

For very dilute Na-smectite systems, where  $h$  is in the order of the lateral dimensions of the clay layers, the rotational degrees of freedom will start to contribute to the repulsion and the parallel layer approximation breaks down. The effect of the rotational degrees of freedom is manifested as a plateau in the pressure versus clay concentration diagrams. Michot et al. (2004) used osmotic stress to determine the swelling pressures of Wyoming (SWy-2) Na-montmorillonite at salinities below the CCC in the clay concentration range 5 to 50 g/l. Comparison to the DLVO theory shows that the measured swelling pressures are higher than the calculated DLVO pressures and displays a pseudo plateau, that is particularly noticeable in the case of 10 mM NaCl as can be seen in Figure 4-4. The osmotic pressure of the pseudo plateau is  $\sim 500 \text{ Pa}$ , independently of NaCl concentration. Similar observations have also been made in osmotic stress measurements on laponite (a synthetic hectorite) that displays a pseudo plateau at  $\sim 1000 \text{ Pa}$  (Martin et al., 2006; Mourchid et al., 1995). The appearance of the pseudo plateau is explained in terms of an isotropic (free rotational state) to nematic (parallel layers) transition (Mourchid et al., 1995) as first suggested by Onsager (1949). Permanent birefringence appears for clay concentrations in the plateau region which demonstrates the presence of nematic ordering (Michot et al., 2004). So far, there is no straightforward equation that can capture this deviation from DLVO, although the Carnahan-Starling approximation for hard spheres seems promising for describing the pressures of the isotropic state, to the left of the plateau in the case of laponite (Mourchid et al., 1995).

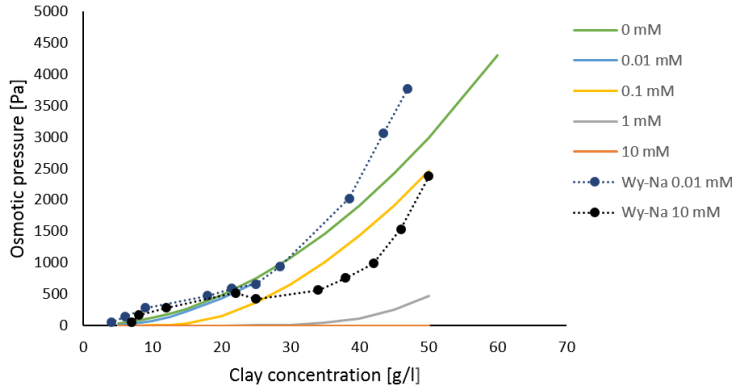


**Figure 4-4 Comparison between experimental osmotic pressure data (markers connected with dotted lines) (Michot et al., 2004) and calculated pressures from DLVO theory (smooth lines) (Börjesson et al., 2018).**

### Attractive forces

Colloidal systems are often sticky, so the colloidal particles tend to aggregate and settle under gravity (Witten and Pincus, 2010). Of the various attractive forces, the van der Waals interaction is always present and operates between any two molecules or atoms regardless of the species being electrically charged or not. Furthermore, the van der Waals force dominates at long distances because it falls off less rapidly than the repulsive forces. The van der Waals interaction between two large molecules or non-metallic colloidal particles is often calculated assuming that the interaction is pairwise additive (Evans and Wennerström, 1999; Russel et al., 1992). For coin-shaped or hexagonal clay layers, simulations based on pairwise additivity, show that the van der Waals interaction is greater for face-to-face arrangements than for edge-to-face arrangements (Jönsson et al., 2008). In the Hamaker theory, the van der Waals interaction between two colloidal particles is explicitly calculated based on strict pairwise additivity. The van der Waals interaction energy,  $U_{vdW}$ , of two clay layers (or other layered materials) in a face-to-face arrangement separated by a distance  $h$  is in the Hamaker treatment given by (Israelachvili, 2011; Russel et al., 1992)

$$\frac{U_{vdW}}{\text{area}} = -\frac{A_H}{12\pi} \left( \frac{1}{h^2} + \frac{1}{(h+2\delta)^2} - \frac{2}{(h+\delta)^2} \right) \quad (8)$$

which gives the force ( $-dU_{vdW}/dh$ )

$$\frac{F_{vdW}}{\text{area}} = -\frac{A_H}{6\pi} \left( \frac{1}{h^3} + \frac{1}{(h+2\delta)^3} - \frac{2}{(h+\delta)^3} \right) \quad (9)$$

where  $\delta$  is the thickness of each layer ( $\sim 1$  nm for smectites) and  $A_H$  is the effective Hamaker constant that incorporates the material properties of the colloidal particles and the intervening medium. Typical values of  $A_H$  for smectite-smectite interactions across an aqueous interlayer are  $1\text{-}2 \cdot 10^{-20}$  J, equivalent to  $2.5\text{-}5 k_B T$  at  $T = 298$  K (Iwata, 1994).

Eq. 8 shows that the interaction is attractive; at infinite separation  $U_{vdW} = 0$  and at finite separation  $U_{vdW} < 0$ . Likewise,  $F_{vdW} < 0$  showing that the force acts to prevent further separation, i.e., the force is attractive. Note that there are always repulsive forces present to prevent  $h$  become zero and therefore  $U_{vdW}$  and  $F_{vdW}$  will always be finite. Eqs. 8 and 9 also

show that  $U_{\text{vdW}}$  and  $F_{\text{vdW}}$  are proportional to the particle area or size since  $\delta$  is fixed. This means that clays with large lateral dimensions are more prone to stick together than clays with small lateral dimensions. Phase separation would occur if the attractive forces dominate repulsive forces and the magnitude of the energy minimum is larger than  $\sim k_B T$ . Thus, for a sol to be stable, the repulsive forces must prevent the particles from reaching a critical separation  $h_c$  where the attractive potential is on the order of  $k_B T$ , the thermal energy (Witten and Pincus, 2010). In the DLVO theory for parallel clay layers, the repulsive force is the mean-field electrostatic force calculated from Poisson-Boltzmann theory and the attractive force is solely given by Eq. 9 (Evans and Wennerström, 1999; Israelachvili, 2011; Witten and Pincus, 2010). Within this model for smectite, a cohesive state cannot be formed if  $h > h_c$  such that  $-U_{\text{vdW}}(h_c) \leq k_B T$ . For sufficiently large  $h > \delta$ ,  $U_{\text{vdW}}$  can to zeroth order be approximated by

$$U_{\text{vdW}} \approx U_{\text{vdW}}^{(0)}(h) = -\frac{A_H}{12\pi} A \cdot \frac{6\delta^2}{(h+\delta)^4} \quad (10)$$

where  $A$  is the surface area of the smectite particles. By setting  $U_{\text{vdW}}^{(0)} = -k_B T$ , Eq. 10 readily gives a zeroth order approximation to  $h_c$

$$h_c^{(0)} + \delta = \left( \frac{A_H}{k_B T} \frac{A\delta^2}{2\pi} \right)^{1/4} \quad (11)$$

Eq. 11 can be used as the initial value for an iterative solution of Eq. 8 that may be required in the case of small values of  $A_H$  and/or  $A$ . However, for  $h_c/\delta > 6$ , Eq. 11 gives the basal distance,  $h_c + \delta$ , within less than 1% error, so for realistic values of  $A_H$  and representative montmorillonite particle areas  $A \sim 10^4$ - $10^5$  nm<sup>2</sup> (Michot et al., 2004; Ploehn and Liu, 2006) Eq. 11 suffice. The variation of critical basal distance and critical particle volume fraction as a function of particle size is shown in Figure 4-5. The smectite particles are assumed to be coin-shaped and their size is represented by the diameter in Figure 4-5. When the single-porosity (interlayer only) model (Birgersson et al., 2017) is applicable, which by definition is the case when the particles are arranged in parallel, the particle volume fraction is given by (Neretnieks et al., 2009)

$$\phi = \frac{\delta}{h+\delta} \quad (12)$$

From the results in Figure 4-5, it is clear that larger particles have larger van der Waals interaction and therefore must be separated further to ensure the thermal energy to overcome attraction. The interaction strength as represented by  $A_H$  has similar influence on  $h_c$ . Note that  $A_H = 5 k_B T$  is the most representative value for smectite and the other values are presented for reference only (Iwata, 1994). For a realistic clay particle with  $A \sim 10^5$  nm<sup>2</sup> (Ploehn and Liu, 2006), Eq. 11 gives  $h_c = 15.8$  nm which is a large distance in contrast to the conditions in the bentonite buffer where  $h < 1$  nm. However, in comparison with the lateral dimensions the separation is still small, as illustrated in Figure 4-6. The critical volume fraction is  $\phi_c = 6\%$  which correspond to a dry density of  $\rho_d = \rho_s \phi = 165$  kg/m<sup>3</sup> based on a grain density of  $\rho_s = 2780$  kg/m<sup>3</sup> (Karnland et al., 2006). The value of 165 kg/m<sup>3</sup> is in stark contrast to experimental findings for montmorillonite gels.

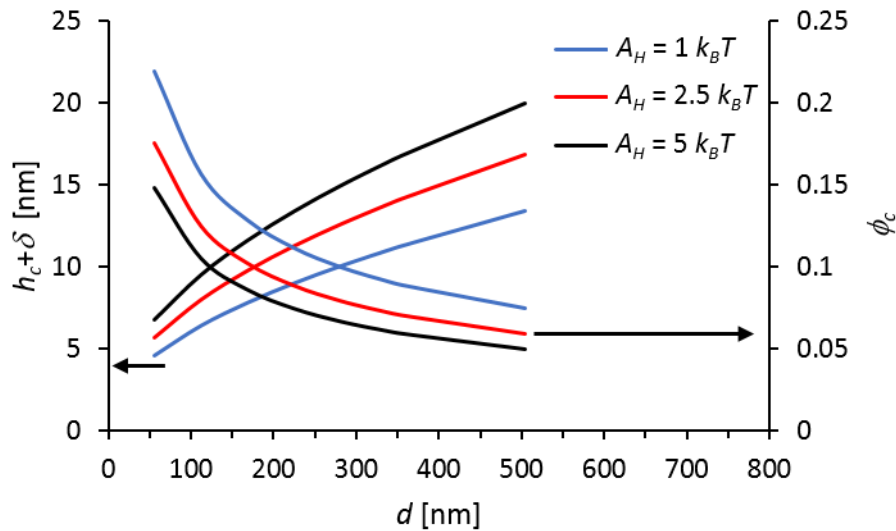


**Figure 4-5** Critical basal distance (left y-axis) and corresponding critical particle volume fraction (right y-axis) obeying  $-U_{vdW}(h_c) = k_B T$  in Eq. 8, as a function of the diameter of coin-shaped 1 nm thick particles, for three different values of the Hamaker constant.

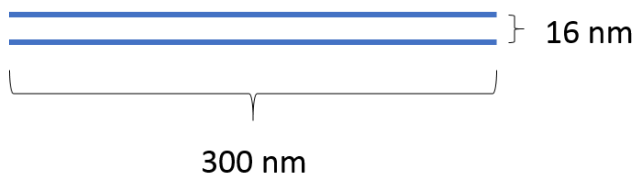


**Figure 4-6** Side view of two montmorillonite layers at a separation where the van der Waals attraction is of the order of  $k_B T$  (Hedström et al., 2016). The Hamaker constant is set to  $5 k_B T$ .

Gels have been observed at substantially lower values of  $\phi$  or  $\rho_d$  which consequently rules out van der Waals interaction between parallel clay layers as an explanation for gelling. The most commonly found explanation for gel formation is interaction between clay particle edges and faces (van Olphen, 1977, 1964). Two types of arrangements that can arise from the edge-face interactions are the house-of-cards and the overlapping coin structures shown in Figure 4-7.

Abend and Lagaly (2000) used a variety of rheological techniques to characterise Na-montmorillonite dispersions with different solid contents for a range of NaCl concentrations. Above the CCC, gels were formed at the lowest solid contents included in the study, 0.5% w/w ( $\rho_d \approx 5 \text{ kg/m}^3$ ,  $\phi = 0.18\%$ ) for Turkey 50M montmorillonite and 2% w/w ( $\rho_d \approx 20 \text{ kg/m}^3$ ) for Wyoming M40A montmorillonite. Direct observation can also be used to determine whether a gel is formed. Figure 4-8 shows a stable Na-montmorillonite gel with estimated  $\phi = 0.07\%$ . To put these values of  $\phi$  into perspective, consider the threshold volume fraction where montmorillonite layers with radius  $r$  can rotate freely. Each particle can be viewed as occupying a sphere, and at dense random packing the volume fraction of spheres is 0.64 (Goodwin and Hughes, 2008; Torquato et al., 2000). The threshold volume fraction is thus given by (Martin et al., 2006)

$$\phi = 0.64 \frac{\pi r^2 \delta}{(4/3)\pi r^3} = 0.96 \frac{\delta}{r} \quad (13)$$

With  $r = 150$  nm (Figure 4-6),  $\phi$  becomes 0.64% which is significantly higher than the values discussed above. For gels with  $\phi > 0.64\%$ , the house-of-cards structure would be possible, while for more dilute gels the overlapping coin configuration is required to provide a space-filling percolated network (Hedström et al., 2016). Coarse-grained simulations of pairs of laponite-sized particles ( $r = 18$  nm) showed that the overlapping coin configuration was more stable than a T-shaped arrangement of the two particles (Jönsson et al., 2008). With an increased number of laponite particles, a larger variety of configurations were found, house-of-cards, overlapping coins (Delhorme et al., 2012a) and various liquid crystalline phases (Delhorme et al., 2012b) depending on volume fraction and concentration of excess NaCl (aq).

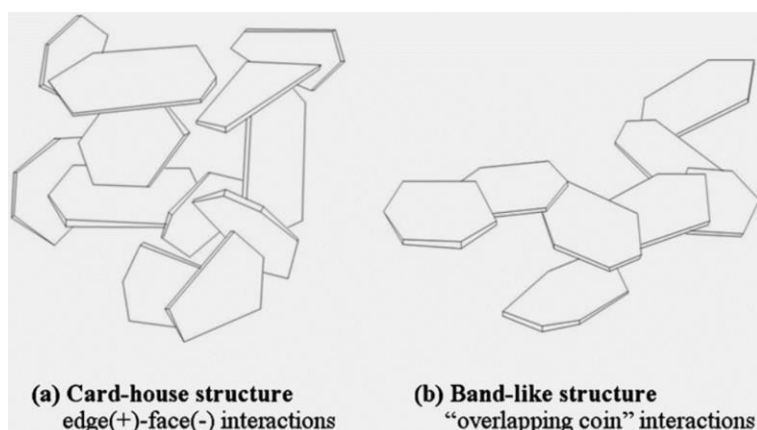


**Figure 4-7** Cartoons of proposed clay gel structure (Goh et al., 2011).



**Figure 4-8** Na-montmorillonite gel formed in mixed NaCl/NaOH solution of ionic strength 15 mM and pH ~11. Initially the vial was standing upright and filled with montmorillonite sol that was settling and slowly gelling and consolidating. After the gel was formed, the vial was placed horizontally, and the gel eventually unfastened from the glass and flipped forward. Based on turbidity, the clay concentration in the gel is estimated to be less than 2 g/l, equivalent to a volume fraction of 0.07%. Note that the gel is fully surrounded by electrolyte. The snapshot to the left was taken ca 7 years after gelling (Hedström et al., 2016) and the right snapshot is recent to demonstrate that the gel remains stable.

Although gels are formed because of the interaction between clay particle edges and faces there is still, after almost seven decades, no consensus regarding the nature of this interaction. Transmission electron microscope images of kaolinite clay particles mixed with negatively charged gold colloids showed that the gold particles only adsorbed to the edges (Thießen, 1947). Van Olphen suggested that the flocculation in Na-montmorillonite is due to the interaction of the negatively charged face with a positively charged edge that behaves similarly to aluminium oxide (van Olphen, 1956, 1951). For neutral and acidic conditions, the idea of positive edge charge seems uncontroversial, while for basic conditions the opinions

differ. In principle, acid-base titrations have the potential to provide pKa values for the titratable edge sites (Avena and De Pauli, 1998; Kraepiel et al., 1998; Tertre et al., 2006; Tombácz and Szekeres, 2004; Wanner et al., 1994) that could help resolve the issue of protonation state at high pH, in particular. However, a study of published data showed that the pKa values were spread over 10 pH units (Duc et al., 2005).

Avena (2003) used the Multi-Site Complexation (MUSIC) model (Hiemstra et al., 1989), which is based on Pauling's bond valence concept, to analyse the protonation of clay. The MUSIC model suggested the edge Si-OH groups to be rather unreactive (neutral < pH ~11.9) while the edge Al-OH<sup>1/2-</sup> can undergo protonation and become positively charged at pH ≤ 10. The small influence on the CCC with increasing pH as observed by several authors could be rationalised with the assumption of a net positive edge charge (Birgersson et al., 2009; Tawari et al., 2001). For example, an increase in pH from 6 to 9 CCC resulted in a change in CCC from about 10 to 30 mM NaClO<sub>4</sub> in Wyoming SWy-1 montmorillonite, while the effect of pH was even less for Otay montmorillonite where CCC increased from 8 to 12 mM (Hetzel and Doner, 1993). Similarly, the CCC for Wyoming montmorillonite was 30 mM for both NaCl (pH 6.5) and NaOH (pH 12) (Lagaly and Ziesmer, 2003). The effect of the pyrophosphate anion (P<sub>2</sub>O<sub>7</sub><sup>4-</sup>) is often also used to support the notion of a positive edge charge. The argument assumes that this polyvalent anion binds to the positive edge charges and thereby prevent the Coulombic attraction between edges and faces (Martin et al., 2002; Mongondry et al., 2004). Indeed, a small addition of Na<sub>4</sub>P<sub>2</sub>O<sub>7</sub><sup>4-</sup> to a 7 % wt. bentonite slurry caused the yield strength to vanish in the pH range 5-10 (Goh et al., 2011) and 0.1 mM Na<sub>4</sub>P<sub>2</sub>O<sub>7</sub><sup>4-</sup> added to a dilute Wyoming Na-montmorillonite suspension raised the CCC to 195 mM NaCl (Lagaly and Ziesmer, 2003).

On the other hand, several authors argue that the montmorillonite edge is positively charged only below pH 6.5-7 and increasingly negative at higher pH (Abend and Lagaly, 2000; Permien and Lagaly, 1994; Tombácz and Szekeres, 2004). The suggested mechanism for the formation of gels at high pH, is van der Waals attraction between negatively charged edges and faces. The repulsion between an edge and a face will be smaller and therefore a lower salinity is required to screen the Coulomb repulsion compared to a face-face aggregation (Abend and Lagaly, 2000). Further, the binding of pyrophosphate to the edge is said to be caused by ligand exchange, P<sub>2</sub>O<sub>7</sub><sup>4-</sup> replacing structural OH groups, thereby increasing the negative edge charge density (Permien and Lagaly, 1994).

However, the suggestion of face(-)—edge(-) aggregation is somewhat contradicted by the simulation results on laponite-sized particles. It was shown that van der Waals attraction only plays a minor role at low salt concentrations. The van der Waals interaction modulates the balance between attractive and repulsive interactions and can reinforce the attractive minimum between a positive edge and a negative face. However, if the amount of positive edge charges is reduced, both types of minima (house of cards and overlapping coins Figure 4-7) disappear (Jönsson et al., 2008).

A third type of attraction that is especially important for polyvalent counterions is caused by ion-ion correlations. These correlations are the reason for the failure of the PB equation to describe Ca-montmorillonite (Kjellander et al., 1988). It was shown above that on average there is no electric field at the midplane between the two halves of a clay interlayer (Figure 4-3). However, individual ions are mobile in both the transverse and the lateral directions. The lateral fluctuations in ion positions cause each configuration to produce instantaneous fields at the midplane. Each half of the system respond to the electric field fluctuations caused by the other half to adjust the instantaneous charge distribution to lower the total energy. This

correlation implies an attractive force. The magnitude of the attraction depends on the layer charge density, layer separation, and valence of the counterion (Evans and Wennerström, 1999). This is a classical counterpart to the quantum mechanical dispersion force (van der Waals) and for spherical colloids it can be shown that the correlation free energy decays like  $r^{-6}$ ,  $r$  being the separation between the centres of the colloids (Jönsson et al., 1998). For layered systems, there is no algebraic expression for the correlation attraction. Instead, it must be evaluated with either simulations (Bratko et al., 1986; Guldbrand et al., 1984; Wennerström et al., 1982) or through numerical solutions of advanced integral equation theories for inhomogeneous fluids (Kjellander, 1988; Kjellander et al., 1988; Kjellander and Marčelja, 1984). For divalent counterions, the correlation interaction can outweigh the entropic contribution from the midplane concentration. Ion-ion correlation is the most plausible explanation to the observed limited swelling of Ca-montmorillonite (Jönsson et al., 2009; Kjellander et al., 1988). Ca-montmorillonite in contact with deionised water through 100 $\mu$ m filters did not erode despite the swelling pressure in the clay was above 5 MPa (Birgersson et al., 2009). This test demonstrates that Ca-montmorillonite do not transform to a sol which is attributed to the limited expansion ability because of the correlation attraction.

## 4.2 Rheology of different clay phases

The rheology of bentonite is of great practical importance. One of the main uses for bentonite is in the oil and gas industry as a drilling fluid. Therefore, a lot of work has been put into determining the rheological properties of bentonite slurries, and how these properties can be modified with various additives (Abend and Lagaly, 2000; Goh et al., 2011). Using water-based drilling fluids also presents a challenge as it can cause wellbore instability due to swelling in reactive clay-based shale formations. This necessitates swelling inhibitor additives to the drilling fluids, traditionally high concentration of KCl but other polymer-based compounds are being developed (Anderson et al., 2010). The issues that the oil and gas industry must deal with are in principle complementary to the issues that arise in the case of chemical erosion in a repository for spent nuclear fuel. Since chemical erosion is a scenario that may occur only after a very long time, one cannot rely on artificial modifications of bentonite. Instead the rheological properties of the montmorillonite will depend on the groundwater evolution. Thus, a large amount of work on clay rheology will be omitted in this review, in favour, with a few exceptions, of studies that are directly relevant to and focussed on future repository conditions. Rheology is a tool to understand and predict the overall behaviour of the different montmorillonite phases. Both gels and pastes have solid-like features, and the determination of yield strength will answer whether these phases are expected to withstand the shear forces of the flowing water in a fracture intersecting the deposition hole (Eriksson and Schatz, 2015; Hedström et al., 2016). The montmorillonite sol is a fluid, so an important property is the viscosity and its dependence on concentration. The sol viscosity, together with hydraulic gradient and fracture aperture, determines the flow field outside the paste in the fracture intersecting the deposition hole (Neretnieks et al., 2009).

### 4.2.1 Rheology of pastes and gels

Phase diagrams of three different Na-montmorillonites have been determined by means of visual inspection and Figure 4-9 illustrates how this was done (Hedström et al., 2016).



**Figure 4-9 Identification of a) sol, b) gel, and c) paste (Hedström et al., 2016). Note that the test tubes are filled with electrolyte. The lines on the test tubes mark the initial volume of clay/electrolyte mix before the additional electrolyte was added. The lack of yield strength is clearly observable in the sol. Likewise, the gel shows yield strength and does not expand beyond its original volume, nor does any mixing of montmorillonite with the excess electrolyte occur. The paste in c) expands beyond its original volume due to the osmotic pressure.**

The test tubes were first partially filled with a montmorillonite/NaCl(aq) mixture, which could be paste-like or more fluid, depending on NaCl concentration and montmorillonite concentration. The height of the montmorillonite/NaCl(aq) mixture was marked on the test tubes. Subsequently, additional NaCl solution of the same concentration as in the clay mixture was added to completely fill each test tube. After the test tubes were filled and sealed, they were placed on the side or completely horizontally if the samples displayed yield strength. Visual inspection of how the montmorillonite/NaCl(aq) mixture evolve in the test tube reveals the phase, sol, gel or paste as shown in Figure 4 9. In Figure 4 9 c, the electrolyte concentration is above the CCC, therefore as the paste expands, it turns into a gel.

The phase diagram for Wyoming Na-montmorillonite (from MX-80) is shown in Figure 4-10. The salinity range is 5-35 mM, in steps of 5 mM. With this grid the CCC is located between 15 and 20 mM NaCl, since below this salinity only pastes or sols have been detected. For salinities above the CCC, the phase diagram can be used to predict the density of gel at the front of a swelling paste, which is indicated by the solid line between paste and gel in Figure 4-10. Gels to left of the dividing line cannot be reached from a swelling paste, but only obtained by adding NaCl to Na-montmorillonite suspensions/sols. Thus, these gels are not directly related to the erosion scenario in a repository, but of a more academic interest. The methodology outlined Figure 4-9 gives unambiguous answers for gels, dilute sols, and pastes at NaCl concentrations above 20 mM. The method is less accurate to determine the paste/sol border, because the swelling of the paste may dilute it to a sol. For example, 40 g/l Na-montmorillonite in 10 mM NaCl is labelled as a sol in Figure 4-10, because the system showed liquid behaviour, but it cannot be ruled out that this was caused by paste to sol transformation at the front that eventually progressed to the whole sample. Wyoming Na-montmorillonite from SWy2 at 40 g/l has a substantial yield stress (> 100 Pa) in deionised water, which is clearly indicative of a paste (Baravian et al., 2003), while a 28 g/l ( $\phi = 1\%$ ) Wyoming Na-montmorillonite suspension in 1 mM NaCl is a shear thinning sol with only marginal yield stress (< 0.02 Pa) (Eriksson and Schatz, 2015).

The expected shear stress on the bentonite front from flowing water in a fracture can be obtained from a force balance of flow in a slit with no-slip conditions. The shear stress on the fracture walls is readily calculated, and can be shown to be larger than the stress on the bentonite front (Börgesson et al., 2018) and therefore represents an upper value given by (Börgesson et al., 2018; Eriksson and Schatz, 2015; Neretnieks et al., 2009)

$$\tau = \frac{1}{2} a \rho_w g \frac{\Delta L}{L} \quad (14)$$

where  $a$  is the fracture aperture and  $\Delta L/L$  is the hydraulic gradient. Even for an unrealistically large hydraulic gradient of 0.1 m/m and a wide aperture of 1 mm, the estimated shear stress on the bentonite front is less than 0.5 Pa (Neretnieks et al., 2009). This value is still well below measured yield stresses for montmorillonite gels (Birgersson et al., 2009; Børgesson et al., 2018; Eriksson and Schatz, 2015; Hedström et al., 2016).

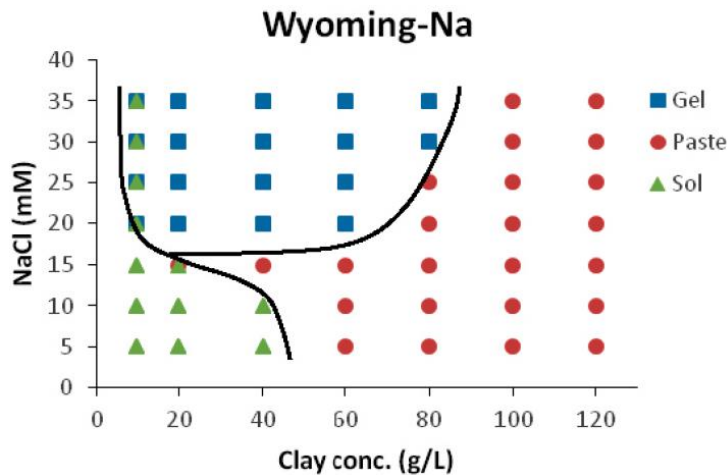


**Figure 4-10 Phase diagram for Wyoming Na-montmorillonite (Hedström et al., 2016).**

With the purpose to investigate the effect of increasing NaCl concentration on the yield stress of montmorillonite (Mt) gels, rotating-vane rheometry was performed on Kutch-Mt (montmorillonite extracted from Asha 505 bentonite from the Kutch area, Gujarat region, Ashapura Group India) gels at clay concentrations 10 and 20 g/l. The CCC value for Kutch Na-montmorillonite is 3-5 mM NaCl, i.e., much lower than for Wyoming Na-montmorillonite. This makes Kutch-montmorillonite suitable for testing the effect of NaCl concentration. The chosen clay concentrations are also to the left of the paste-gel border and significantly lower than the expected clay concentration at the bentonite front in a repository. Still, the measured yield stress values at the lowest NaCl concentration (5 mM) were 1.1 and 7.7 Pa for montmorillonite concentrations of 10 and 20 g/l, respectively (Hedström et al., 2016).

In a subsequent study, the rheology of Wyoming Na-montmorillonite at the gel/paste border was examined (Børgesson et al., 2018). The shear stress vs time (strain) behaviour of the Na-montmorillonite samples was determined by means of rotating-vane rheometry, using a four-bladed vane-spindle (Brookfield V-74). All tests were performed at a rotational speed of 0.05 rpm. The shear stress response for three Wyoming Na-montmorillonite samples in 20 mM NaCl are shown Figure 4-11. Initially there is an elastic response while for larger strain (time) the stress deviate from the linear and eventually at a critical strain the stress reaches a maximum before the structure breaks. The maximum stress was recorded as the yield stress of the gel. The yield stress increased with increasing rest time. This is especially evident as the rest time is increased from 1 to 18 hours as shown in Table 4-1. For all three gels the yield stress is significantly higher than the maximum expected shear from flowing water in a fracture intersecting the repository. The same tests were also performed on the three samples before NaCl was added. In this case of no excess salt, the systems were pastes and this was reflected in a substantially different shape of the stress response to shearing time and shown in Figure 4-12. The elastic response lasted longer for all three samples and after the maximum stress there was no drop in the stress. This was interpreted as the structure was constantly

healed, due to the repulsive forces that dominate the pastes, while for gels that are held together by attraction forces, the rupture does not heal within the timeframe relevant for the test. The maximum stresses of the pastes were also significantly higher than for the gels. Further, a rest time of 2 hours gave virtually no difference in the stress-time curve for the 50 g/l sample compared to a rest time of 4 days. Figure 4-12 demonstrates that the pastes would withstand the estimated shear from flowing water in a fracture. However, pastes could still expand in contact with water in the fracture and thereby be susceptible to erosion due to transformation to sol. This process is not governed by flow but by the swelling pressure in the paste and possibly modulated by wall friction (Birgersson et al., 2009; Börgesson et al., 2018).

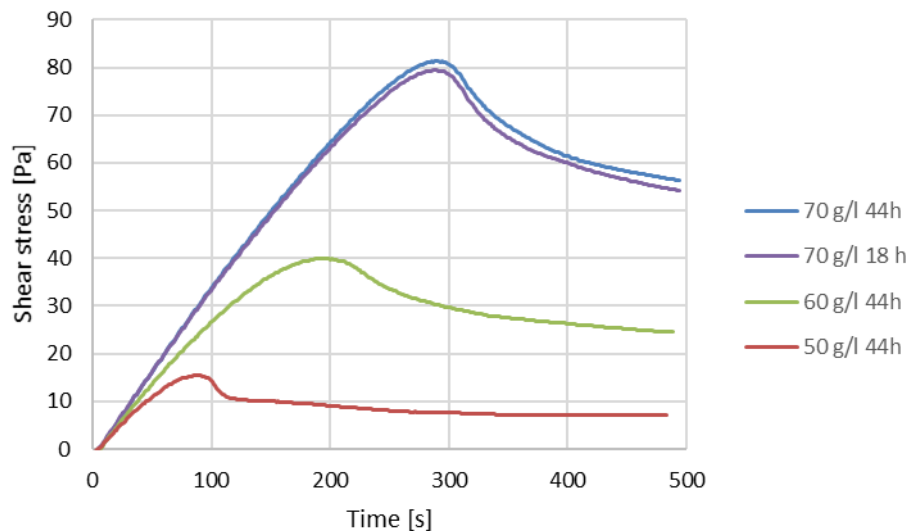


**Figure 4-11** Shear stress vs shearing time of Wyoming Na-montmorillonite in 20 mM NaCl concentration. The rest time after vigorous agitation was 44 h for all samples. For comparison the result after 18 h rest time is also shown for the 70 g/l sample. (Börgesson et al., 2018).

**Table 4-1** Maximum yield stress at 20 mM NaCl after different rest times for the three Wy-Na samples.

C <sub>Clay</sub> [g/l]	$\sigma_{max}$ [Pa] (after different rest times)		
	1 h	18 h	44 h
50	5.3	11.5	15.3
60	16.5	33.6	39.8
70	53.5	79.4	81.3

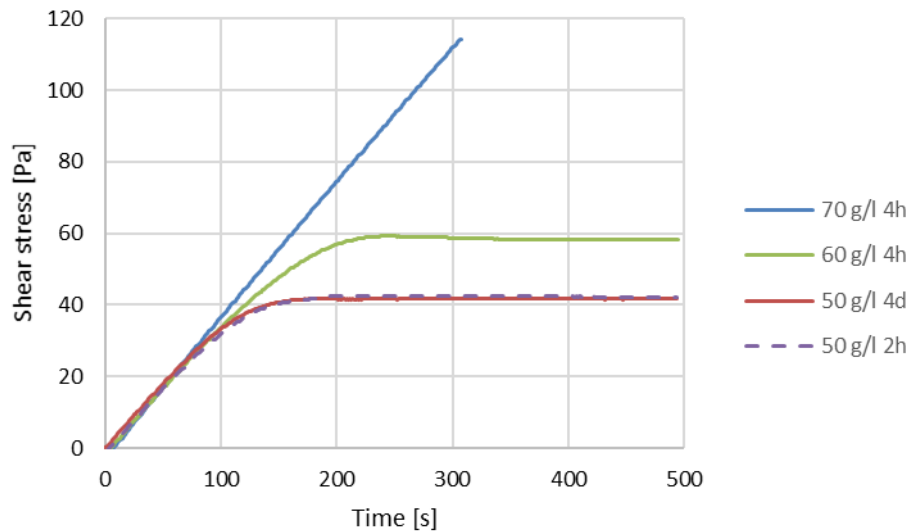


**Figure 4-12** Shear stress vs shearing time of Wyoming Na-montmorillonite under salt free conditions. The rest time after agitation was 4 hours for the 60 and 70 g/l samples and for the 50 g/l sample it was 4 days, and then a repeated test with 2 hours rest time after vigorous agitation was performed. For the 70 g/l sample the test was terminated when the stress reached the limit of the instrument. (Börgesson et al., 2018).

The rheology of Wyoming montmorillonite (extracted and purified from MX-80 bentonite) was also studied by Eriksson and Schatz (2015) for a number of solids volume fractions, ranging 0.5 to 15 vol%. Homoionic Na-montmorillonite as well as 50/50 Na/Ca-montmorillonite were included in the study and examined at two different NaCl concentrations, 1 and 17 mM respectively. The authors use the term gel for any state that display yield stress instead of distinguishing between gels and pastes. However, the information about the studied systems is abundant, so gels and pastes can readily be identified and related to, e.g., the phase diagram in Figure 4-10. The study was motivated by the observed difference between paste and sol in artificial fracture tests. The artificial fracture tests are discussed in more detail in section 4.3.1 and a schematic of the setup is given in Figure 4-18. An overhead image of such test with Wyoming Na-montmorillonite and flowing deionised water is shown in Figure 4-13. There is an inner solid zone (paste) that is unaffected by the flow, and an outer zone (sol) that is transported by the flow. By rotating the artificial fracture 90°, it was observed that the sol sedimented while the paste largely resisted gravity. It was concluded that erosion involves mass transfer from paste to sol. The solids content of the paste near the boundary to the sol zone was estimated to be less than 5 vol.%. No estimate of the solids content of the sol in the outer zone was given.

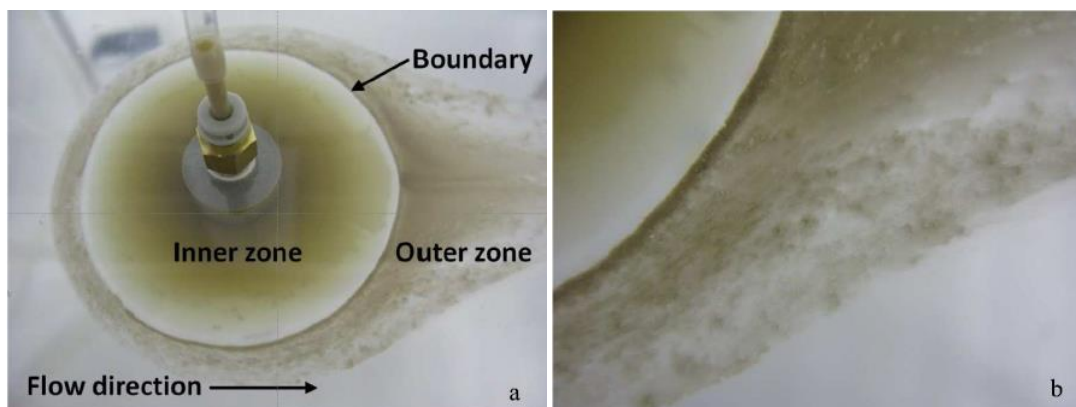


**Figure 4-13** Overhead images of an artificial fracture test with sodium montmorillonite against deionised water flowing at a velocity of  $\sim 2 \times 10^{-4}$  m/s in a 1 mm aperture fracture 456 h after start of test showing a) the complete inner and outer zones, and b) a close-up of the sharp boundary between them. The direction of flow in the fracture is from left to right in the above images (Eriksson and Schatz, 2015).

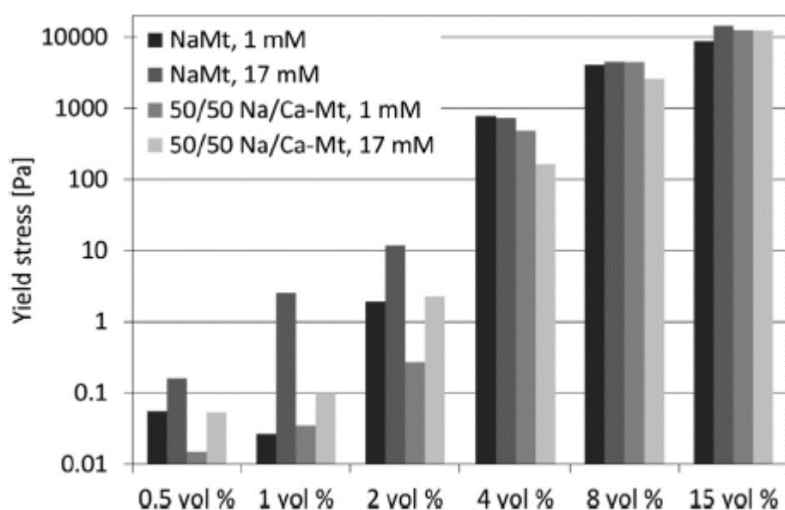


**Figure 4-14** Summary of yield stress measurements as given in (Eriksson and Schatz, 2015). The tests were performed at two NaCl concentrations 1 and 17 mM, respectively.

The yield stress measurements are summarised in Figure 4-14. At the lowest particle volume fraction  $\phi = 0.5\%$ , the measured yield stress is very low for all systems. At  $\phi = 1\%$ , the result for Na-montmorillonite in 17 mM NaCl clearly stands out. As yield stress can only develop as a result of either repulsive forces as in the case of pastes or as a result of attractive forces as in the case of gels, the result in Figure 4-14 suggests that Na-montmorillonite with  $\phi = 1\%$  in 17 mM NaCl is a gel, which is also consistent with the phase diagram for Wy-Na in Figure 4-10. Note that the repulsive PB force (Eq. 5) is larger for Na-montmorillonite in 1 mM NaCl than in 17 mM NaCl. Therefore, the difference in yield stress between these two systems cannot be explained by the repulsive force. For the systems with  $\phi = 2\%$ , one observes a significant increase in yield stress for the low salt systems. This is mainly due to repulsive interactions and one may conclude that the mixed 50/50 Na/Ca has lower repulsion, which is also in accordance with theoretical predictions. The finding that 50/50 Na/Ca-Mt in

17 mM NaCl gives the same yield strength at Na-Mt in 1 mM NaCl, strongly suggests that the former system is a gel. For  $\phi \geq 4\%$ , the results in Figure 4-14 suggests that these systems are pastes and located to the right in the phase diagram.

Both the pastes and the gels were found to have yield stresses well above the shear stress of flowing water, confirming the observations made with the artificial fracture setup (Figure 4-13). This further strengthens the conclusion that erosion involves a mass transfer process from paste to sol (Eriksson and Schatz, 2015).

#### 4.2.2 Rheology of suspensions/sols

The viscosity measurements by Eriksson and Schatz on  $\phi = 1\%$  suspensions gave results that are somewhat in contradiction with other measurements. Firstly, it is suggested that these suspensions show predominantly Newtonian character, with marginal shear thinning with increasing shear rate. Other studies have found strongly shear-thinning behaviour for these systems (Baravian et al., 2003; Birgersson et al., 2009). Further, these studies also suggest about an order of magnitude larger viscosity for Wy-Na montmorillonite at  $\phi = 1\%$ .

An example of shear-thinning of Wyoming Na-Mt (SWy2) is shown in Figure 4-15. The authors state that some NaCl from the homo-ionisation procedure remains in the montmorillonite and the estimated concentration in the suspensions is 1 mM (Baravian et al., 2003). The suspension with 5 g Mt/l is Newtonian and the viscosity is just slightly above that of water. With Mt concentrations above 30 g/l the viscosity diverges at low shear stresses which would give the suspensions a solid appearance.

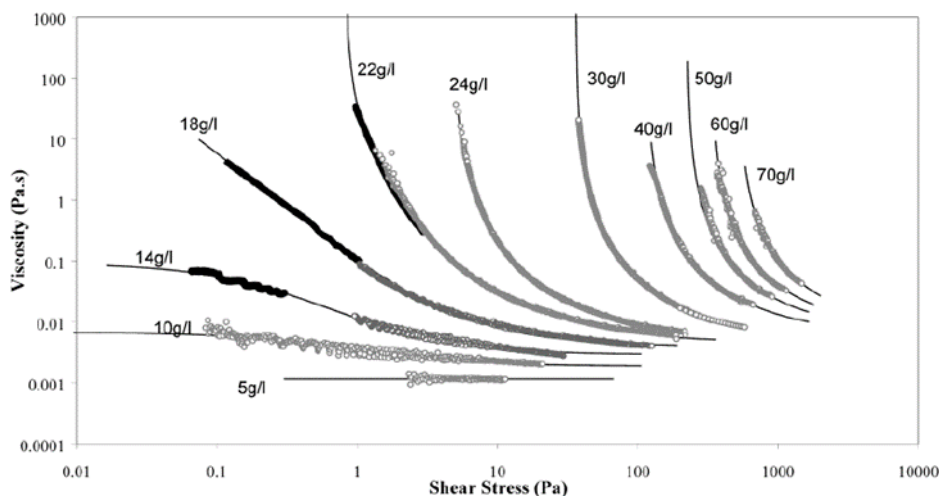


**Figure 4-15 Viscosity-shear stress variation for Wyoming Na-Mt (SWy2) suspension at various concentrations: solid curve, model; black symbols, cone and plate experiments; grey symbols, parallel plate experiments (Baravian et al., 2003).**

In partial agreement with Figure 4-15, Birgersson et al. (2009) found that suspensions with water content ( $w$ ) below 35 ( $\sim 28\text{g/l}$ ) were too stiff to be tested with the Brookfield LV cylindrical spindle (concentric cylinder and bob) setup. However, the results for water content of 35 shown in Figure 4-16, suggest lower viscosities than reported by Baravian et al. (2003). In addition to shear-thinning behaviour of the  $w = 35$  suspension, one also notices the decrease in shear stress and therefore viscosity with increasing NaCl concentration (Figure 4-16). The reason for this is the decreasing repulsion with increasing salinity as discussed earlier (Eq. 5). Prior to each measurement the suspension was vigorously shaken, and the viscometer was started immediately after the suspension was transferred (using a syringe) to

the cylindrical cup. This procedure explains why even systems with NaCl concentration above the CCC (~20 mM) behave like liquids. Any gel in the suspension was disrupted by the shaking, and the time before the measurement was started was shorter than the time for the gel to regenerate.

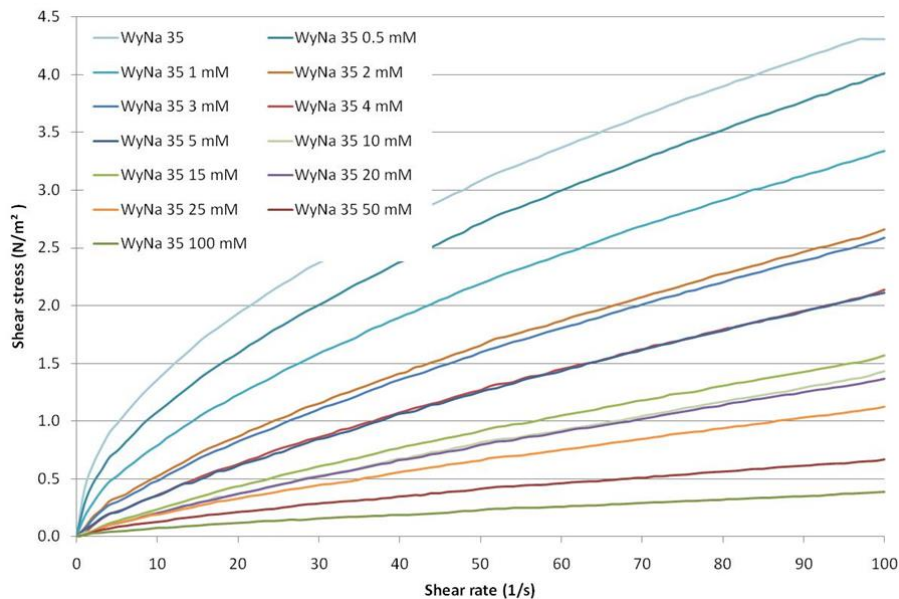


**Figure 4-16** Shear stress as a function of shear rate for Wy-Na-Mt at water content 35 and different NaCl concentrations (Birgersson et al., 2009).

The stress vs shear rate curves in e.g., Figure 4-16, could be modelled with a power law (Birgersson et al., 2009), but with parameters that change with salinity. Thus, such model gives little idea of the physics behind both the non-Newtonian behaviour and the influence of salt.

Baravian et al. (2003) developed an extended hard-sphere model for interacting discs: In dilute suspensions the diameter of the hard sphere is given by the diameter of a coin-shaped clay layer, while for more concentrated suspensions the clay layers will be forced to align. The model captures the measurements well as shown by the solid lines in Figure 4-15. However, the coin diameter is a fitting parameter and is somewhat different from the expected physical diameter of a clay layer, suggesting that it incorporates additional effects such as hydrodynamic forces, counterion swarm and non-rigidity of the particles (Baravian et al., 2003).

Neretnieks et al. (2009) also proposed a viscosity model based on the concept of effective spherical volume of the clay particles. In an unconventional manner, the Debye length is added to the rim of the clay particle, which makes the effective volume of each particle to increase with decreasing salinity. The viscosity is evaluated as a polynomial up to third order in the effective volume fraction (co-volume fraction) and it fits measured viscosities well for a range of clay concentrations and NaCl concentrations below the CCC (Figure 4-17). The model assumes that the clay particles can rotate freely and is thus limited to more dilute systems, although it seems to work also when the spherical volumes interpenetrate. The clay diameter is a fitting parameter, and the best fit was obtained with a diameter of 220 nm.

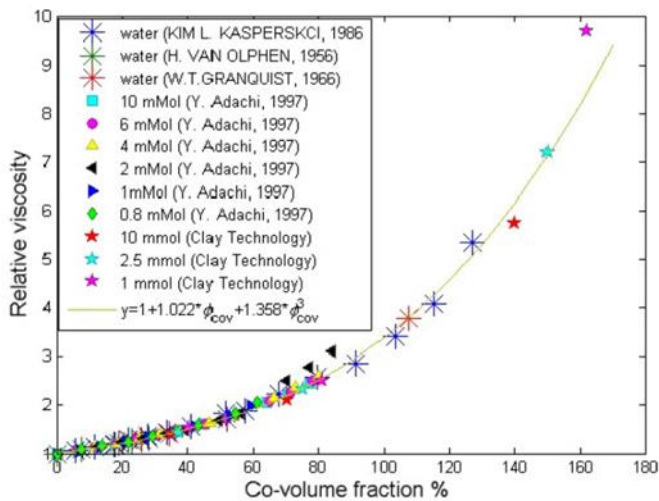


**Figure 4-17** Relative viscosity of montmorillonite suspensions as a function of co-volume fraction. The highest actual volume fraction is <0.9%. From Neretnieks et al. (2009).

### 4.3 Erosion experiments involving bentonite or montmorillonite

Unless otherwise stated, the tests reviewed in this section will be those performed under conditions where erosion is expected. The bentonite/montmorillonite will contain enough Na<sup>+</sup> to be sol forming and the contacting solution having a salinity below the CCC (Birgersson et al., 2011, 2009; Hedström et al., 2011).

#### 4.3.1 Erosion tests using artificial fractures

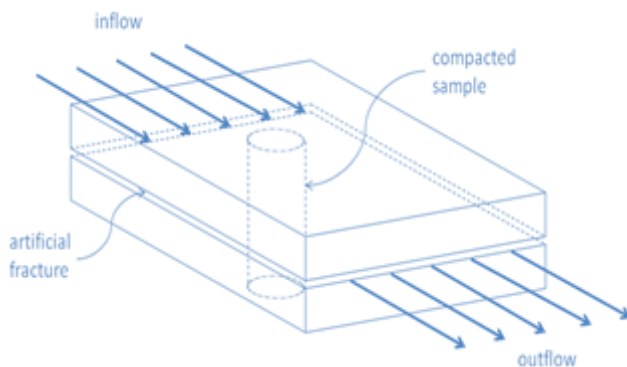


**Figure 4-18** Example of artificial fracture setup for erosion tests (Schatz et al., 2013).

Several groups have performed erosion tests using artificial fractures (Alonso et al., 2019; Hedström et al., 2016; Reid et al., 2015; Schatz et al., 2013; Schatz and Akhanoba, 2017; Vilks and Miller, 2010) and a compilation of the setup parameters used by the various groups is summarised in Table 4-2. An often-used setup is based on a modified Hele-Shaw cell made from transparent polymer, e.g. poly(methyl methacrylate). The setup has an inflow and outflow and, in most experiments, a cylindrical compartment for the clay sample as illustrated in Figure 4-18. The aperture is regulated using spacers of various thickness. One potential problem with this setup is that the swelling pressure of the emplaced clay will to various degree cause bulging and thereby introduce aperture uncertainty, especially near the clay. One group has circumvented this problem by using an annular compartment that allows for a bolt through the middle of the emplaced specimen. This design feature prevents deformation of the test cell as the swelling pressure builds up and makes certain that the aperture at the specimen

is the same as the nominal aperture of the setup (Hedström et al., 2016). The transparent setup allows for monitoring the extrusion by photography. Erosion rates are deduced from the clay concentration in the effluent which can be measured by a number of methods including fluorescence spectrophotometry (Vilks and Miller, 2010), turbidity (Hedström et al., 2016), Photon Correlation Spectrometry (PCS) (Alonso et al., 2019), and gravimetric either after the liquid has evaporated (Schatz et al., 2013) or by filtering the effluent and weighing the dried filter paper (Reid et al., 2015).

The experiments with artificial fractures performed in the BELBaR project have been summarised before (Neretnieks and Moreno, 2018b). To compare the reported erosion rates between different tests as well as between different laboratories, the erosion rate can be normalised to the area at which the erosion takes place. This area is calculated from the circumference of the extruded clay times the assumed fracture aperture. The reported normalised erosion rates in the BELBaR project range from 5.4 to 1288 kg/m<sup>2</sup>/a, Table 4-1 in (Neretnieks and Moreno, 2018b). With such a range of reported values, any attempt at empirical modelling of a single dataset is fruitless. Note that a rate of 100 kg/m<sup>2</sup>/a would translate to an erosive mass loss of 60 kg over a period of 1000 years, assuming a diameter of 2 m of the extruded bentonite and a fracture aperture of 100 µm. In the present report, the normalised erosion rate will not be further discussed. Instead, factors that may have contributed to the large differences in the reported data, will be examined.

**Table 4-2 Compilation of experimental setup parameters used by the different research groups. Deionised water (DI), Grimsel water (GW), montmorillonite (Mt), bentonite (Bt). 50/50 Na/Ca Mt are produced by mixing equal weights of Na- and Ca-Mt.**

Aperture (mm)	Sample dimensions diameter, height	Clay type	Water type	Reference
1, 5	37 mm (d) 10 mm (h)	Bt Wy, Osage Wy-Na-Mt Wy-Ca-Mt	DI GW	Vilks and Miller (2010)
1	20 mm (d) 20 mm (h)	MX-80 Bt Wy-Na-Mt 50/50 Wy- Na/Ca-Mt	DI GW (2xGW) NaCl: 2.1, 4, 4.3, 17, 171 mM	Schatz et al. (2013)
0.12, 0.24	Annulus 35 mm (d <sub>o</sub> ) 15 mm (d <sub>i</sub> ) 10 mm (h)	Wy-Na-Mt 50/50 Wy- Na/Ca-Mt	DI GW NaCl: 1-7, 10, 15, 20, 25 mM	Hedström et al. (2016)

Hydraulic aperture: 0.054	20 mm (d) 10 mm (h)	MX-80 Bt	DI	Reid et al. (2015)
0.1, 0.2, 0.4, 1, 1.7	19 mm (d) 10 mm (h)	Nanocor® Na-Mt  MX-80 raw & washed  Wy-Na-Mt  Wy-Ca-Mt  Ibeco Bt  MCA-C saponite	NaCl: 1, 10, 100 mM	Alonso et al. (2019)

### ***Erosion in horizontal artificial fractures***

The modified Hele-Shaw cell can be used for studying the expansion of the clay vs time in either stagnant water or flowing water. In stagnant water, it is mostly found that the expansion is rapid in the beginning but will reach a plateau where no more expansion is discernible within the experimental timeframe. In tests with fracture aperture  $\geq 1$  mm, expansion had been reported to be continuing at test termination.

Figure 4-19 shows the state of Na-Mt after 30 days of expansion into a 0.12 mm aperture fracture filled with stagnant deionised water. The clay was water saturated in a swelling pressure test cell with diameter 35 mm and the height was set to 10 mm. The nominal dry density was  $1257 \text{ kg/m}^3$  which corresponds to a water-saturated density of  $1800 \text{ kg/m}^3$ . After water saturation was completed a hole with diameter 15 mm was drilled in the centre of the clay cylinder, and then the clay was fitted into the annular compartment of the artificial fracture test cell. The fracture was filled with deionised water and was placed horizontally. Outside the emplaced montmorillonite there is an approximately 1 cm wide opaque region of denser montmorillonite paste. It should be noted that this paste region never expanded beyond 10-15 mm in any of the tests with 0.12 mm aperture (Hedström et al., 2016). The paste is strong enough that as it expands, it pushes air bubbles in the fracture ahead of itself, rather than surrounding them, and that in all tests, the paste withstood the shear forces of flowing water even up to velocities of 2.5 m/h. In deionised water the expansion of the paste was fast and completed within a week. Outside the paste there is an almost transparent region that exhibits a fingering instability akin to the Rayleigh-Taylor instability (RTI). Hedström et al. (2016) viewed this phase as a dense sol, because the occurrence of RTI suggests a liquid and this phase also flows under shear. But one could speculate that it is a nematic liquid crystalline phase as discussed by Michot et al. (2004). The average clay concentration of the erodible clay outside the paste region was measured to about 30 g/l (Hedström et al., 2016), which also fits the concentration where permanent birefringence was observed (Michot et al., 2004). Outside the fingers there seems to be yet another transition from the denser sol or nematic phase to a presumably more dilute state that looks diffuse and scatters light to a larger extent, indicating density fluctuations whose size is comparable to the wavelength of visible light. Observing a free swelling clay into a narrow fracture filled with dilute water, hints that there are several phase transitions involved in the colloid release erosion scenario.



**Figure 4-19** Top view of Wy-Na after 30 days of free expansion in deionised water (Hedström et al., 2016). The fracture aperture is 0.12 and the outer diameter of the annular disc is 35 mm. The dry density of the pre-saturated emplaced clay was nominally 1257 kg/m<sup>3</sup>. Outside the emplaced montmorillonite there is an approximately 1 cm wide opaque region of denser montmorillonite paste. Beyond the paste follows an almost transparent region that at its outer edge displays fingers suggesting that it is a sol. For further details see the main text.

Alonso et al. (2019) investigated a number of clays (Table 4-2) and concluded that in all tests with the exception for Nanocor and MX-80 with the largest tested aperture 1.7 mm, expansion stopped. All tests were performed with a nominal dry density of  $\sim 1400 \text{ kg/m}^3$ , and the total time for expansion in stagnant solution was 30 days.

As an example, the expansion vs aperture for Nanocor in contact with 1 mM NaCl(aq) is shown in Figure 4-20. It is, however, difficult to compare the expansion vs aperture in these tests because not only the aperture differs but also the average dry density due to the small amount of emplaced clay.

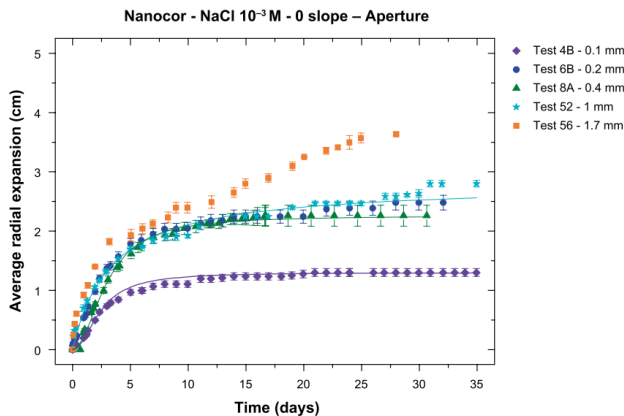


**Figure 4-20** Average radial expansion of Nanocor within smooth horizontal fractures (apertures 0.1, 0.2, 0.4, 1 mm and 1.7 mm) filled with 1 mM NaCl (aq) (Alonso et al., 2019).

The volume of the extruded clay is  $\pi(r_o^2 - r_i^2)a$ , where  $r_o$  and  $r_i$  are the outer and inner radii of the clay, respectively, and  $a$  is the fracture aperture. At an aperture of 0.1 mm the clay expands 1.4 cm, thus the volume of the clay in the fracture is 0.15 cm<sup>3</sup>, i.e., 5% of the volume of cylindrical compartment for the emplaced clay sample. With 0.4 mm aperture, the clay expands 2.26 cm giving a volume fraction of extruded clay to cylindrical compartment of 40%. There will be a substantial difference in the remaining clay mass and therefore dry

density between the 0.1 mm and 0.4 mm aperture cases. With 1 mm aperture, the volume of extruded clay even exceeds the compartment volume.

Erosion tests were conducted for 0.1, 0.2, and 0.4 mm apertures, by applying water flow after the 30-day expansion phase. Generally, the expansion was found to increase during the period with flowing water, and the results for Nanocor Mt montmorillonite are listed in Table 4-3. The eroded mass as determined from the effluent concentration was in all tests extremely small so the mass loss in Table 4-3 essentially reflects the mass of the extruded clay. The large difference between emplaced and remaining masses, suggest that in order to compare the effects of aperture on swelling and erosion, a much larger clay compartment would be needed when the aperture is larger than 0.1 mm. Assuming that the average dry density of extruded clay is half the dry density of the remaining clay, one can estimate the mass of the extruded clay, based on the emplaced mass and volume of the extruded clay. For tests with Nanocor in Table 4-3, such estimate gives 3.6, 20.5, and 20.5% mass loss for 0.1, 0.2, and 0.4 mm aperture, respectively. In the case of the smallest aperture, the more than twice as high measured mass loss than given by the estimate might reflect that the swelling pressure caused bulging and therefore the aperture may have been larger than the nominal 0.1 mm.

**Table 4-3 Erosion by flow experiments with Nanocor montmorillonite in 1 mM NaCl. The remaining mass is determined by drying and weighing the clay remaining in the cylindrical compartment (Alonso et al., 2019).**

Aperture	Flow	Radial expansion Flow start	Radial expansion Flow end	Emplaced mass	Remaining mass	Mass loss	Eroded Mass
(mm)	(m/s)	(cm)	(cm)	(g)	(g)	(%)	(mg)
0.1	$1.5 \times 10^{-6}$	1.43	1.81	3.9617	3.6238	8.5	0.62
0.2	$6.1 \times 10^{-7}$	2.48	3.97	3.9617	3.248	18.0	6
0.4	$1.4 \times 10^{-7}$	2.26	2.59	3.9617	3.031	23.5	9.9

Increased expansion during flow was not seen in previous studies, as long as the salinity was kept constant (Hedström et al., 2016; Schatz et al., 2013). In a constant flow test with 50/50 Wy-Na/Ca montmorillonite with increasingly dilute NaCl solutions, the rate of expansion increased significantly when the NaCl concentration was lowered from 4.2 to 2.1 mM (Schatz et al., 2013). Perhaps, there is a similar effect involved in the tests on Nanocor. Although labelled as Na- montmorillonite, an analysis of major anions revealed 4.4 and 10.68 mmol/100g clay of  $\text{Cl}^-$  and  $\text{SO}_4^{2-}$ , respectively (Alonso et al., 2019). It is therefore likely that during the flow phase of the tests dissolved salt is removed and thereby the actual salinity outside the extruded clay is lowered. Further, the amount of erosion from Nanocor is significantly lower than previously reported erosion rates for homoionic Na- montmorillonite. Generally, erosion decreased with increasing salinity and would cease (be below detection limit) at a critical concentration (Hedström et al., 2016; Schatz et al., 2013). In view of the previous studies, it is plausible that the measured salt content in Nanocor contributed both to the swelling during flow and to the low erosion rates.

Limited extrusion was also found in the tests with 1 mm aperture by Schatz et al. (2013) as shown in Figure 4-21. Tests 3 and 5 are Na- montmorillonite expanding and eroding in deionised water and differ in flow velocities only, 0.7 and 0.1 m/s, respectively. This difference does not influence the extrusion suggesting that the paste that can withstand a flow velocity of 0.1 m/s also withstand 0.7 m/s. However, there appear to be some influence on extrusion due to the flow because in both Test 3 and 5 the extrusion distances decrease somewhat after ~200 h. Test 6 is done with Na- montmorillonite in Grimsel water simulant (0.7 mM NaCl and 0.14 mM CaCl<sub>2</sub>) at a lower flow velocity of 0.02 m/s and the extrusion is larger than in Tests 3 and 5 at the end. During the initial 100 h the extrusion is almost the same in the three tests, indicating that the repulsion is similar. Test 9 is done with mixed 50/50 Na/Ca- montmorillonite and shows less expansion and deviate earlier from the other three tests with Na- montmorillonite. This is also to be expected because at lower dry densities, the presence of Ca gives lower swelling pressure.

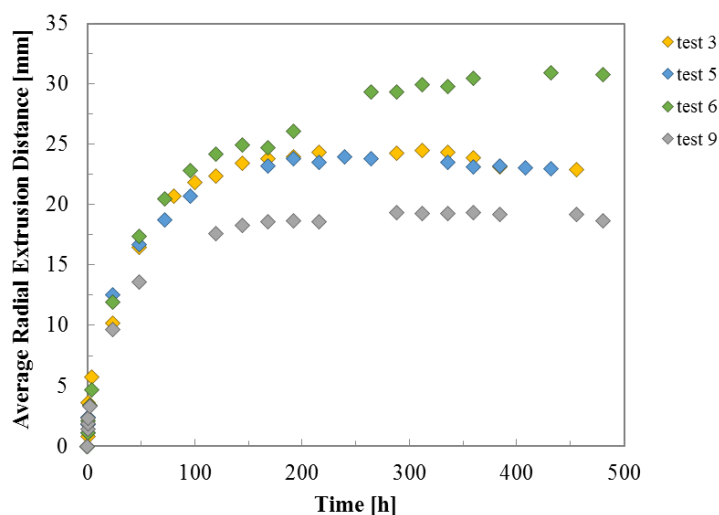


**Figure 4-21 Average radial extrusion distance as a function of time for tests 3, 5, 6, and 9. Tests 3 and 5 (Na-Mt in deionised water) were performed at flow velocities 0.7 and 0.1 m/h, respectively. Test 6 (Na-Mt) was performed with Grimsel water simulant at flow velocity 0.02 m/h. Test 9 (50/50 Na/Ca-Mt) was done with deionised water at flow velocity 0.12 m/h. From (Schatz et al., 2013).**

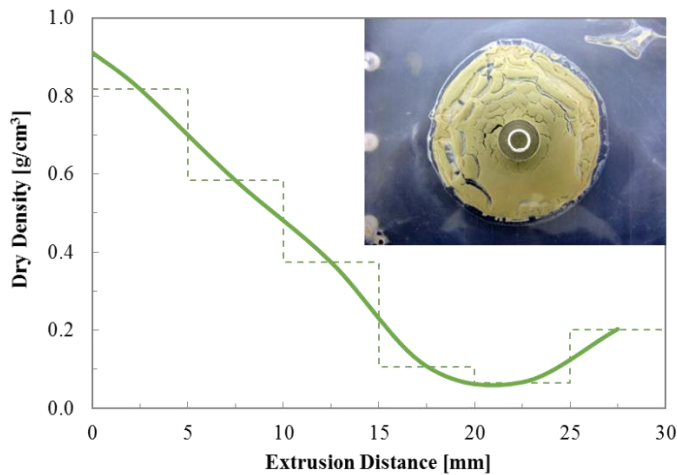


**Figure 4-22** Dry density gradient of the extruded material zone, over 5 mm thick layers, into the 1 mm fracture at the termination of test 6 (Figure 4-21). Dotted line represents measured values over corresponding distance intervals; smoothed solid line from the residual density through distance midpoints is included for illustrative purposes only. The inset shows the clay after drying. From (Schatz et al., 2013).

As discussed above a 1 mm fracture aperture and small sample compartment implies that a large portion of the clay will end up in the fracture. One advantage with large aperture, though, is that it facilitates the determination of the density of the extruded clay. After test termination, Schatz et al. (2013) dried the test cell before dismantling and could thereby determine the dry density gradient from sample compartment to outermost rim of the extruded paste. Figure 4-22 shows the dry density profile from Test 6 (Figure 4-21). Within the accuracy of the measurement, the dry density falls linearly with extrusion distance. The outermost increase in dry density is most likely an artefact caused by the drying.

The limited extrusion of the clay paste implies that there must be friction between extruding clay paste and fracture wall to balance the swelling pressure (Birgersson et al., 2009; Börgesson et al., 2018). The introduction of a friction force would also lead to a linear decay of the dry density (strictly true in linear geometry but only approximate for radial extrusion), which is corroborated by Figure 4-22. The effect of friction in swelling models is further discussed in section 4.4.2.

### 4.3.2 The role of surface roughness and accessory minerals

Reid et al. (2015) performed a test with the specific aim to investigate the clogging of a fracture with variable aperture by the accessory minerals in the bentonite. The artificial fracture was made from a clear two-part epoxy resin and constructed by taking a cast of a granite fracture. The average hydraulic aperture was determined to 54  $\mu\text{m}$ , which is clearly smaller than the apertures used in other experiments (Table 4-2). The test cell was circular with a diameter of 26 cm and with a 2 cm diameter hole at the centre to house a compacted MX-80 bentonite plug. The hole in the top plate was threaded to fit a brass plug to keep the bentonite in place. The bentonite plug protruded 5 mm into the bottom plate so that it was intersected by the fracture. A load cell, in direct contact with the bentonite plug via a piston, was mounted on the underside of the bottom plate. (Figure 4-23). The load cell measurements were used to calculate the swelling pressure in the bentonite. In this respect, this set-up is unique as no other group has combined the monitoring of extrusion and erosion with simultaneous swelling pressure measurements.

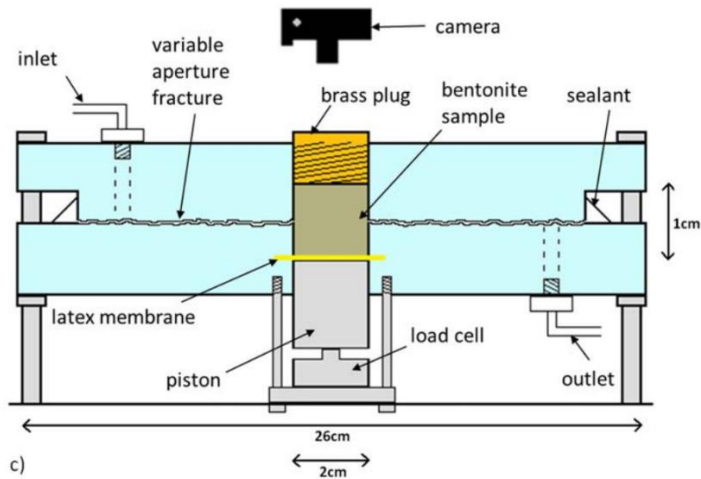


**Figure 4-23 Schematic of the artificial fracture flow cell used by Reid et al. (2015).**

The bentonite sample was compacted uniaxially in a compaction mould with a slightly smaller diameter (18.65 mm) than the sample compartment in the artificial fracture cell. The dry density of the compacted bentonite sample was  $1660 \text{ kg/m}^3$  and the water content was 18%. The compacted bentonite plug was then placed in the artificial fracture. In case there would be no extrusion into the fracture, the average dry density of the emplaced plug after it had filled the sample compartment would be  $(18.65/20)^2 \cdot 1660 = 1440 \text{ kg/m}^3$ . After installation of the bentonite plug in the fracture test cell, deionised water, as a proxy for glacial water, was flowed through at an average rate of  $\sim 0.95 \text{ ml/min}$  for a period of 130 days.

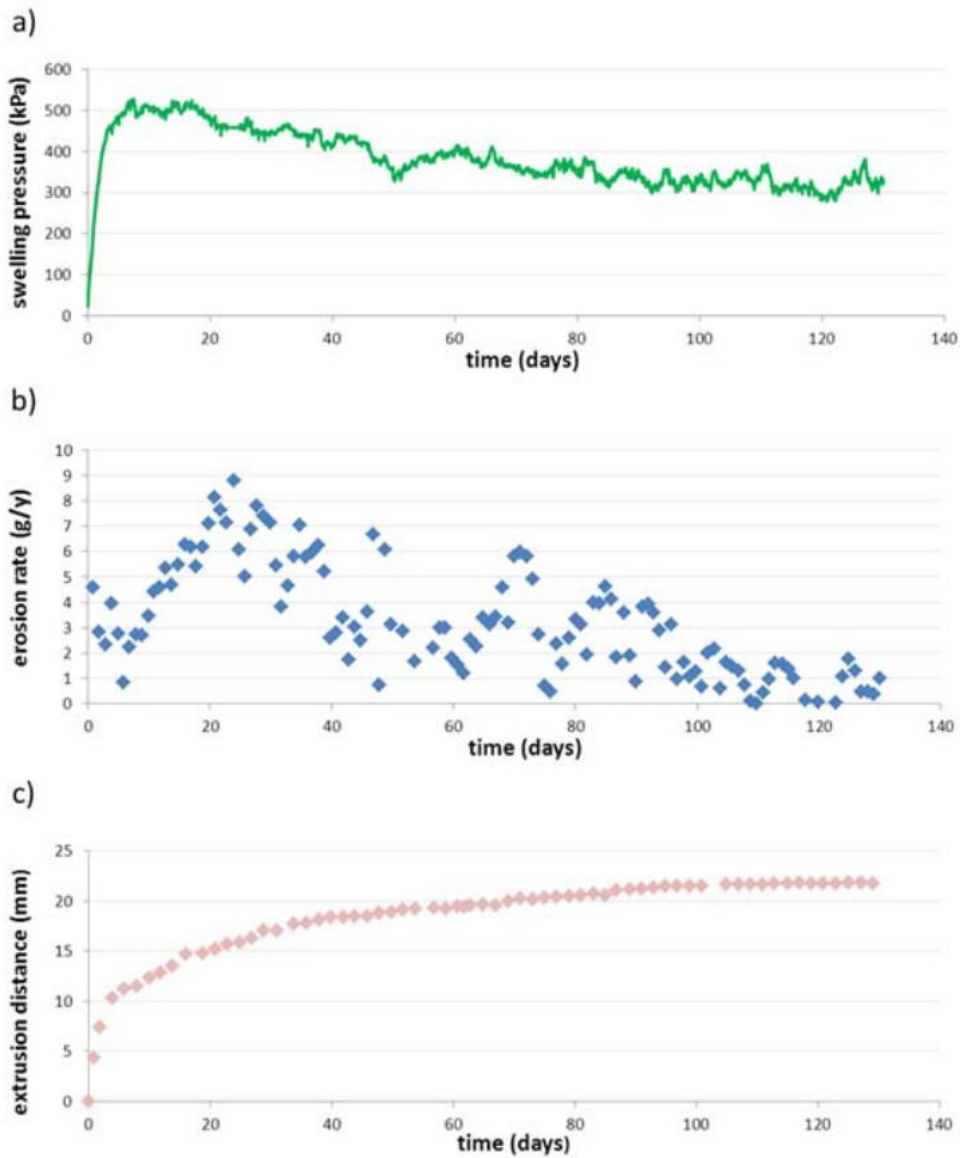


**Figure 4-24 Results from Reid et al. (2015): a) swelling pressure vs time; b) erosion rate vs time; c) extrusion distance vs time.**

Figure 4-24 shows the development of swelling pressure (a), erosion rate (b) and the extrusion distance into the fracture (c) during the test. The swelling pressure reached a maximum value of 515 kPa during the first week of the test and oscillated around 500 kPa until day 20, after which a steady decline began, albeit with oscillations, down to ~300 kPa at the end of the test. Simultaneously with the pressure build-up, a rapid extrusion took place. The extrusion rate decreased over time and the extrusion gradually levelled out at 22 mm. During the first stage of pressure build-up and extrusion, the erosion rate was relatively low. The eroded amount was determined gravimetrically once a day so there is naturally some scatter in the data since one may assume that the erosion process has a stochastic component. The erosion rate gradually decreased after the maximum was reached after about 20 days. Reid et al. (2015) suggest that the erosion rate oscillate with a period of ~10 days and propose that this oscillation is coupled to a cyclic two-stage mechanism that is correlated with variations in swelling pressure and breakthrough events of the rim of accessory minerals left behind at the front of the extruded bentonite (Figure 4-25). The proposed mechanism states that during the

first stage when erosion is low, the swelling pressure increases because the water uptake is larger than the bentonite loss. Stage two is claimed to start when the swelling pressure exceeds the strength of the forces that keep the accessory mineral ring intact. The breach of the mineral ring triggers an erosion event which in turn leads to decreasing swelling pressure. The erosion will lead to further transport of accessory minerals which repair the mineral ring. When the filtering capacity of the mineral ring is restored, erosion decreases, and the process returns to stage 1. This explanation is rather tenuous and is difficult to justify based on the data. In particular, the correlation between fluctuations in erosion rates and fluctuations in swelling pressure is weak. Further, fluctuations in swelling pressure in the bentonite plug would not be transferred to the accessory mineral ring due to wall friction.



**Figure 4-25** Top view of bentonite extrusion into the fracture after 90 days. The ring of accessory minerals is clearly visible outside the MX-80 bentonite. From Reid et al. (2015).

However, the gradual decrease in swelling pressure is clearly correlated with erosion. The measured swelling pressures are significantly lower than expected and the authors point out that the internal threading in the top plate makes the volume slightly larger, which would lead to a further reduction of the average dry density. The swelling pressure of fully saturated MX-80 with a dry density of  $1440 \text{ kg/m}^3$  is 4 - 4.2 MPa (interpolating the data in Karnland et al. (2006)), while the maximum swelling pressure in the test was 515 kPa, which would correspond to a dry density of  $1020 \text{ kg/m}^3$ . It seems improbable that such difference in dry density would be accounted for by swelling of the top half of the bentonite plug into the threading. It should be noted, however, that the bentonite plug was not fully saturated when mounted in the fracture test cell. In contact with the flowing water, the bentonite immediately expanded into the fracture, as seen in (Figure 4-24) creating a ring of bentonite with low hydraulic conductivity in the fracture outside the emplaced bentonite plug. This would cause the water saturation of the bentonite plug to slow down and it is likely that full water saturation is not achieved when the maximum swelling pressure is measured. In addition, the oscillations in the swelling pressure may reflect homogenisation processes. Another issue that may influence the swelling pressure is bulging of the epoxy resin plates, as no measures seem to have been taken to ensure a fixed sample volume.

Assuming that the bentonite plug is fully saturated at the end of the test (no analysis of the plug after test termination is reported) a dry density of  $920\text{-}950 \text{ kg/m}^3$  can be deduced from the measured swelling pressure of 300-350 kPa. The erosive loss during the 130 days of the test is 1.11 g, i.e., 24% of the initial sample mass (Reid et al., 2015). Based solely on this mass loss, the dry density of the bentonite plug at termination would be  $1100 \text{ kg/m}^3$ . It is not unreasonable to think that the dry density could be below  $1000 \text{ kg/m}^3$  if one also considers the mass of the extruded clay and possibly also the swelling into the threading and bulging of the

fracture. Thus, the trend of falling swelling pressure during the test is largely explained by the erosive loss.

The test demonstrates that accessory minerals can be deposited in a rough fracture outside the swelling front, while the montmorillonite continues to erode as seen in Figure 4-25. The amount of accumulated accessory minerals was in the test increasing with time. Contrary to what the authors claim, due to the design of the test, it is not possible to attribute the decreasing erosion rate over time to any filtration effect of the deposited accessory minerals. At present, it cannot be excluded that the large total erosion, 24% of the emplaced bentonite source, contributed to the decreasing erosion rate. The source bentonite was MX-80 including all the accessory minerals. The dissolution of especially gypsum has been shown to reduce erosion and under some circumstances also contribute to gel formation (Birgersson et al., 2009). In a more recent study, the swelling behaviour of MX-80, washed MX-80 (depleted of soluble minerals), and the montmorillonite fraction extracted from MX80, was investigated. The average radial extrusion in planar fractures with 0.2 mm aperture and 1 mM NaCl(aq), levelled at 25-30 mm for the montmorillonite and the washed MX-80, while the extrusion of MX-80 only reached 10-12 mm (Alonso et al., 2019). The authors concluded that soluble salts have greater effect restricting clay expansion than the (*non-soluble*) accessory minerals.

Alonso et al. (2019) also conducted erosion tests of MX-80 in rough fractures and did not observe any enrichment region of accessory minerals during the 30 days of flowing water. While Reid et al. (2015) based the fracture on a cast of a real fracture, Alonso et al. (2019) designed a regular roughness pattern, that likely yielded a larger aperture. Therefore, it is not straightforward to compare the two studies. Also, the time differ significantly between the two studies.

In the application for a permit to build a Spent Fuel Repository, SKB disregarded the process of accumulation of accessory minerals, since there is a lack of evidence that that the accessory minerals can actually form efficient filters (SKB, 2011).

To date, there has not been any study of erosion in rough fractures, using washed MX-80 or other bentonite depleted of soluble minerals.

### 4.3.3 Influence of temperature

Homoionic montmorillonites are prepared by separating the heavier accessory minerals from the clay fraction by centrifugation of dilute suspensions of the raw bentonite. The clay fraction is subsequently ion exchanged by repeated washings with high ionic strength solutions of the relevant chloride salt. Excess salt is finally removed by dialysis. The homoionic clay is the finally oven dried at 60°C (Karlund et al., 2006; Schatz et al., 2013). There are to our knowledge no studies on colloid release erosion that has considered bentonite/montmorillonite exposed to temperatures higher than 60°C.

Couture (1985) reported that exposing bentonite to steam (150-250°C) led to a rapid loss in swelling capacity. Reduced swelling capacity may influence the colloid release erosion since it is related to the extensive swelling of sodium-dominated bentonite/montmorillonite. A more recent study on swelling and sedimentation behaviour of steam-exposed Na- and Ca-montmorillonite as well as bentonite concluded that it is not the swelling capacity that is influenced by the steam exposure but the final sediment volume of actively dispersed clay that was left to settle (Leupin et al., 2014). The homoionic montmorillonites were largely unaffected by steam in the tests, both with respect to sediment volume and volume after

unconfined swelling. Couture did not examine the volume after unconfined swelling and the study concluded that what Couture meant by reduced swelling capacity in fact referred to sediment volume (Leupin et al., 2014). Nevertheless, these studies suggest that steam may reduce gel formation or weaken the gels. Possibly, this effect is more pronounced in tests on bentonites than in the tests on the homoionic smectite, because in the former there may be soluble accessory minerals that can increase the ionic strength above the critical value for gel formation. Figure 4-26 illustrates the effect of steam (150°C) on Ikosorb. The reference material clearly formed a voluminous gel with no noticeable colloid particles in the supernatant above. After steam treatment the gel-forming interactions are much weaker and most clay has settled, and the sediment fills less than a quarter of the gel volume (Leupin et al., 2014). The clays SPV200 and Tixoton (#1 and #3 from left in Figure 4-26) also showed a large difference in sediment volume.

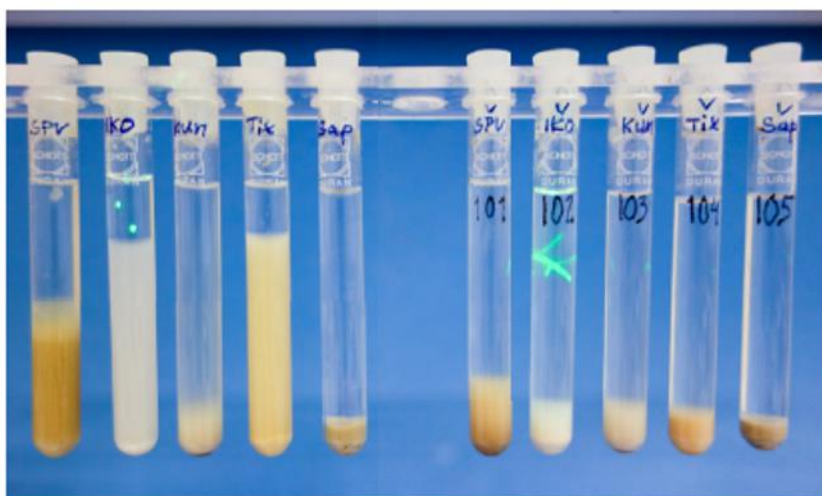


**Figure 4-26 Illustration of the clay/water volume after active dispersion and sedimentation for five materials in Series MmS-1000 (Leupin et al., 2014). The group of five test tubes to the left are the reference material and the test tubes to the right show the steam exposed clays. A laser beam is used to illustrate the presence or absence of colloidal particles in the supernatant of the Ikosorb material. The lack of light scattering in the reference shows that no colloidal particles are present in the supernatant above the gel. In contrast, there is considerable light scattering in the steam exposed material, indicating significant presence of colloidal particles above the sediment.**

There are no reported mineralogical changes associated to steam exposure. Oscarson and Dixon (1989) found that exposing clay to steam did not affect its cation-exchange capacity (CEC), nor cause any detectable change in the mineralogical composition of the clay as indicated by X-ray diffraction analysis. The observed changes in gel formation as illustrated in Figure 4-26 could possibly be related to changes to the clay edge charges so the edge-face interaction is weakened. Similar conclusions were reached in a recent review on the effects of steam on bentonite (Hoch et al., 2020). Such changes would not be detectable with X-ray diffraction or CEC measurements.

To investigate the strength of Na-montmorillonite gels, Hedström et al. (2016) heated low-density gels in a water bath. In the case of the lowest densities and NaCl concentrations the gels eventually melted but solidified once the temperature decreased. For the gels with sufficiently high density, heating to 75°C did not cause any change, while for others the heating caused the gel to yield but not completely melt. A few examples of Kutch-Na (Na-montmorillonite extracted from Asha 505 bentonite from the Kutch area, Gujarat region,

Ashapura Group India) are shown in Figure 4-27. The temperature for causing the gel to yield increased with increasing clay concentration at constant NaCl concentration. Gels with 40 g Mt/l never yielded. Gels with montmorillonite content < 40g/l could only be formed by adding NaCl solution to a clay dispersion, while a paste that expand in NaCl solution with concentration above the CCC would stop expanding and turn into a gel at the swelling front with a higher concentration. For Wyoming Na-montmorillonite (MX-80) this concentration was found to be ~60 g/l (Börgesson et al., 2018; Hedström et al., 2016). Thus, in a repository, gel melting would not be an issue, both because the gel is too dense, and the groundwater temperature is not likely to be critically high. Possible temperatures in a UK GDF are discussed in section 2.3.

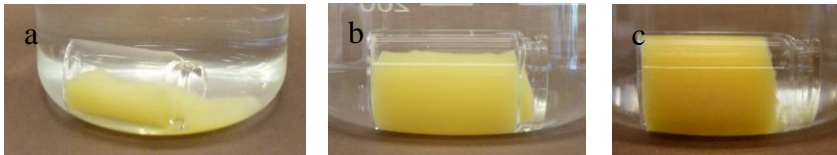


**Figure 4-27** Three Kutch Na-montmorillonite gels after rapid heating to 75 °C. (a) Gel (10 g/l) in 5 mM NaCl solution. The gel underwent almost complete melting transition during heating to 75°C and solidified as the temperature was lowered. (b) Gel (10 g/l) in 6 mM NaCl-solution. The gel underwent large deformation (partial melting) during heating to 75°C. (c) Gel (20 g/l) in 200 mM NaCl-solution. The gel showed no sign of change. From (Hedström et al., 2016).

## 4.4 Modelling work

Modelling of the penetration of bentonite into a fracture and the subsequent possible erosion is a difficult task. Attempts have been done with models derived by Börgesson et al. (Birgersson et al., 2009; Börgesson et al., 2018) and Neretnieks et al. (Liu et al., 2009a; Neretnieks et al., 2009; Neretnieks and Moreno, 2018a). These models will be briefly discussed here, and it will be shown that both models are problematic, being either inconsistent and/or lacking key physicochemical components.

### 4.4.1 Dynamic force-balance model by Neretnieks et al.

The purpose of the so-called dynamic force-balance model is to quantify swelling of bentonite or montmorillonite (Liu et al., 2009a; Neretnieks et al., 2009). For the calculation of erosive loss of bentonite in a fracture, additional models are needed. The advective transport of water and sol outside the expanded clay is described by Darcy’s law. The transport of ions that, e.g., may partake in ion exchange reactions with the montmorillonite is described with advection and diffusion (Neretnieks et al., 2009). In addition to the developers, the model or suite of models, has also been implemented by others to investigate its reproducibility (Benbow et al., 2015; Schatz et al., 2013). However, those studies primarily focussed on the numerical difficulties rather than the underlying science. For example, the objective by The Swedish Radiation Safety Authority (SSM) was to “reproduce all or a sub-set of SKB’s corrosion calculation cases. If requested by SSM, the application of SKB’s buffer erosion model to estimate the “erosion time” used in the corrosion calculations shall also be explored using hydrological simulation results” (Benbow et al., 2015).

However, as will be demonstrated below, the dynamic force-balance model is not internally consistent and therefore gives unphysical predictions. This is illustrated most easily by examining the model prediction of the CCC. The model is formulated as a one-dimensional expansion of parallel montmorillonite layers, in which each montmorillonite layer only interacts with its nearest neighbours. The local volume fraction  $\phi$  at each position in the column of parallel montmorillonite layers can be obtained from the local layer separation  $h$  by means of Eq. 12. The forces that are included in the model are the friction force exerted by the moving clay layer, gravity  $F_s$ , and attraction and repulsion forces between clay layers,  $F_A$  and  $F_R$ , respectively. The model is expressed as a generalised diffusion equation that describes the time evolution of the volume fraction of colloidal particles under the effect of drift and diffusion. (Liu et al., 2009a)

$$\frac{\partial \phi}{\partial t} = F_s \frac{\partial}{\partial x} \left( \frac{\phi}{f} \right) + \frac{\partial}{\partial x} \left( D_F \frac{\partial \phi}{\partial x} \right) \quad (15)$$

where  $f$  is the friction coefficient and  $D_F$  is termed the diffusivity function. The diffusivity function is central to the model because it contains the thermal motion (Brownian) as well as the effect on the clay layers from the attraction and repulsion forces.  $D_F = k_B T / f \cdot \xi$  where  $\xi$  is given by

$$\xi = 1 + \frac{(h+\delta)^2}{k_B T} \left( \frac{\partial F_A}{\partial h} - \frac{\partial F_R}{\partial h} \right) \quad (16)$$

For large separations the forces between the particle vanish and  $\xi = 1$  and as a consequence, Eq. 15 reduces to the normal diffusion equation describing Brownian motion of non-interacting clay particles.

For clay separations where the clay particles interact, it turns out that Eq. 16 gives inconsistent and therefore wrong predictions. The model predictions were done by using the DLVO forces in Eq. 16 (Liu et al., 2009a, 2009b; Neretnieks et al., 2009). Within the model, clay expansion will cease if  $\xi$  becomes zero, because according to Eq. 16, then the thermal motion (represented by the 1) is balanced by the forces between clay particles. Within the DLVO realisation of the model, the only force that can balance the thermal motion is the van der Waals force as shown earlier (Eq. 9). Therefore, the conditions under which a cohesive state could possibly be formed are known, and the maximum clay layer separations for various particle sizes and values of the Hamaker constant are given in Figure 4-5.

The prediction from Eq. 16, on the other hand give too large separations between the clay layers. That is, the predicted cohesive state has separations that are too large for the van der Waals interaction to overcome the thermal motion. With the following parameter values:  $A = 9 \cdot 10^{-14} \text{ m}^2$  (smectite particle surface area),  $\delta = 1 \text{ nm}$  (smectite particle thickness), and Hamaker constant,  $A_H = 2.5 k_B T$ , the CCC is found to be  $\sim 50 \text{ mM}$  (NaCl) and the critical volume fraction where expansion stops is  $\sim 3.4\%$  (Liu et al., 2009b).

The analytical solution to Eq. 16 is confirmed in the simulations (Liu et al., 2009b) with NaCl concentrations below (40 mM) and above (60 mM) the CCC as shown in Figure 4-28. The authors comment that in the numerical results, gravity is also included, suggesting that this would somewhat influence (increase) the critical volume fraction, and at 60 mM one can see a sharp drop in the volume fraction at  $\phi = 4.5\%$  and no clay particles are present in the solution above the clay phase. This is in contrast to the modelling result at NaCl concentration of 40 mM, (left panel in Figure 4-28) where there is a diffusive tail of clay particles above the denser suspension, indicating the absence of cohesion. A critical volume fraction of 4.5%

corresponds to a separation of clay layers of  $h = 21$  nm (Eq. 12). As mentioned above, this separation is far beyond the separation where the van der Waals attraction equals the thermal energy.

With the parameters used in the calculation by Liu et al. (2009b), the largest possible layer separation for having a cohesive state is just  $h = 12.8$  nm as can be deduced from the red curve ( $A_H = 2.5 k_B T$ ) in Figure 4-5 or from Eq. 11. Note that a particle area  $A = 9 \cdot 10^{-14}$  m<sup>2</sup> corresponds to a coin-like particle with diameter  $d = 340$  nm. From Eq. 8 we obtain the van der Waals attraction  $U_{vdW}(h = 21 \text{ nm}) = -0.15 k_B T$ . Obviously, such tiny attraction energy cannot overcome the thermal energy  $k_B T$ . Thus, one can conclude that Eq. 16 is incorrect, which renders the model unsafe to use for any kind of assessment of swelling and erosion.

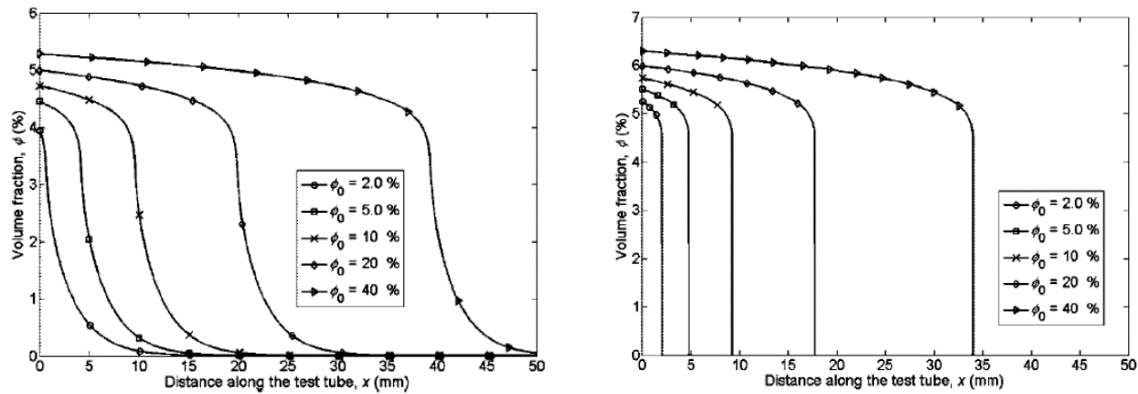


**Figure 4-28** Vertical swelling of 5 mm thick montmorillonite pellets against gravity in a test tube filled with 1:1 electrolyte, e.g., NaCl. The volume fraction profile at steady state as a function of initial volume fractions for electrolyte concentrations 40 mM (left) and 60 mM (right) (Liu et al., 2009b).

#### 4.4.2 Model by Börgesson et al.

##### General

A swelling model based on effective stress theory, developed at Clay Technology (Börgesson et al., 1995), has been further adopted for the swelling into fractures. The rheological properties of bentonite and pure Na-montmorillonite depend strongly on water content (clay concentration) and the NaCl concentration. Based on rheology, four domains were identified and quantified at low ionic strength, i.e., below the CCC (Börgesson et al., 2009)

- Na-montmorillonite with a water content below 35 (clay concentration above about 30 g/l) is a paste with shear strength,
- Between 35 and 100 in water content (clay concentrations between about 10 and 30 g/l), Na-montmorillonite is a non-Newtonian sol.
- Between 100 and 1000 in water content (clay concentrations between about 1 and 10 g/l), Na-montmorillonite is a Newtonian fluid with a viscosity larger than that for water.
- Above 1000 in water content, the influence of montmorillonite is lost.

MX-80 bentonite behaves essentially as Na-montmorillonite, but the water content limits for the different rheological regions are generally lower.

The swelling model is assumed to be valid in the region with the highest clay concentration, termed solid mass or paste.

Above the CCC, the swelling of Wy-Na stops at clay concentration 60-80 g/l and there is no erosive loss of gel for flow velocities relevant for the repository (Börgesson et al., 2018). Below the CCC the swelling of the paste continues until the clay concentration of about 30, where the paste turns to a sol and clay is susceptible to erosion. The rate of loss of the sol depends on many factors as described earlier in this report. Figure 4-29 illustrates the model for Na-montmorillonite.

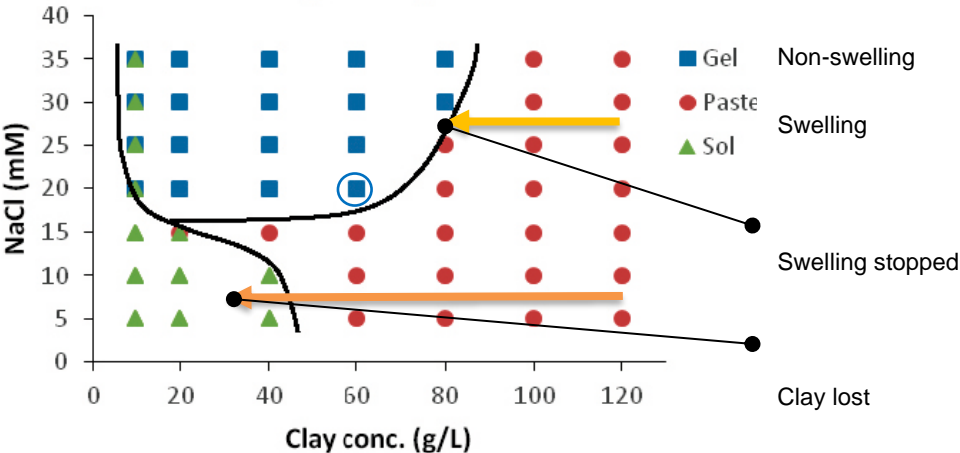


**Figure 4-29** State diagram of Wyoming Na-montmorillonite. The gel is characterised by non-swelling properties and the paste and sol by swelling properties. The swelling above CCC (yellow) and below CCC (orange) is illustrated. The blue circle indicates the highest clay concentration (approximately) for which a gel is formed at the CCC (20 mM in this case). From Börgesson et al. (2018).

The swelling paste, illustrated as red dots in Figure 4-29, is assumed to swell as a solid mass of Na-bentonite according to relations derived for that clay.

**Model**

Swelling of the clay in the region illustrated in Figure 4-29 into a fracture is modelled by force equilibrium. The force equilibrium state, that will prevail in a fracture after completed swelling into a plane fracture, has been considered and a formula for the swelling pressure distribution in the fracture has been derived without considering the stress path up to the equilibrium state.

The bentonite swelling into an ideal plane fracture is modelled as controlled by the swelling pressure of the bentonite and the friction against the fracture wall. Figure 4-30 shows the equilibrium situation of an infinitesimal part of a bentonite (*dr*) penetrating from a deposition hole into a horizontal fracture.

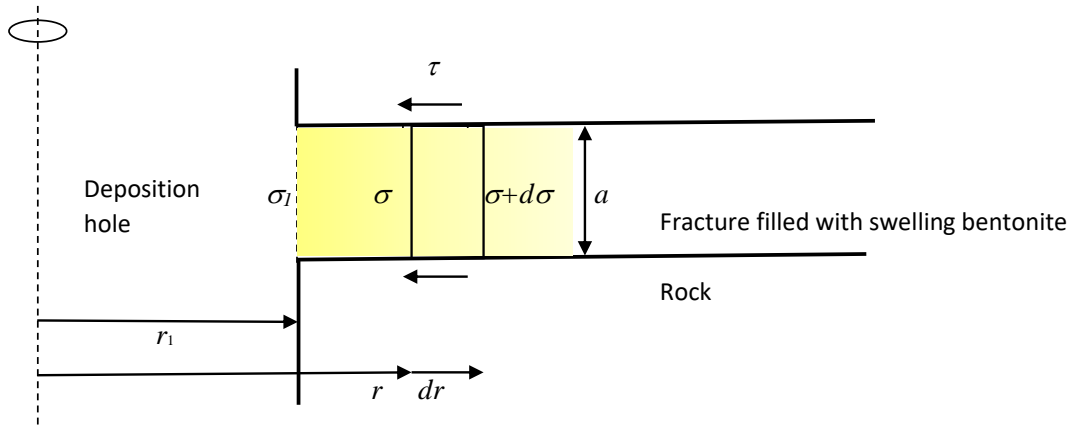


**Figure 4-30 State of equilibrium of an infinitesimal part of bentonite  $dr$  after swelling into a fracture.**

$r_1 =$  deposition hole radius

$a =$  fracture aperture

$\sigma_1 =$  swelling pressure at the deposition hole wall

$\sigma =$  swelling pressure at the distance  $r - r_1$  into the fracture

$d\sigma =$  change in swelling pressure at the increased distance  $dr$

$\tau =$  shear stress at the fracture wall

The shear stress between the penetrating bentonite and the fracture wall can be expressed as

$$\tau = \sigma \tan \phi \quad (17)$$

where  $\phi$  is the friction angle between the bentonite and the fracture surface. Assuming that the penetration depth is small compared to the radius  $r_1$ , ( $r/r_1 \approx 1$ ), force equilibrium in radial direction gives (after integration)

$$\sigma = \sigma_1 \exp \left( -\frac{2z}{a} \tan \phi \right) \quad (18)$$

Equation 18 thus describes the relation between the swelling pressure  $\sigma$  in the fracture and the penetration depth  $z$  into the fracture at the fracture aperture  $a$  and the buffer swelling pressure  $\sigma_1$ .

### **Calculated fracture penetration**

Figure 4-31 shows the swelling pressure distribution in a plane fracture with the aperture 0.1 mm at different friction angles calculated according to Eq. 18.

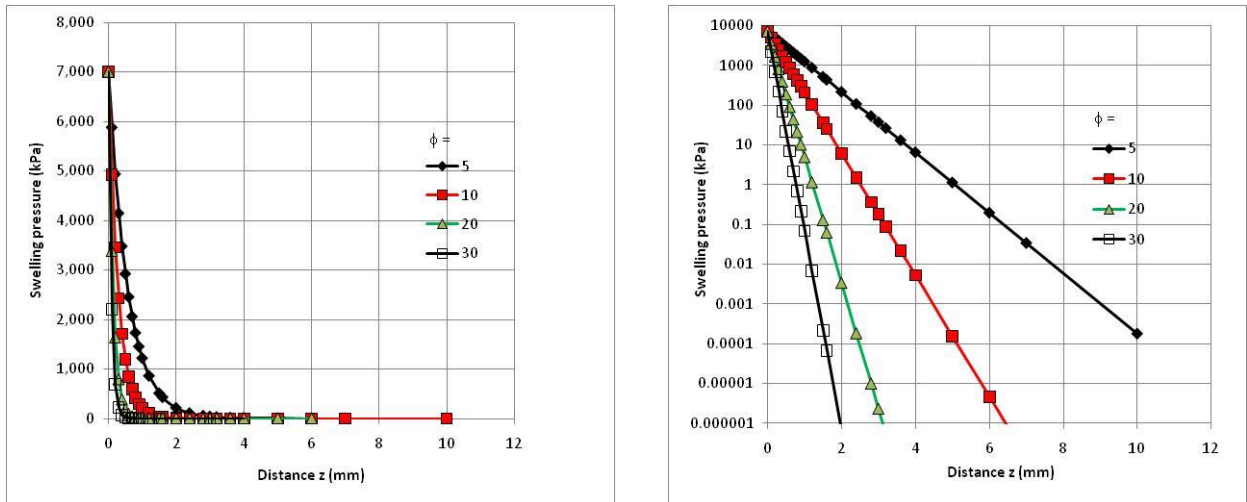


**Figure 4-31** Calculated swelling pressure as a function of depth after penetration of bentonite into a plane fracture with the aperture 0.1 mm at different friction angles.

Figure 4-31 shows that the swelling pressure drops rapidly. At the friction angle 10° it drops from 7 MPa at the deposition hole to below 10 Pa at 4 mm depth of a 0.1 mm wide fracture.

**Above the CCC**

A problem is the insufficient knowledge of the swelling pressure and friction angle at the very low clay concentration of 60-80 g/l, where swelling stops when the ground water has a salinity above CCC (as illustrated in Figure 4-29). It could be interesting to make a sensitivity analysis in order to study how much the penetration can vary above CCC at the clay concentration 60 g/l, which was done in Börgesson et al. (2018).

The penetration depth can be derived from Eq. 18

$$z = \frac{a}{2 \tan \phi} \ln \frac{\sigma_1}{\sigma} \tag{19}$$

Varying  $\phi$  between the extreme values  $0.5^\circ < \phi < 30^\circ$  and  $\sigma$  between the extreme values  $0.01 \text{ kPa} < \sigma < 1.1 \text{ kPa}$  at the clay concentration 60 g/L we get the penetration depths shown in Table 4-4. The fracture width is in this case  $a = 100 \mu\text{m}$  and the swelling pressure of the buffer at the fracture entrance  $\sigma_1 = 7\,000 \text{ kPa}$ .

**Table 4-4** Calculated fracture penetration depths, z, at different friction angles and swelling pressure limits  $\sigma$

	$\phi = 0.5^\circ$	$\phi = 1.0^\circ$	$\phi = 5^\circ$	$\phi = 10^\circ$	$\phi = 30^\circ$
$\sigma = 0.01 \text{ kPa}$	$z = 77 \text{ mm}$	$z = 39 \text{ mm}$	$z = 7.7 \text{ mm}$	$z = 3.8 \text{ mm}$	$z = 1.2 \text{ mm}$
$\sigma = 0.1 \text{ kPa}$	$z = 64 \text{ mm}$	$z = 32 \text{ mm}$	$z = 6.4 \text{ mm}$	$z = 3.2 \text{ mm}$	$z = 0.97 \text{ mm}$
$\sigma = 1.1 \text{ kPa}$	$z = 50 \text{ mm}$	$z = 25 \text{ mm}$	$z = 5.0 \text{ mm}$	$z = 2.5 \text{ mm}$	$z = 0.76 \text{ mm}$

Table 4-4 shows that the penetration depth varies up to a factor 100 at the extreme cases of friction angles 0.5 and 30 degrees and swelling pressure 0.01 and 1.1 kPa at the dry density  $\rho_d=60 \text{ kg/m}^3$  but is anyway not larger than 77 mm at the most extreme case.

The uncertainties of these calculations are besides the friction angle and the swelling pressure, mainly the validity of Eq. 18 and the simplification that we have a fracture with the same properties as parallel plates. The derivation of Eq. 18 is based on force equilibrium after completed swelling and does not take into account the swelling phase. The influence of the history of swelling is regarded as small compared to the uncertainties of the swelling pressure and the friction angle. The assumption of parallel plates was judged to increase the penetration compared to if variable fracture apertures were considered.

### **Below the CCC**

Below the CCC the swelling into a fracture can be calculated in the same way as above CCC until the swelling paste has turned into a swelling sol as illustrated in Figure 4-29. As illustrated in Table 4-4 the swelling of the paste into a fracture of the width 0.1 mm is not very strong. The loss of the swelling sol cannot be modelled in the same way and a good model for that is today not at hand. As shown in Figure 4-4, below the CCC, Na-montmorillonite displays a pseudo plateau of ~500 Pa in the osmotic pressure curve. The pseudo plateau starts at clay concentration of ~30 g/l and ends at ~10g/l, demonstrating that systems that rheologically are sols (see section 4.2.2) also have osmotic or swelling pressure, hence the term swelling sol. One difficulty in using this swelling pressure information in the present model is the absence of friction angle in a fluid.

In order to study if the swelling of the paste can delay the loss of clay by the chemical erosion of the sol a simplified FEM calculation that models the swelling of a clay into a fracture was done. In this calculation the clay was assumed to be lost as soon as the clay turned into a sol i.e. at a clay concentration of 30 g/l. The swelling pressure at that clay concentration was assumed to be 10 Pa. The calculation considers that water has to be taken from the fracture and sucked into the buffer in order to compensate for the clay that is lost in the buffer. The calculation showed that when only repulsive forces are accounted for, the swelling rate cannot limit the loss of bentonite. This conclusion is independent of whether one uses an empirical relation or the Poisson-Boltzmann equation of the density/swelling pressure relation.

### ***Influence of temperature***

Below 100°C the influence of temperature on the models of the swelling paste should be small compared to the uncertainty of the models and the assumptions of the swelling pressure/clay concentration relation. Above 100°C current knowledge does not allow any final conclusions to be drawn, but any transformations or other changes of the properties of the Na-montmorillonite should lead to less fracture penetration and thus less erosion.

## **4.5 Gap analysis**

### **4.5.1 Experimental parameter space**

Potential sub-surface conditions near a UK GDF are discussed in chapter 2. While there are uncertainties inherent in the climate modelling, one cannot exclude the possibility of future glaciations. Mineralogical, geochemical and isotopic analyses of drillcore rock samples and groundwater samples from deep boreholes near Sellafield, West Cumbria, suggest that glacial

waters reached to more than 700 m depth during the Pleistocene (Milodowski et al., 2018). The process of colloid release (chemical erosion) is thus relevant also in a UK context.

#### **4.5.2 Effect of elevated temperature**

There are some observations suggesting that the gelling ability of steam-exposed bentonite is altered. These studies concerned the sediment volume of steam-exposed clay and were not conducted with the purpose for investigating erodibility. It has not been tested if steam exposure would lead to larger erosion or if the CCC is increased.

Steam exposure seemed not to induce any measurable chemical alteration of the montmorillonite. Changes to the montmorillonite particle edges that may influence the edge charge, are difficult to verify experimentally. The observed changes in sediment volume after steam exposure suggest alteration of the edge charges (Hoch et al., 2020). This could have an impact on the gel / sol properties. Whether elevated temperature in general can induce mineralogical processes in montmorillonite that would have a negative impact on erosion has not been investigated.

#### **4.5.3 Time-dependence of erosion rates**

Some tests using artificial fractures indicate that erosion rates may decrease over time. It is still uncertain if such conclusions are robust as the experimental times are relatively short. The conclusions are also uncertain because the mass of the emplaced bentonite / montmorillonite has been too small in relation to the extruded / eroded amount in many tests. The results of tests with raw bentonite may also have been misinterpreted / overinterpreted due to the presence of soluble accessory minerals.

There are a few long-term tests on erosion of bentonite / montmorillonite plugs confined by porous metal filters that strongly indicate decreasing erosion rates with time (Birgersson et al., 2009; Bouby et al., 2020). Of course, erosion of bentonite through a filter does not correspond to erosion of bentonite in a fracture, so these tests are difficult to use for quantification of erosion in a repository environment. But these studies indicate that it may be fruitful to pursue the study of erosion rates using artificial fractures.

The main design principles for such studies would be to: a) ensure that the bentonite source is large relative the expected extrusion and erosive loss; b) use washed bentonite or montmorillonite so the results are not obscured by the dissolution of soluble accessory minerals, such as gypsum, that may cause gelling; c) also test homoionic Na-montmorillonite to confirm the slowdown of the erosion rates, even in the absence of accessory minerals, as observed for erosion through filters (Bouby et al., 2020); d) ensure the emplaced bentonite / montmorillonite source is fully water saturated to avoid water saturation and extrusion / erosion occurring at the same time. So far, there are no theoretical or even conceptual models to explain why erosion rates would decrease in the case of erosion of montmorillonite without accessory minerals. One might speculate that the differences in reported normalised erosion rates (Neretnieks and Moreno, 2018b) may not only reflect the above-mentioned artefacts. Perhaps, the experimental runtimes have not been long enough to give converged results. Anyway, repeating many of the artificial fracture experiments but over a much longer period of time could provide valuable information.

#### **4.5.4 Modelling and conceptual understanding**

To date, there are no reliable models available, that can describe the clay swelling into a fracture and the erosion process. It has been shown that current models are mathematically and physically inconsistent and / or lack a sound description of the processes at the swelling

front. Unless these models are fundamentally reworked, they cannot be used to assess chemical erosion and erosion rates.

Conceptually, wall friction appears to be important to capture the observed limited extrusion at water salinities above as well as below the CCC. Wall friction may also be influenced by fracture roughness. There are conflicting observations regarding the effect of fracture roughness on montmorillonite extrusion and erosion.

Understanding the rate and mechanism of montmorillonite mass transfer from paste to sol seem crucial. Such understanding is currently missing from all models.

## 5 References

- Abend, S., Lagaly, G., 2000. Sol–gel transitions of sodium montmorillonite dispersions. *Applied Clay Science* 16, 201–227. [https://doi.org/10.1016/S0169-1317\(99\)00040-X](https://doi.org/10.1016/S0169-1317(99)00040-X)
- Åkesson, M., 2012. Temperature Buffer test. Final report. SKB TR-12-04.
- Åkesson, M., Olsson, S., Dueck, A., Nilsson, U., Karnland, O., Kiviranta, L., Kumpulainen, S., Lindén, J., 2012. Temperature Buffer test. Hydro-mechanical and chemical/mineralogical characterizations. SKB P-12-06.
- Alemán, J.V., Chadwick, A.V., He, J., Hess, M., Horie, K., Jones, R.G., Kratochvíl, P., Meisel, I., Mita, I., Moad, G., Penczek, S., Stepto, R.F.T., 2007. Definitions of terms relating to the structure and processing of sols, gels, networks, and inorganic-organic hybrid materials (IUPAC Recommendations 2007). *Pure and Applied Chemistry* 79. <https://doi.org/10.1351/pac200779101801>
- Alexander, R., Börgesson, L., Hedström, M., Jefferies, N., Wilson, J., 2018. Sealing Site Investigation Boreholes: Phase 2. Aspects of the evolution and longevity of bentonite seals (Contractor Report to RWM). Radioactive Waste Management, RWM.
- Alonso, U., Missana, T., Gutiérrez, M.G., Morejón, J., Mingarro, M., Fernández, A.M., 2019. CIEMAT studies within POSKBAR Project. Bentonite expansion, sedimentation and erosion in artificial fractures. SKB, TR-19-08.
- Anderson, R.L., Ratcliffe, I., Greenwell, H.C., Williams, P.A., Cliffe, S., Coveney, P.V., 2010. Clay swelling — A challenge in the oilfield. *Earth-Science Reviews* 98, 201–216. <https://doi.org/10.1016/j.earscirev.2009.11.003>
- Asensio, L., De la Morena, G., López-Vizcaíno, R., Yustres, Á., Navarro, V., 2018. Salinity effects on the erosion behaviour of MX-80 bentonite: A modelling approach. *Applied Clay Science* 161, 494–504. <https://doi.org/10.1016/j.clay.2018.05.013>
- Avena, M.J., De Pauli, C.P., 1998. Proton Adsorption and Electrokinetics of an Argentinean Montmorillonite. *Journal of Colloid and Interface Science* 202, 195–204. <https://doi.org/10.1006/jcis.1998.5402>
- Avena, M.J., Mariscal, M.M., De Pauli, C.P., 2003. Proton binding at clay surfaces in water. *Applied Clay Science* 24, 3–9. <https://doi.org/10.1016/j.clay.2003.07.003>
- Baravian, C., Vantelon, D., Thomas, F., 2003. Rheological Determination of Interaction Potential Energy for Aqueous Clay Suspensions. *Langmuir* 19, 8109–8114. <https://doi.org/10.1021/la034169c>
- Bath, A., Richards, H., Metcalfe, R., McCartney, R., Degnan, P., Littleboy, A., 2006. Geochemical indicators of deep groundwater movements at Sellafield, UK. *Journal of Geochemical Exploration, Geochemistry for the Safe Isolation of Hazardous Wastes* 90, 24–44. <https://doi.org/10.1016/j.gexplo.2005.09.003>
- Bath, A.H., Edmunds, W.M., 1981. Identification of connate water in interstitial solution of chalk sediment. *Geochimica et Cosmochimica Acta* 45, 1449–1461. [https://doi.org/10.1016/0016-7037\(81\)90278-7](https://doi.org/10.1016/0016-7037(81)90278-7)
- Benbow, S.J., Metcalfe, R., Jenny Burrow, 2015. Independent Modelling of Engineered Barrier Evolution and Coupled THMC: Canister Corrosion Calculations in SR-Site. SSM Technical note 2015:49.
- Bethke, C.M., 2008. *Geochemical and Biogeochemical Reaction Modeling*. Cambridge University Press.
- Bethke, C.M., 1996. *Geochemical Reaction Modeling, Concepts and Applications*. Oxford University Press.

- Birgersson, M., Börgeron, L., Hedström, M., Karnland, O., Nilsson, U., 2009. Bentonite erosion Final report. SKB TR-09-34.
- Birgersson, M., Hedström, M., Karnland, O., 2011. Sol formation ability of Ca/Na-montmorillonite at low ionic strength. *Physics and Chemistry of the Earth, Parts A/B/C* 36, 1572–1579. <https://doi.org/10.1016/j.pce.2011.07.017>
- Birgersson, M., Hedström, M., Karnland, O., Sjöland, A., 2017. 12 - Bentonite buffer: Macroscopic performance from nanoscale properties, in: *Geological Repository Systems for Safe Disposal of Spent Nuclear Fuels and Radioactive Waste (Second Edition)*, Woodhead Publishing Series in Energy. Woodhead Publishing, pp. 319–364. <https://doi.org/10.1016/B978-0-08-100642-9.00012-8>
- Börgeron, L., Hedström, M., Birgersson, M., Karnland, O., 2018. Bentonite swelling into fractures at conditions above the critical coagulation concentration. SKB TR-17-11.
- Börgeron, L., Johannesson, L.-E., Sandén, T., Hernelind, J., 1995. Modelling of the physical behaviour of water saturated clay barriers. Laboratory tests, material models and finite element application. SKB Technical Report TR-95-20.
- Börgeron, L., Sandén, T., 2006. Piping and erosion in buffer and backfill materials. Current knowledge. SKB R-06-80.
- Börgeron, L., Sandén, T., Dueck, A., Andersson, L., Jensen, V., Nilsson, U., Olsson, S., Åkesson, M., Kristensson, O., Svensson, U., 2015. Consequences of water inflow and early water uptake in deposition holes EVA project. SKB TR-14-22.
- Börgeron, L., Sandén, T., Fälth, B., Åkesson, M., Lindgren, F., 2005. Studies of buffer behaviour in KBS-3H concept. Work during 2002-2004. SKB R-05-50.
- Bouby, M., Kraft, S., Kuschel, S., Geyer, F., Moisei-Rabung, S., Schäfer, T., Geckeis, H., 2020. Erosion dynamics of compacted raw or homoionic MX80 bentonite in a low ionic strength synthetic water under quasi-stagnant flow conditions. *Applied Clay Science* 198, 105797. <https://doi.org/10.1016/j.clay.2020.105797>
- Busby, J., 2014. Geothermal energy in sedimentary basins in the UK. *Hydrogeol J* 22, 129–141. <https://doi.org/10.1007/s10040-013-1054-4>
- Busby, J., 2010. Geothermal prospects in the United Kingdom., in: *Proceedings World Geothermal Congress 2010*. Presented at the World Geothermal Congress 2010, Bali, Indonesia.
- Couture, R.A., 1985. Steam rapidly reduces the swelling capacity of bentonite. *Nature* 318, 50–52. <https://doi.org/10.1038/318050a0>
- De Craen, M., Wang, L., Van Geet, M., Moors, H., 2004. Geochemistry of Boom Clay pore water at the Mol site. Scientific Report Waste & Disposal Department SCK•CEN-BLG-990.
- Delhorme, M., Jönsson, B., Labbez, C., 2012a. Monte Carlo simulations of a clay inspired model suspension: the role of rim charge. *Soft Matter* 8, 9691–9704. <https://doi.org/10.1039/C2SM25731A>
- Delhorme, M., Labbez, C., Jönsson, B., 2012b. Liquid Crystal Phases in Suspensions of Charged Plate-Like Particles. *J. Phys. Chem. Lett.* 3, 1315–1320. <https://doi.org/10.1021/jz300380n>
- Derjaguin, B., Landau, L., 1941. Theory of the stability of strongly charged lyophobic sols and of the adhesion of strongly charged particles in solutions of electrolytes. *Acta Physico Chemica URSS* 14, 633–662.
- Dubois, M., Zemb, T., Belloni, L., Delville, A., 1992. Osmotic pressure and salt exclusion in electrostatically swollen lamellar phases. *The Journal of chemical physics* 96, 2278–2286.

- Duc, M., Gaboriaud, F., Thomas, F., 2005. Sensitivity of the acid–base properties of clays to the methods of preparation and measurement: 1. Literature review. *Journal of Colloid and Interface Science* 289, 139–147. <https://doi.org/10.1016/j.jcis.2005.03.060>
- Engström, S., Wennerström, H., 1978. Ion condensation on planar surfaces. A solution of the Poisson-Boltzmann equation for two parallel charged plates. *J. Phys. Chem.* 82, 2711–2714. <https://doi.org/10.1021/j100514a017>
- Eriksson, R., Schatz, T., 2015. Rheological properties of clay material at the solid/solution interface formed under quasi-free swelling conditions. *Applied Clay Science* 108, 12–18. <https://doi.org/10.1016/j.clay.2015.02.018>
- Evans, D.F., Wennerström, H., 1999. *The Colloidal Domain: Where Physics, Chemistry, Biology, and Technology Meet*, 2nd ed. ed. Wiley-VCH, New York.
- Goh, R., Leong, Y.-K., Lehane, B., 2011. Bentonite slurries—zeta potential, yield stress, adsorbed additive and time-dependent behaviour. *Rheol Acta* 50, 29–38. <https://doi.org/10.1007/s00397-010-0498-x>
- Goodwin, J., 2009. *Colloids and Interfaces with Surfactants and Polymers*, 2 edition. ed. Wiley, Chichester, U.K.
- Goodwin, J.W., Hughes, R.W., 2008. *Rheology for Chemists: An Introduction*, 2nd edition. ed. Royal Society of Chemistry, Cambridge, UK.
- Guldbrand, L., Jönsson, B., Wennerström, H., Linse, P., 1984. Electrical double layer forces. A Monte Carlo study. *The Journal of chemical physics* 80, 2221–2228.
- Hackley, V.A., Ferraris, C.F., 2001. *The Use of Nomenclature in Dispersion Science and Technology* (SP No. 960–3). NIST.
- Halonen, M., Adesola, O., 2020. Downscaled tests on buffer pellet behavior in steel cells. Posiva Working Report 2018-25.
- Hamley, I.W., 2007. *Introduction to Soft Matter: Synthetic and Biological Self-Assembling Materials*, Revised Edition edition. ed. Wiley, Chichester.
- Hedström, M., Birgersson, M., Nilsson, U., Karnland, O., 2011. Role of cation mixing in the sol formation of Ca/Na-montmorillonite. *Physics and Chemistry of the Earth, Parts A/B/C* 36, 1564–1571. <https://doi.org/10.1016/j.pce.2011.07.019>
- Hedström, M., Ekvy Hansen, E., Nilsson, U., 2016. Montmorillonite phase behaviour Relevance for buffer erosion in dilute groundwater. SKB TR-15-07.
- Hedström, M., Karnland, O., 2011. Ca/Na selectivity coefficients from the Poisson–Boltzmann theory. *Physics and Chemistry of the Earth, Parts A/B/C* 36, 1559–1563. <https://doi.org/10.1016/j.pce.2011.07.020>
- Hensen, E.J.M., Smit, B., 2002. Why Clays Swell. *J. Phys. Chem. B* 106, 12664–12667. <https://doi.org/10.1021/jp0264883>
- Hetzel, F., Doner, H.E., 1993. Some colloidal properties of beidellite; comparison with low and high charge montmorillonites. *Clays and Clay Minerals* 41, 453–460.
- Hiemstra, T., Van Riemsdijk, W.H., Bolt, G.H., 1989. Multisite proton adsorption modeling at the solid/solution interface of (hydr)oxides: A new approach: I. Model description and evaluation of intrinsic reaction constants. *Journal of Colloid and Interface Science* 133, 91–104. [https://doi.org/10.1016/0021-9797\(89\)90284-1](https://doi.org/10.1016/0021-9797(89)90284-1)
- Hoch, A., Metcalfe, R., Benbow, S., 2020. *The Effects of Steam on Bentonite: Literature Review and Gap Analysis* (Contractor Report to RWM No. RWM164). Radioactive Waste Management, RWM.
- Holmboe, M., Wold, S., Jonsson, M., 2012. Porosity investigation of compacted bentonite using XRD profile modeling. *Journal of contaminant hydrology* 128, 19–32. <https://doi.org/10.1016/j.jconhyd.2011.10.005>

- Hsiao, Y.-W., Hedström, M., 2017. Swelling Pressure in Systems with Na-Montmorillonite and Neutral Surfaces: A Molecular Dynamics Study. *J. Phys. Chem. C* 121, 26414–26423. <https://doi.org/10.1021/acs.jpcc.7b09496>
- Israelachvili, J.N., 2011. *Intermolecular and Surface Forces*, 3rd ed. Elsevier. <https://doi.org/10.1016/C2009-0-21560-1>
- Iwata, 1994. *Soil-Water Interactions: Mechanisms Applications*, Second Edition, Revised Expanded. CRC Press.
- Johannesson, L.-E., Sandén, T., Dueck, A., Ohlsson, L., 2010. Characterization of backfill candidate material, IBECO-RWC-BF. Baclo Project-Phase 3. SKB R-10-44.
- Jönsson, B., Labbez, C., Cabane, B., 2008. Interaction of Nanometric Clay Platelets. *Langmuir* 24, 11406–11413. <https://doi.org/10.1021/la801118v>
- Jönsson, B., Lindman, B., Holmberg, K., Kronberg, B., 1998. *Surfactants and Polymers in Aqueous Solution*, 1st ed. John Wiley & Sons, Ltd.
- Jönsson, Bo, Åkesson, T., Jönsson, Bengt, Meehdi, S., Janiak, J., Wallenberg, R., 2009. Structure and forces in bentonite MX-80 (Technical Report No. 09–06). SKB.
- Kahn, A., 1958. The flocculation of sodium montmorillonite by electrolytes. *Journal of Colloid Science* 13, 51–60. [https://doi.org/10.1016/0095-8522\(58\)90008-4](https://doi.org/10.1016/0095-8522(58)90008-4)
- Karnland, O., Muurinen, A., Karlsson, F., 2005. Bentonite swelling pressure in NaCl solutions - Experimentally determined data and model calculations, in: Alonso, E.E., Ledesma, A. (Eds.), *Advances in Understanding Engineered Clay Barriers*. Taylor & Francis Group, London, pp. 241–256.
- Karnland, O., Olsson, S., Dueck, A., Birgersson, M., Nilsson, U., Hernan-h\aa kansson, T., Pedersen, K., Nilsson, S., Eriksen, T.E., Rosborg, B., 2009a. Long term test of buffer material at the Äspö Hard Rock Laboratory, LOT project - final report on the A2 test parcel (TR-09-29) (No. 09–29). SKB.
- Karnland, O., Olsson, S., Nilsson, U., 2006. Mineralogy and sealing properties of various bentonites and smectite-rich clay material. SKB Technical Report TR-06-30.
- Karnland, O., Olsson, S., Sandén, T., Fälth, B., Eriksen, T.E., Jansson, M., Svärdström, K., Rosborg, B., Muurinen, A., 2009b. Long term test of buffer material at the Äspö HRL, LOT project. Final report on the A0 test parcel. SKB TR-09-31.
- Kjellander, R., Marčelja, S., Quirk, J.P., 1988. Attractive double-layer interactions between calcium clay particles. *Journal of Colloid and Interface Science* 126, 194–211. [https://doi.org/10.1016/0021-9797\(88\)90113-0](https://doi.org/10.1016/0021-9797(88)90113-0)
- Kraepiel, A.M.L., Keller, K., Morel, F.M.M., 1998. On the Acid–Base Chemistry of Permanently Charged Minerals. *Environ. Sci. Technol.* 32, 2829–2838. <https://doi.org/10.1021/es9802899>
- Lagaly, G., Ziesmer, S., 2003. Colloid chemistry of clay minerals: the coagulation of montmorillonite dispersions. *Advances in Colloid and Interface Science* 100–102, 105–128. [https://doi.org/10.1016/S0001-8686\(02\)00064-7](https://doi.org/10.1016/S0001-8686(02)00064-7)
- Laurila, T., Olin, M., Koskinen, K., Sane, P., 2013. Current Status of Mechanical Erosion Studies of Bentonite Buffer. Posiva 2012-45.
- Leupin, O., Birgersson, M., Karnland, O., Korkeakoski, P., Sellin, P., Mäder, U., Wersin, P., 2014. Montmorillonite stability under near-field conditions. Nagra Technical Report 14-12.
- Liu, L., Moreno, L., Neretnieks, I., 2009a. A dynamic force balance model for colloidal expansion and its DLVO-based application. *Langmuir* 25, 679–87. <https://doi.org/10.1021/la8026573>
- Liu, L., Moreno, L., Neretnieks, I., 2009b. A Novel Approach to Determine the Critical Coagulation Concentration of a Colloidal Dispersion with Plate-like Particles. *Langmuir* 25, 688–697. <https://doi.org/10.1021/la802658g>

- Liu, L., Neretnieks, I., 2008. Homo-interaction between parallel plates at constant charge. *Colloids and Surfaces A: Physicochemical and Engineering Aspects* 317, 636–642. <https://doi.org/10.1016/j.colsurfa.2007.11.055>
- Manning, D. a. C., Younger, P.L., Smith, F.W., Jones, J.M., Dufton, D.J., Diskin, S., 2007. A deep geothermal exploration well at Eastgate, Weardale, UK: a novel exploration concept for low-enthalpy resources. *Journal of the Geological Society* 164, 371–382. <https://doi.org/10.1144/0016-76492006-015>
- Martin, C., Pignon, F., Magnin, A., Meireles, M., Lelièvre, V., Lindner, P., Cabane, B., 2006. Osmotic compression and expansion of highly ordered clay dispersions. *Langmuir* 22, 4065–4075. <https://doi.org/10.1021/la052605k>
- Martin, C., Pignon, F., Piau, J.-M., Magnin, A., Lindner, P., Cabane, B., 2002. Dissociation of thixotropic clay gels. *Phys. Rev. E* 66, 021401. <https://doi.org/10.1103/PhysRevE.66.021401>
- Metcalf, R., Ball, D.R., Gale, I.N., Higgs, J.J.W., Hooker, P.J., Noy, D.J., Rochelle, C.A., Savage, D., 2000. Hydrogeology and hydrogeochemistry. Chapter 6, in: Plant, J.A., Haslam, H.W. (Eds.), *Integrated Resource Analysis of the Cheshire Basin*. British Geological Survey Report.
- Metcalf, R., Crawford, M.B., Bath, A.H., Littleboy, A.K., Degnan, P.J., Richards, H.G., 2007. Characteristics of deep groundwater flow in a basin marginal setting at Sellafield, Northwest England: 36Cl and halide evidence. *Applied Geochemistry* 22, 128–151. <https://doi.org/10.1016/j.apgeochem.2006.09.004>
- Metcalf, R., Watson, S.P., McEwen, T., 2015. Geosphere parameters for generic geological environments. Quintessa Report to RWM, QRS-1712C-1, Version 4.0.
- Michot, L.J., Bihannic, I., Porsch, K., Maddi, S., Baravian, C., Mougél, J., Levitz, P., 2004. Phase diagrams of Wyoming Na-montmorillonite clay. Influence of particle anisotropy. *Langmuir* 20, 10829–37. <https://doi.org/10.1021/la0489108>
- Milodowski, A.E., Bath, A., Norris, S., 2018. Palaeohydrogeology using geochemical, isotopic and mineralogical analyses: Salinity and redox evolution in a deep groundwater system through Quaternary glacial cycles. *Applied Geochemistry* 97, 40–60. <https://doi.org/10.1016/j.apgeochem.2018.07.008>
- Mongondry, P., Nicolai, T., Tassin, J.-F., 2004. Influence of pyrophosphate or polyethylene oxide on the aggregation and gelation of aqueous laponite dispersions. *Journal of Colloid and Interface Science* 275, 191–196. <https://doi.org/10.1016/j.jcis.2004.01.037>
- Mourchid, A., Delville, A., Lambard, J., LeColier, E., Levitz, P., 1995. Phase Diagram of Colloidal Dispersions of Anisotropic Charged Particles: Equilibrium Properties, Structure, and Rheology of Laponite Suspensions. *Langmuir* 11, 1942–1950. <https://doi.org/10.1021/la00006a020>
- Navarro, V., Asensio, L., Yustres, Á., De la Morena, G., Pintado, X., 2016. Swelling and mechanical erosion of MX-80 bentonite: Pinhole test simulation. *Engineering Geology* 202, 99–113. <https://doi.org/10.1016/j.enggeo.2016.01.005>
- Neretnieks, I., Liu, L., Moreno, L., 2009. Mechanisms and models for bentonite erosion. SKB TR-09-35.
- Neretnieks, I., Moreno, L., 2018a. Some mechanisms that influence bentonite erosion in a KBS-3 repository – an exploratory study. SKB TR-18-13.
- Neretnieks, I., Moreno, L., 2018b. Revisiting bentonite erosion understanding and modelling based on the BELBaR project findings. SKB TR-17-12.
- Nirex, 1998. Sellafield Geological and Hydrogeological Investigations: The hydrochemistry of Sellafield, 1997 update. Nirex Science Report S/97/089.
- Norrish, K., 1954. The swelling of montmorillonite. *Discussions of the Faraday Society* 18, 120–134. <https://doi.org/10.1039/df9541800120>

- Norrish, K., Rausell-Colom, J., 1962. Effect of freezing on the swelling of clay minerals. *Clay Miner. Bull* 5, 9–16.
- Onsager, L., 1949. The Effects of Shape on the Interaction of Colloidal Particles. *Annals of the New York Academy of Sciences* 51, 627–659. <https://doi.org/10.1111/j.1749-6632.1949.tb27296.x>
- Oscarson, D.W., Dixon, D.A., 1989. The effect of steam on montmorillonite. *Applied Clay Science* 4, 279–292. [https://doi.org/10.1016/0169-1317\(89\)90035-5](https://doi.org/10.1016/0169-1317(89)90035-5)
- Permien, T., Lagaly, G., 1994. The rheological and colloidal properties of bentonite dispersions in the presence of organic compounds III. The effect of alcohols on the coagulation of sodium montmorillonite. *Colloid Polym Sci* 272, 1306–1312. <https://doi.org/10.1007/BF00657786>
- Pintado, X., Adesola, F., Turtiainen, M., 2013. Downscaled tests on buffer behaviour. . Posiva Working report 2012-100.
- Ploehn, H.J., Liu, C., 2006. Quantitative Analysis of Montmorillonite Platelet Size by Atomic Force Microscopy. *Industrial & Engineering Chemistry Research* 45, 7025–7034. <https://doi.org/10.1021/ie051392r>
- Posiva OY, 2012. Safety Case for the Disposal of Spent Nuclear Fuel at Olkiluoto – Performance Assessment 2012. POSIVA 2012-4.
- Quirk, J.P., Marčelja, S., 1997. Application of Double-Layer Theories to the Extensive Crystalline Swelling of Li-Montmorillonite. *Langmuir* 13, 6241–6248. <https://doi.org/10.1021/la970484l>
- Reid, C., Lunn, R., Mountassir, G.E., Tarantino, A., 2015. A mechanism for bentonite buffer erosion in a fracture with a naturally varying aperture. *Mineralogical Magazine* 79, 1485–1494. <https://doi.org/10.1180/minmag.2015.079.6.23>
- Russel, W.B., Saville, D.A., Schowalter, W.R., 1992. *Colloidal Dispersions*. Cambridge University Press.
- Ruths, M., Israelachvili, J.N., 2008. Surface Forces and Nanorheology of Molecularly Thin Films, in: *Nanotribology and Nanomechanics*. Springer Berlin Heidelberg, pp. 417–515. [https://doi.org/10.1007/978-3-540-77608-6\\_9](https://doi.org/10.1007/978-3-540-77608-6_9)
- RWM, 2017. Geological Disposal: Geosphere Status Report. Radioactive Waste Management Limited, Report DSSC/453/01.
- Salas, J., Gimeno, M.H., Auqué, L., Molinero, J., Gómez, J., Juárez, I., 2010. SR-Site – hydrogeochemical evolution of the Forsmark site. SKB Technical Report TR-10-58.
- Sandén, T., Börgesson, L., 2010. Early effects of water inflow into a deposition hole. SKB R-10-70.
- Sandén, T., Börgesson, L., 2008. Deep repository Engineered barrier system. Piping and erosion in tunnel backfill. Laboratory tests to understand processes during early water uptake. SKB R-06-72.
- Sandén, T., Börgesson, L., Dueck, A., Goudarzi, R., Lönnqvist, M., 2008. Deep repository-Engineered barrier system Erosion and sealing processes in tunnel backfill materials investigated in laboratory. SKB R-08-135.
- Schatz, T., Akhanoba, N., 2017. Bentonite Buffer Erosion in Sloped Fracture Environments. Posiva 2016-13.
- Schatz, T., Kanerva, N., Martikainen, J., Sane, P., Olin, M., Seppälä, A., Koskinen, K., 2013. Buffer Erosion in Dilute Groundwater. Posiva 2012-44.
- Sedighi, M., Bennett, D., Masum, S.A., Thomas, H.R., Johansson, E., 2014. Analysis of temperature data at the Olkiluoto. Posiva Working Report 2013-58.
- Shand, P., Edmunds, W.M., Lawrence, A.R., Smedley, P.L., Burke, S., 2007. The natural (baseline) quality of groundwater in England and Wales. British Geological Survey Groundwater Programme Research Report RR/07/06.

- Shelton, A., Sellin, P., Missana, T., Schäfer, T., Cervinka, R., Koskinen, K., 2018. Synthesis report: Colloids and related issues in the long term safety case. SKB TR-17-17.
- SKB, 2019. RD&D Programme 2019. Programme for research, development and demonstration of methods for the management and disposal of nuclear waste. SKB Technical Report TR-19-24.
- SKB, 2011. Long-term safety for the final repository for spent nuclear fuel at Forsmark. Main report of the SR-Site project. SKB Technical Report TR-11-01.
- Smedley, P.L., Edmunds, W.M., 2002. Redox patterns and trace-element behavior in the East Midlands Triassic sandstone aquifer, U.K. *Ground Water* 40, 44–58.
- Smith, P., Schatz, T., Reijonen, H., Hellä, P., 2017. Chemical Erosion and Mass Redistribution of Bentonite in a KBS-3H Repository. POSIVA 2016-12.
- Summerhayes, C.P., Thorpe, S.A., 1996. , in: *Oceanography: An Illustrated Guide*. Chapter 11. CRC Press, pp. 165–181.
- Sundberg, J., Wrafter, J., Ländell, M., Back, P.-E., Rosén, L., 2008. Thermal properties Forsmark. Modelling stage 2.3. Complementary analysis and verification of the thermal bedrock model, stage 2.2. SKB research report R-08-65.
- Suzuki, K., Asano, H., Yahagi, R., Kobayashi, I., Sellin, P., Svemar, C., Holmqvist, M., 2013. Experimental investigations of piping phenomena in bentonite-based buffer materials for an HLW repository. *Clay Minerals* 48, 363–382. <https://doi.org/10.1180/claymin.2013.048.2.15>
- Swartzen-Allen, S.L., Matijevic, E., 1976. Colloid and surface properties of clay suspensions. III. Stability of montmorillonite and kaolinite. *Journal of Colloid and Interface Science* 56, 159–167. [https://doi.org/10.1016/0021-9797\(76\)90158-2](https://doi.org/10.1016/0021-9797(76)90158-2)
- Tambach, T.J., Hensen, E.J.M., Smit, B., 2004. Molecular Simulations of Swelling Clay Minerals. *J. Phys. Chem. B* 108, 7586–7596. <https://doi.org/10.1021/jp049799h>
- Tawari, S.L., Koch, D.L., Cohen, C., 2001. Electrical Double-Layer Effects on the Brownian Diffusivity and Aggregation Rate of Laponite Clay Particles. *Journal of Colloid and Interface Science* 240, 54–66. <https://doi.org/10.1006/jcis.2001.7646>
- Tertre, E., Castet, S., Berger, G., Loubet, M., Giffaut, E., 2006. Surface chemistry of kaolinite and Na-montmorillonite in aqueous electrolyte solutions at 25 and 60°C: Experimental and modeling study. *Geochimica et Cosmochimica Acta* 70, 4579–4599. <https://doi.org/10.1016/j.gca.2006.07.017>
- Thießen, P.A., 1947. Kennzeichnung submikroskopischer Grenzflächenbereiche verschiedenartiger Wirksamkeit. *Z. Anorg. Chem.* 253, 161–169. <https://doi.org/10.1002/zaac.19472530307>
- Tombácz, E., Szekeres, M., 2004. Colloidal behavior of aqueous montmorillonite suspensions: the specific role of pH in the presence of indifferent electrolytes. *Applied Clay Science* 27, 75–94. <https://doi.org/10.1016/j.clay.2004.01.001>
- Torquato, S., Truskett, T.M., Debenedetti, P.G., 2000. Is Random Close Packing of Spheres Well Defined? *Phys. Rev. Lett.* 84, 2064–2067. <https://doi.org/10.1103/PhysRevLett.84.2064>
- van Olphen, H., 1977. *An Introduction to Clay Colloid Chemistry*, 2nd Edition edition. ed. Wiley-Blackwell, New York.
- van Olphen, H., 1964. Internal mutual flocculation in clay suspensions. *Journal of Colloid Science* 19, 313–322. [https://doi.org/10.1016/0095-8522\(64\)90033-9](https://doi.org/10.1016/0095-8522(64)90033-9)
- van Olphen, H., 1956. Forces between suspended bentonite particles, in: *Clays and Clays Minerals. Proc. 4th Natl. Conf., Natl. Acad. Sci. Publ.* 456. Natl. Res. Council, University Park, Pennsylvania, pp. 204–224.
- van Olphen, H., 1951. Rheological phenomena of clay sols in connection with the charge distribution on the micelles. *Discussions of the Faraday Society* 11, 82–84.

- Verwey, E.J.W., Overbeek, J.Th.G., 1948. Theory of the stability of lyophobic colloids. Dover.
- Vilks, P., Miller, N.H., 2010. Laboratory Bentonite Erosion Experiments in a Synthetic and a Natural Fracture (No. NWMO TR-2010-16). Nuclear Waste Management Organization, NWMO TR-2010-16.
- Wanner, H., Albinsson, Y., Karnland, O., Wieland, E., Charlet, L., Wersin, P., 1994. The Acid/Base Chemistry of Montmorillonite. *Radiochimica Acta* 66–67, 157–162. <https://doi.org/10.1524/ract.1994.6667.special-issue.157>
- Wilson, J., Bond, A., 2016. Impact of elevated temperatures on bentonite buffers. Quintessa Report QRS-1384Q-R3, v 1.2 for NDA RWMD, Nuclear Decommissioning Authority, Harwell, UK.
- Wilson, J., Savage, D., Bond, A., Watson, S., Pusch, R., Bennett, D., 2011. Bentonite: A Review of key properties, processes and issues for consideration in the UK context. Quintessa Report QRS-1378ZG v1.1 for NDA RWMD. Nuclear Decommissioning Authority, Harwell, UK.
- Witten, T.A., Pincus, P.A., 2010. *Structured Fluids: Polymers, Colloids, Surfactants*. Oxford University Press.
- Zhang, F., Low, P.F., Roth, C.B., 1995. Effects of Monovalent, Exchangeable Cations and Electrolytes on the Relation between Swelling Pressure and Interlayer Distance in Montmorillonite. *Journal of Colloid and Interface Science* 173, 34–41. <https://doi.org/10.1006/jcis.1995.1293>





**Radioactive Waste Management Limited**

Building 329  
Thomson Avenue  
Harwell Oxford  
Didcot  
OX11 0GD

**t** +44 (0)1925 802820  
**w** [www.gov.uk/rwm](http://www.gov.uk/rwm)

© Nuclear Decommissioning Authority 2021